FLOW EFFECTS ON VISCO-RESISTIVE MHD IN A TOKAMAK

By

JERVIS RITESH MENDONCA

PHYS06201304009

Institute for Plasma Research, Gandhinagar

A thesis submitted to the

Board of Studies in Physical Sciences

In partial fulfillment of requirements

for the Degree of

DOCTOR OF PHILOSOPHY

of

HOMI BHABHA NATIONAL INSTITUTE

July, 2019

Homi Bhabha National Institute

As members of the Viva Voce Committee, we certify that we have read the dissertation prepared by **Jervis Ritesh Mendonca** entitled **"Flow Effects on Visco-resistive MHD in a Tokamak"** and recommend that it may be accepted as fulfilling the thesis requirement for the award of Degree of Doctor of Philosophy.

S mukherjee ________________ **Date :** 11/11/2019

Chairman - Prof. Subroto Mukherjee

D. Chandra ________________ **Date :** 11/11/2019

Guide/Convener - Dr. Debasis Chandra

________________ **Date :** 11/11/2019

Co-Guide - Prof. Abhijit Sen

Vinod Krishan ________________ **Date :** 11/11/2019

Examiner - Prof. Vinod Krishan

________________ **Date :** 11/11/2019

Member - Prof. Rajaraman Ganesh

________________ **Date :** 11/11/2019

Member - Dr. R. Srinivasan

Final approval and acceptance of this thesis is contingent upon the candidate's submission of the final copies of the thesis to HBNI.

We hereby certify that we have read this thesis prepared under our direction and recommend that it may be accepted as fulfilling the thesis requirement.

D. Chandra

Date: 11/11/2019

Place: Gandhinagar

Dr. Debasis Chandra

Guide

STATEMENT BY AUTHOR

This dissertation has been submitted in partial fulfilment of requirements for an advanced degree at Homi Bhabha National Institute (HBNI) and is deposited in the Library to be made available to borrowers under rules of the HBNI.

Brief quotations from this dissertation are allowable without special permission, provided that accurate acknowledgement of source is made. Requests for permission for extended quotation from or reproduction of this manuscript in whole or in part may be granted by the Competent Authority of HBNI when in his or her judgement the proposed use of the material is in the interests of scholarship. In all other instances, however, permission must be obtained from the author.

JERVIS RITESH MENDONCA

DECLARATION

I, hereby declare that the investigation presented in the thesis has been carried out by me. The work is original and the work has not been submitted earlier as a whole or in part for a degree/diploma at this or any other Institution or University.

JERVIS RITESH MENDONCA

List of Publications arising from the thesis

Publications in Peer Reviewed Journals:

- **Modelling and analytic studies of sheared flow effects on tearing modes**, Debasis Chandra, Anantanarayanan Thyagaraja, Abhijit Sen, Christopher J. Ham, Tim C. Hender, Robert James Hastie, John William Connor, Predhiman Krishan Kaw and Jervis Mendonca
Nuclear Fusion **55**, 053016 (2015).

- **Visco-resistive MHD study of internal kink (m = 1) modes**,
Jervis Mendonca, Debasis Chandra, Abhijit Sen, Anantanarayanan Thyagaraja
Physics of Plasmas **25**, 022504 (2018).

- **Simulation of the internal kink mode in visco-resistive regimes**,
Jervis Mendonca, Debasis Chandra, Abhijit Sen, Anantanarayanan Thyagaraja
submitted for publication to Nuclear Fusion

Conferences/Schools:

International Participation

- 52nd Culham Plasma Physics Summer School, Culham Centre for Fusion Energy, Abingdon, Oxfordshire, OX14 3DB, United Kingdom, July 13-24, 2015

- Simulation of the internal kink mode in visco-resistive regimes,
Jervis Mendonca, Debasis Chandra, Abhijit Sen, Anantanarayanan Thyagaraja
Proc. 27th IAEA Fusion Energy Conference (Gandhinagar, India),22-27 October 2018 TH/P5-21

- Investigations of the visco-resistive kink(m=1,n=1) mode using the two fluid CUTIE code,
Jervis Mendonca, Debasis Chandra, Abhijit Sen, Anantanarayanan Thyagaraja
Oral Presentation, Sixty-First Annual Meeting of the American Physical Society Division of Plasma Physics (APS DPP), October 21-25, 2019, Fort Lauderdale, Florida, U.S.A., Abs. Id. JO6.00003

National Participation

- Fluid Simulation of the Drift Tearing Instability. (Poster), Jervis Mendonca, Debasis Chandra, Abhijit Sen and Anantanarayanan Thyagaraja
  29th National Symposium on Plasma Science and Technology, Mahatma Gandhi University, Kottayam, Kerala, India, 8-11 December, 2014

- Visco-resistive MHD study of internal kink(m=1) modes. (Poster), Jervis Mendonca, Debasis Chandra, Abhijit Sen and Anantanarayanan Thyagaraja
  32nd National Symposium on Plasma Science and Technology, Institute for Plasma Research, Gandhinagar,Gujarat,07-10 November 2017

- Two fluid Simulations Of Internal Kink(m=1) Modes,
  Jervis Mendonca, Debasis Chandra, Abhijit Sen, Anantanarayanan Thyagaraja
  Oral presentation, 33rd National Symposium on Plasma Science and Technology, Delhi University, Delhi, India, December, 4-7 2018, Abs. Id 254

JERVIS RITESH MENDONCA

Dedicated to

Family and Friends

ACKNOWLEDGEMENTS

The completion of a thesis represents far more than a single student and supervisor's research accomplishments. It is the culmination of a long journey, where many people contribute in big and small ways, and it isn't possible to acknowledge each person, despite one's best efforts. To those who have helped me but I have inadvertently not mentioned here, I offer my apologies and I am grateful to your assistance in my journey to become a physicist. I also would acknowledge all those in years past who I have encountered before I arrived in IPR, and have contributed in my intellectual and personal growth. It is indeed a moment of reflection for me as this marks the end of my time as a student and I enter the real world, later than many of my peers who did not choose to enter a doctoral program. I have learnt a lot beyond physics during my time here, lessons I believe should stand me in good stead as I go ahead. The PhD also offers an opportunity for introspection, and has helped me personally to build on my strengths and tackle my weaknesses. I have mixed feelings, happiness at accomplishing what I set out, and sadness that it has ended. There have been many physicists I have encountered personally and through books during my bachelors and masters studies, who have been a source of inspiration for me to take up this career. Physics remains as fascinating a subject to me today as it was all those years ago in school since I first encountered it. While a lot has changed in my life since then, physics has remained a constant part of my life, though waxing and waning in importance at various times. It is also to my mind a tragedy that many of those I wish could have read this will probably not due to its technical nature, and perhaps very few people will ever read this voluminous document. I forever am sad that I could not explain to those of my friends and family as to what I have been doing all these years. With this mind, and all the multitude of emotions and thoughts going through me as I write this, I will move on to specifically acknowledge those who have helped to make this thesis possible.

At the outset, I wish to express my deep gratitude and reverence to my thesis supervisor Dr. Debasis Chandra and co-supervisor Prof. Abhijit Sen. They have been the reason that this thesis is possible today, and words fail me in expressing my gratitude to them for advising and teaching me all these years. I believe I am extremely fortunate in terms of the rich interaction I have had with them regarding MHD and tokamak physics in general and the opportunities to learn from the many leading scientists they have been in collaboration with. Dr. Chandra has been a guiding light in my research work, and has been like a parent here to me. I will be forever grateful to him for his insights, know-how and learning from his mastery of solving physics problems using computational means. Prof. Sen is one of the leading scientists not only of IPR, but perhaps the country and internationally in subject of Flows and Nonlinear Physics. He has guided students for decades, and I am fortunate to have also had the opportunity to count myself among them. Despite his stature, and vast knowledge, he has been extremely approachable and is very friendly to all students in the institute. He has remained an extremely active researcher for several decades and he continues to be a source of inspiration to scientists and students at IPR. There are so many things that I have learnt as a researcher and a person from him that it is impossible to list here, but I could say he has left an indelible mark on my approach to life and hope I have his blessings going forward from here.

I also wish to express my gratitude to Dr. Anantanarayanan Thyagaraja, who though has not been formally a co-supervisor, this thesis would have been possible without his guidance and help at all stages from the very beginning. He has provided the CUTIE code for us at IPR to work with for our simulations and helped us in various issues regarding using it. He is a highly accomplished physicist, with a command over disparate areas ranging from mathematics to Tamil and English literature and has published in many areas of physics, while being one of the leading plasma physicists of our generation. It has been an honour to have worked with him and I have learnt a lot from him about numerics and tokamak physics.

I wish to also remember Late Prof. P.K. Kaw who unfortunately is no more with us. I am sad I did not get much of an opportunity to interact with him during the last stages of my PhD, and his passing has had a profound impact on me as it did on people in IPR and his many friends, students and well wishers around the world. He was perhaps one of India's best scientists since Independence and has inspired many around the world, doing seminal research from a very young age. India's tokamak program is largely due to his efforts as a founder and director of IPR for decades. A genius of the mould of great physicists of past and present, interacting with him was an unforgettable experience due to his extraordinary ability in physics, his ability to solve equations just looking at them, his vast knowledge of every area of physics, all these extensively attested to by many people. It is my fortune to have known him, first as one of teachers in course work, and later as chairman of my doctoral committee. He will be deeply missed.

I would like to thank my doctoral committee members Prof. Subroto Mukherjee, Prof. Rajaraman Ganesh, Dr. R. Srinivasan who have been very helpful in my progress and the discussions that took place had a profound impact on me. I would also like to thank Prof. Sudip Sengupta, Dr. Mainak Bandhopadhyay who are former and current Academic committee Chairmen respectively for their motivation and assistance along with the other members of the Academic committee. I am grateful to my course work teachers for their efforts.

I would like to mention Dr. Nirmal Bisai with whom I interacted briefly on the CENTORI code, and he has been very warm and knowledgeable to interact with.

I would like to thank all the administrative, library, accounts and computer center staff for their support during my studies. I would like to mention Harish Chandra Khanduri, Hitesh Mehta, Saroj Das, Shirin S Bhesania, Shilpa Khandker, Arvind Singh, Prashant Kumar, Govind Lokhande, Rekha Singh, Avadhesh Maurya and the others who I have interacted with numerous times for many matters and they have kindly assisted me.

Certainly, the acknowledgements section is incomplete without mentioning my hostel colleagues and a few scholars who didn't stay in the hostel. The hostel has been the center of our life in IPR and there isn't space enough here to detail how it has been over the few years I was here. I have learnt and been influenced by the various people I met here, who hail from various different backgrounds.

I would like to remember my old friends and teachers, some of whom I have lost contact with, some who have passed away. I offer my apologies for being unable to mention names here due to a lack of space but I'm deeply grateful to them.

I would like to bring the section to a conclusion by mentioning my family, my father, mother and sister who have been supportive throughout my studies. My other relatives, my maternal grandparents, cousins and their families, uncles, aunts all have given me a lot of love and encouragement over the years. I would like to recall my Late paternal grandparents, my grandfather who I never saw, and grandmother who passed away when I was a child, also my dear uncle William Mendonca, who recently passed, and was very fond of me. I am grateful for all the love and support I received from them, it has been helpful in the arduous process of reaching here today. My parents have been always supportive of whatever decisions I took and left it entirely to me as to what career and courses I should take. I like to dedicate this thesis to them.

Contents

SYNOPSIS

Due to the increasing cost of non-renewable energy and its ultimate depletion, and ever increasing demand of energy from both developed and developing countries, every future alternative energy source needs to be comprehensively investigated. The main source of energy in the solar system is the Sun, and it is powered by nuclear fusion. Nuclear fusion is a process in which two light nuclei combine to form a heavier nucleus with a net release in energy. In order to do so, the nuclei should overcome the Coulomb barrier, which is achieved by increasing temperatures to nearly 10 keV. The Sun is able to confine particles due to a massive gravitational field, but that is not possible on earth. Therefore, various schemes have been devised starting from magnetic mirrors, and currently the most successful scheme, which uses magnetic fields to confine plasma is called the tokamak. The word tokamak is a Russian acronym, "toroidalnaya kameras magnitnymi katushkami", meaning toroidal chamber with magnetic coils, and is a literal description of the device. The principal magnetic field in a tokamak is in the toroidal direction, around the full length of the torus. This alone, however, is insufficient to contain the plasma, whose positively and negatively charged particles, although following magnetic field lines, would drift vertically in opposite directions due to the non-uniform magnetic field. Hence a poloidal magnetic field is required to prevent particle motion resulting in this effect . The combination of these two magnetic fields produces helical nested magnetic flux surfaces around the full domain of the torus. This magnetic configuration confines the plasma away from the walls of a vacuum vessel which is the boundary of the tokamak device. The amount of twist the magnetic field experiences in this way at a given radius, r, is measured by the safety factor, or winding number q(r). The toroidal field is created by the use of an external current in poloidal coils, while the poloidal field, which is typically weaker by an order of magnitude except in some spherical tokamaks like MAST, is produced by an internal toroidal current in the plasma. Tokamak performance is affected by various instabilities, particularly Macro-instabilities which affect stability and Micro-instabilities which affect transport. Here, we have studied a particular class of Macro-instabilities, which are current driven resistive instabilities, such as the tearing and kink instabilities, which play a role in stability and disruptions. We have investigated the effect of flows, which have a beneficial effect on these instabilities, hence are of great importance experimentally. The summary of salient works carried out under this thesis work has been elaborated below.

CUTIE code

An approach to better understand plasma turbulence and anomalous transport involves global simulations for a two fluid plasma and Maxwell's equations. Global simulations take into account length scales all the way up to the device size, and a two fluid theory accounts for the different physics of the ion and electron species by treating them as separate interacting fluids. CUTIE (CUlham Transporter of Ions and Electrons) is a plasma fluid initial value code which provides such simulations. CUTIE is a nonlinear, global, electromagnetic, quasi neutral ($n_e \approx n_i$), two fluid, turbulent large eddy simulation code, which allows interaction between plasma property profiles and electromagnetic turbulence. Details of the code are primarily available in [44] amongst others. The CUTIE model is solved for the so-called mesoscale, defined to be an intermediatescale between the device size and the ion gyroradius, incorporating approximations for the underlying classical and neoclassical transport effects. Thus ions feel their neoclassical conductivities (due to transport effects arising from toroidal geometry) and electrons the bootstrap current (a plasma current produced by tokamak plasmas) and neoclassical resistivities. CUTIE is based on a periodic cylinder model of the tokamak geometry in which the magnetic flux surfaces are concentric circles, and which is an appropriate approximation for large aspect ratio devices in which the aspect ratio, R/a, is significantly greater than unity, or equivalently the inverse aspect ratio is small, i.e. a/R « 1. The low β Shafranov shift is adopted. Single fluid studies of (2,1) modes: Equilibrium flows can influence the stability of tearing modes through a variety of physical effects arising from the dynamical characteristics of the plasma as well as the confinement geometry. To understand and assess systematically the roles played by these effects, we have carried out a series of numerical and analytic studies on the stability of the (2,1) tearing mode, using a number of model systems that progressively incorporate various effects of changes in geometry and more detailed physics. We begin with a simple reduced MHD description of the plasma in a cylindrical geometry and present a series of numerical computation results carried out with the code CUTIE . The cases include purely axial sheared flows, purely poloidal sheared flows and helical flows that are a combination of the axial and poloidal flows leading to different flow helicities. Then, we present CUTIE simulations using a two fluid model and discuss the differences observed from the single fluid simulations. It contains a discussion of a new and powerful technique (called the "resolvent method") for obtaining the full eigen-spectrum that is applicable to non-self-adjoint problems. The growth rate and real frequencies obtained through the use of this method confirm and further validate our results from the CUTIE code. After that, we examine the equilibrium modifications arising in a toroidal geometry due to the presence of toroidal flows and their impact on the stability of the (2,1) mode. To summarize, we have carried out extensive numerical studies to examine the influence of equilibrium sheared flows on the stability of a tearing mode. Our cylindrical geometry investigations, using a RMHD version of the code CUTIE, show that in the linear regime pure axial sheared flows have a destabilizing influence while pure sheared poloidal flows tend to stabilize the mode. These effects are independent of the sign of the flows. However for a helical flow the sign of the helicity matters with positive helicity providing a stabilizing influence. In the nonlinear regime the independence from the sign of the flow no longer exists (even for purely axial or poloidal flows) and is an important finding of our investigations. The inclusion of two fluid effects provides a further stabilizing effect on the mode presumably due to self consistent excitation of poloidal flows.

This work has been published as : "Modelling and analytic studies of sheared flow effects on tearing modes", Debasis Chandra, Anantanarayanan Thyagaraja, Abhijit Sen, Christopher J. Ham, Tim C. Hender, Robert James Hastie, John William Connor, Predhiman Krishan Kaw and **Jervis Mendonca**, Nuclear Fusion **55**, 053016 (2015)

Single fluid studies of (1,1) mode

The m=1, n=1 internal kink instability is of great importance in tokamaks and has beeen extensively studied in the past by several authors. The (1,1) mode arises within the q=1 rational surface (where q is the safety factor), when the q at the axis is smaller than 1. It can trigger sawtooth oscillations which can influence plasma quality and confinement . It is well known that flows are a common occurence in a tokamak, which can be generated intrinsically,or induced externally e.g. by unbalanced NBI injection. Experiments on NSTX have shown a significant increase of sawtooth period that is attributed to a fast rotation of the plasma. Experimental studies on sawteeth phenomena in presence of NBI in JET, have further shown that there is an asymmetry in sawtooth period depending on the direction of the NBI. The sawtooth period increases with an increase in co-NBI power, and decreases with an increase in counter-NBI power. Thus, these experiments have shown that flow can have a stabilising or destabilising effect on the kink mode depending on the direction of flow. However, there still does not exist a full understanding of the effect of flows on the m=1,n=1 kink instability. It may be noted that most of the past flow studies have been done in the low viscosity regime. However, viscosity can be high in tokamak operations, particularly due to enhancements from turbulent effects and could therefore significantly influence the effect of flow shear on the internal kink mode. Thus, viscosity is an important contributing factor and can change the nature of the effect of flows significantly. Here, we have addressed this issue and investigated the stability of the (1,1) mode in the presence of sheared flows over a range of viscosity regimes. We indeed find that the high viscosity results are often very different from the low viscosity results. In our study, we have systematically examined the effects of several kinds of sheared flows on the (1,1) mode, namely axial, poloidal and combinations of both kinds of flows in the linear as well as nonlinear regimes. Our principal findings are as follows. To begin with, we have done the linear scaling studies of the m=1,n=1 mode in the absence of flow. Here, the variation of linear growth rates have been studied for different S and Pr values. The obtained scalings are in agreement with past analytic theory results in the no flow case. With the application of sheared axial flows, a significant change in the scaling of the growth rates is observed. However, in the presence of poloidal flow, there is no such change in scaling as compared to the no flow case. In our linear studies we have noticed that axial flows destabilise the mode in the low viscosity regime, but it stabilises in the high viscosity regime as compared to the no flow case. On the other hand, poloidal flow always tends to stabilise the linear growth rate. For pure axial and poloidal flows, the results do not change if we change the direction of the flow. This symmetry is broken for helical flows where the time evolution of the modes show a significant dependence on the helicity of the flows even in the linear regime. In the nonlinear regime, there is mostly a reduction of the nonlinear saturation level of the (1,1) mode for both sheared axial and poloidal flows in the high viscosity regime, while in the low viscosity regime, the poloidal and axial flows are destabilising in nature. Helical flows show a strong stabilisation for positive helicity and in most cases, weak stabilisation for negative helicity in the high viscosity regime. In the low viscosity regime, this symmetry breaking of helical flow results gets significantly diminished.

These have been published in a paper entitled : **Visco-resistive MHD study of internal kink(m=1) modes, J. Mendonca et al, Physics of Plasmas, 25, 022504 (2018)**

Two fluid study of (1,1) mode

We have continued our studies in the two fluid regime. The two fluid version of CUTIE solves 5 equations, thus two additional equations, one for electron continuity, and one for parallel momentum. In the linear regime, we have studied how the growth rate as well as diamagnetic flow frequency of the modes changes due to fluid effects for a range of viscosity and resistivity values. We have also found diamagnetic drift stabilisation of the (1,1) mode in the two fluid case, that is, we have seen the growth rate of the (1,1) mode reduces with an increase in density gradient. In the nonlinear case, we will investigate the evolution of the mode with an imposed axial flow.This manuscript is to be submitted to Nuclear Fusion as "Simulation of the internal kink mode in visco-resistive regimes".

Organisation

The Thesis is organised as follows. The chapter 1 contains an introduction to Tokamaks and Fusion Energy. We talk about the MHD model of Tokamaks and Instabilities. We also cover previous investigations of the subject. In chapter 2, we proceed to lay out the FKR analysis of Resistive modes. We talk about tearing modes and Kink modes.

In chapter 3, we discuss the motivation for the simulation of Resistive modes and the CUTIE code, its description and implementation. In chapter 4, we talk about flow studies of (2,1) tearing modes, linear and nonlinear aspects therein. We have used both single and 2fluid models here in our study. In chapter 5, we investigate (1,1) kink mode in a single fluid model. We examine the effect of flows in linear and nonlinear regimes. In chapter 6, we investigate the (1,1) kink mode using a two fluid model and the effects of flows thereon. Finally, we summarise our findings in chapter 7.

List of Figures

List of Tables

1 Introduction

Nuclear Fusion is a process by which two light nuclei combine to form a heavier nucleus with the release of energy. It is being actively pursued as an alternative source of energy from the past few decades due to its enormous potential for fulfilling society's energy needs. Life on Earth is already powered by fusion energy, which it receives from the Sun. However, it is not possible for us on Earth to exactly imitate the Sun in a laboratory or a power plant. This is because we do not have the luxury of a large gravitational field which can confine nuclei in order that fusion is possible, as positively charged nuclei repel. Therefore we need an alternative mechanism to confine the nuclei in such a manner that fusion takes place. This is made clear in the following, where we detail the factors the fusion reaction and the fusion yield would depend on, summarised in the Lawson criterion, which gives us a quantitative criterion for reaction to become self-sustaining. One of the most popular approaches for achieving controlled fusion is magnetic fusion, wherein we employ magnetic fields to confine particles. In this approach, the tokamak is the most successful prototype for a future fusion power plant. Here the particles are confined in a toroidal geometry using a toroidal magnetic field. Though there is no end loss of particles and energy, but there are losses due to several plasma instabilities which occur in the presence of free energy in the system such as current gradients, field gradients, density gradients, temperature gradients etc. In this thesis, we study the physics of plasmas in a tokamak, in particular plasma instabilities in the MHD regime, and the effect of flow on them.

Tokamaks and Fusion Energy, its importance and scope

Nuclear Fusion, as has been mentioned, is the process of combination of light nuclei to produce heavier nuclei with a net output of energy. This process naturally goes on in the cores of stars like the Sun, where gravity helps to confine particles. In the Sun, the dominant process is the combination of two deuterium nuclei as shown in equation 1.1, that is the sun follows a D-D process primarily. The reactions are as follows:

$$ {}_1^2H + {}_1^2H \rightarrow {}_2^3He + {}_0^1n + 3.27MeV \tag{1.1} $$

$$ {}_1^2H + {}_1^2H \rightarrow {}_1^3H + {}_1^1H + 4.03MeV \tag{1.2} $$

$$ {}_1^2H + {}_1^3H \rightarrow {}_2^4He + {}_0^1n + 17.59MeV \tag{1.3} $$

$$ {}_1^2H + {}_2^3H \rightarrow {}_2^4H + {}_1^1H + 18.30MeV \tag{1.4} $$

This gives the overall reaction as follows:

$$ 6{}_1^2H + {}_1^3H + {}_2^3He \rightarrow 2{}_2^4He + {}_2^3He + {}_1^3H + 2{}_1^1He + 2{}_0^1n + 43.19MeV \tag{1.5} $$

There are many mechanisms by which the overall reaction is achieved. However, this cycle is not useful to us in the laboratory as its cross section is too low. The D-T reaction cycle is the most promising reaction in terms of economic viability [1]. We have a large availability of deuterium from the oceans and tritium can be obtained from lithium which is also plentiful, by treatment with neutrons.

Achieving a successful fusion reaction however is more complicated than this. Two nuclei will always repel each other strongly as they are both positively charged. One needs to increase the energy so that reaction rate increases to the extent that it is feasible for our purposes, and confine them so that enough nuclei can collide with each other, which is very difficult at such energies. We also require a sufficient density of the gas. Since the temperatures involved are very high $\sim 10keV$ and can destroy any material we have, confinement of this fusion reaction and controlling it is not a trivial task. These factors are captured in the famous Lawson Criterion[1] which tells us about what parameters we require to achieve ignition, which means a condition where the heat generated by the fusion reactions maintains the temperature of the fusion reaction despite all the heat losses due to various mechanisms. The Lawson criterion states that, once a critical ignition temperature for nuclear fusion has been achieved, it must be maintained at that temperature for a long enough confinement time at a high enough ion density to obtain a net yield of energy. In numbers, $nT\tau_E \geq 3 \times 10^{21} keV s/m^3$ for a D-T reaction.

At fusion relevant temperatures, the D and T gases form a plasma, where nuclei and electrons separate. In order to carry out the reaction on earth, we need a method to keep the gas from touching the walls of any material conductor we use to confine the fusion reactants. For this purpose, we use magnetic fields, and various devices over the years have used magnetic fields in a variety of ways to confine plasma. The most successful of these is called the tokamak. It is an acronym from a Russian name "toroidalnaya kameras magnitnymi katushkami", meaning toroidal chamber with magnetic coils, and is a literal description of the device. We will speak more about the tokamak in what follows.

We have mentioned that magnetic fields are used to confine a plasma. It is because the trajectory of charged particles can be modified by a magnetic field as is well known in electrodynamics. Various types of magnetic fields may be used for the purpose, however in every case it is not possible to confine the particles perfectly. Different types of magnetic field configurations like a screw pinch, stellarators, and tokamaks have been used. Linear devices have large end losses and closed devices like a tokamak have drifts. There are also the issues of instabilities of a plasma, which is the focus of this thesis. Tokamaks are relatively the best among devices which use magnetic fields to confine plasma, and internationally a lot of research effort in the field of controlled magnetic fusion research is devoted to using tokamaks.

Tokamaks essentially are a torus, with two magnetic fields, one toroidal and one poloidal. The toroidal field if used alone cannot confine the plasma. This is because the plasma contains positive and negative particles which will drift in opposite directions. There is an $E \times B$ drift thus created due to the resulting electric field. A poloidal field in combination with a toroidal field can prevent this from happening. It creates a helical field, consisting of nested magnetic flux surfaces. These can be measured by the safety factor $q(r)$ or the rotational transform ι, its inverse. It is important during the operation of a tokamak to ensure we have achieved adequate temperatures and densities for as long as it is possible so that we can obtain as much fusion energy as possible. Our guide in this matter is the aforementioned Lawson Criterion which gives us the condition for ignition. There are many ways in which both heat and density is lost continuously during the operation as well impurities both present prior to the operation and generated during the operation reduce the efficiency of the tokamak. These problems have to be overcome in order to produce fusion in a commercially viable manner. According to our present understanding, we believe that anomalous transport and plasma turbulence may be limiting confinement time in tokamaks. There are several MHD instabilities present in the system which are responsible for enhancement of energy and particle transport in a tokamak. For example, we have the edge localised modes(ELMs) which occur near the edge in the high confinement plasma due to strong pressure gradients. Then we have the tearing modes in the core arising due to current gradient which forms a magnetic island inside the plasma. Similarly, we have the sawteeth near the center of the plasma which are thermal instabilities associated with internal kink modes. To achieve the high confinement and temperature as required for fusion, it is very much necessary to control these instabilities. Much effort has been put by the fusion community to understand how to control these MHD instabilities and achieve high confinement plasma.

Despite these issues, tokamak research has made great advances over the years both experimentally to achieve higher fusion parameters and theoretically to understand the key dynamics of these instabilities and how to control them. Now we have a better understanding of tokamak experiments due to lots of theoretical efforts analytically as well as by doing numerical simulation though it is far from complete. On the other hand, there are instances such as bootstrap current, caused due to the potential difference between trapped and passing particles, which was predicted theoretically [2] and then confirmed experimentally later[3]. All these encouraging results have motivated the international community to build the ITER tokamak, in an international collaboration which seeks to build a working tokamak reactor in France, with an aim to achieve ignition. It will be the biggest tokamak constructed in the world so far.

Literature Survey and Resistive modes in a Tokamak

Many efforts have been made in the past to better understand resistive modes in a Tokamak. We will here try to trace the development of the subject and mention some of the most important works in this and related areas. The importance of flows and its ability to alter the characteristics of resistive modes in a tokamak is brought out.

In our study of tokamak plasmas, our primary focus has been on instabilities in it. An instability is a perturbation which has a positive growth rate, and it draws upon a free energy source for its growth. There are various types of instabilities present in a tokamak depending on the kind of model we use to study it. One of the most common and simple models used to study the tokamak is the MHD(magnetohydrodynamic model), which treats the tokamak plasma as a charged single fluid interacting with magnetic fields. Due to its simplicity it is not able to give answers to some puzzling questions about the tokamak plasma, however it is a very powerful model, and has led to powerful insights into the working and behaviour of the tokamak plasma. An excellent introduction to the ideal MHD model applied to tokamak plasmas can be found in the book by Freidberg[4]. Here, we briefly introduce MHD theory in the following. The equations constituting the MHD model are described in the following.

MHD model

- Continuity equation

$$\frac{\partial \rho}{\partial t} + \nabla \cdot (\rho \mathbf{v}) = 0 \tag{1.6}$$

- Momentum equation

$$\rho \left(\frac{\partial}{\partial t} + \mathbf{v} \cdot \nabla \right) \mathbf{v} = \frac{\mathbf{J} \times \mathbf{B}}{c} - \nabla p \tag{1.7}$$

- Ampere's law

$$\frac{\partial \mathbf{B}}{\partial t} = -c \nabla \times \mathbf{E} \tag{1.8}$$

- Faraday's law

$$\mathbf{E} + \frac{\mathbf{v} \times \mathbf{B}}{c} = 0 \tag{1.9}$$

- Ideal Ohm's law

$$\nabla \cdot \mathbf{B} = 0 \tag{1.10}$$

- Divergence constraint

$$\frac{d}{dt}\left(\frac{p}{\rho^{\gamma}}\right) = 0 \tag{1.11}$$

In these equations 1.6-1.11, we have used the following definitions:

B is the magnetic field; **v** is the plasma velocity; **J** is the current density; **E** is the electric field; ρ, is the mass density; p is the plasma pressure; γ, is the ratio of specific heats C_p/Cv and t is time.

A tokamak plasma generally has two competing forces, pressure expanding outwards and an inward force due to the plasma current. The plasma is at equilibrium when these two forces balance each other. This condition is expressed mathematically as $\vec{\nabla} p = \vec{j} \times \vec{B}$, where "$B$" is the magnetic field and 'p' is the pressure.This condition leads to the Grad-Shafranov equation. It is a differential equation for the poloidal flux function. Various instabilities can affect this equilibrium and it is obtained from the force balance equation, $\vec{\nabla} p = \vec{j} \times \vec{B}$, where "B" is the magnetic field (divergence-free) and $\mu_0 \vec{j} = \vec{\nabla} \times \vec{B}$. It is given as follows:

$$\Delta^* \psi = -\mu_0 R^2 \frac{dp}{d\psi} - \frac{1}{2}\frac{dF^2}{d\psi} \tag{1.12}$$

Here, μ_0 is the magnetic permeability, $p(\psi)$ is the pressure, $F(\psi) = RB_{\phi}$.

The magnetic field and current are, respectively, given by the equations:

$$\vec{B} = \frac{1}{R}\nabla\psi \times \hat{e}_{\phi} + \frac{F}{R}\hat{e}_{\phi} \tag{1.13}$$

$$\mu_0 \vec{J} = \frac{1}{R}\frac{dF}{d\psi}\nabla\psi \times \hat{e}_{\phi} - \frac{1}{R}\Delta^* \psi \hat{e}_{\phi} \tag{1.14}$$

and the elliptic operator Δ^* is given by,

$$\Delta^* \psi \equiv R^2 \vec{\nabla} \cdot \left(\frac{1}{R^2}\vec{\nabla}\psi\right) = R\frac{\partial}{\partial R}\left(\frac{1}{R}\frac{\partial \psi}{\partial R}\right) + \frac{\partial^2 \psi}{\partial Z^2} \tag{1.15}$$

We have chosen here to focus on kink and tearing modes. These are current driven instabilities and are strongly affected by the presence or absence of resistivity. Indeed, tearing modes cannot exist in the absence of resistivity. We will describe kink modes, tearing modes and the effect of flows in some detail in the following. We also assume a cylindrical geometry as our studies are carried out in a cylindrical geometry with periodic boundary conditions.

Flows are an important and unavoidable part of tokamak operation. Flows can be both intrinsically generated within the plasma or externally manipulated. As such, flows can substantially affect plasma equilibrium and stability. The introduction of flows makes MHD equations much harder to solve. Pioneering work in this area has been carried out by Zehrfeld et al[5], who had given an analytic solution due to presence of flow of flux surfaces and their shift. Another seminal work has been carried out by Maschke and Perring[6]. They have found exact solutions for a model with a toroidal flow. They demonstrated a method to incorporate toroidal flow in the Grad Shafranov equation. In this connection, they have shown an outward shift of the constant pressure surface from the magnetic flux surface caused by toroidal rotation or flow. The paper also contains a calculation of outward shifts of the magnetic axis, and pressure due to incorporating toroidal flow into the system. A few studies are noteworthy and we mention them below in this context. There is an analytical theory developed by Betti et al[7] which has demonstrated that radial discontinuities develop at the transonic surface during the transition from subsonic to supersonic velocity of the equilibrium poloidal velocity profile in comparison to the poloidal sound speed. This work has been validated by the simulation work of Guazzotto et al[8], where they have used the FLOW code, and observed a development of pedestal structures which are characterised by radial discontinuities. A derivation of a generalised form of the Grad-Shafranov equations which include both toroidal and poloidal flows has been done by Hameiri[9]. Throumoulopoulos have found several classes of analytic equilibria of a toroidal axisymmetric plasma when it has a toroidal mass flow in the case of isothermal and isentropic magnetic surfaces for various pressure and current density profiles[10].

Flows therefore have been shown to have significant effect on plasma equilibrium. They also have a strong effect on MHD instabilities which has been the focus of this thesis. There exists a large body of literature where these studies have been documented. There were pioneering studies done by Hofmann[11], in which an analysis of resistive tearing modes in plane sheet pinch in the presence of a shear bulk plasma flow. The principal results of this study were a dispersion relation where there is a growth rate scaling of $S^{-1/2}$, and that the region of instability depends on fluid kinetic energy or magnetic field energy where positive or negative stabilisation are likely effects of the flow. The paper of Chen and Morrison[12] is a comprehensive study of the effect of equilibrium velocity shear using the boundary layer approach for constant-ψ and nonconstant-ψ linear tearing modes in the inner resistive region and outer ideal region. They have a number of significant results. One is that Δ' depends strongly on sheared flow in the outer region. In the inner region linear growth rate scaling changes for nonconstant-ψ but remains same for constant-ψ. Also, flow shear is stabilising if it is larger than magnetic field shear. Kleva and Guzdar have studied the stabilization of sawteeth in tokamaks with toroidal flows[13]. They find that as the toroidal flow velocity approaches sound speed, then n=1 resistive tearing mode gets completely stabilized. We can also mention the work of Wahlberg et al[14] and Chapman et al[15] in this context who have studied the stabilisation of the internal kink mode. In this context, it is ought to be mentioned that viscosity can play a very important role to modify the stability of the modes particularly in the presence of flows. The viscosity can be high in tokamak operations due to turbulence etc. which has been reported in tokamak experiments[16]. There are several other studies [17–19] which show that the stability results in the low viscosity regime can be altered significantly in the high viscosity regime.

Thus, in this thesis we have done the systematic studies of MHD resistive instabilities in the presence of flow for a wide viscosity range both in the linear and nonlinear regime.

Layout of the thesis

The Thesis is organised as follows. In **Chapter 1**, we proceed to lay out the FKR[20] analysis of Resistive modes. The paper of Furth, Killeen, Rosenbluth, abbreviated as FKR[20] is a seminal work in the field of tokamak instabilities, and was the first to identify modes such as the tearing mode. Resistive modes occur frequently in a tokamak, and play an important role in disruptions. The resistive modes we have dealt with are the tearing mode and the kink mode. The tearing mode, or more precisely the classical tearing mode which we exclusively deal with, arises at the mode rational surfaces, and plays an important role in disruptions. The origin of this mode, and its importance for the tokamak are discussed. This mode can also couple with other modes like the kink mode, and we could have cascades. Our studies can also be useful for neoclassical tearing modes as the classical tearing mode creates seed islands which can give rise to neoclassical tearing modes. After this, we will discuss the kink mode. It occurs at the m=1 rational surface when the q value at the centre dips below 1. It is of great importance as it is linked to triggering sawtooth oscillations. We will discuss the origin and the importance of the kink mode in this chapter. In **Chapter 2**, we discuss the motivation for the simulation of Resistive modes and the existing literature. In the next **Chapter 3** the CUTIE code, its description and implementation. The CUTIE code has been implemented in IPR for the study of resistive modes. It is written in fortran and incorporates a variety of numerical techniques for efficient solution of single and two fluid equations for the tokamak. We discuss some technical aspects, its numerical and physics capabilities. It is very flexible in terms of the parameters we can use such as specifying profiles, and can be used for a range of simulation studies. It has been very successful in the past in predicting phenomena in a tokamak. In **Chapter 4**, we talk about flow studies of (2,1) tearing modes, linear and nonlinear aspects therein. We have used both single and 2fluid models here in our study. Various new results have been presented in this chapter. We have seen that axial flows destabilise the mode, whereas the poloidal flows stabilise the tearing mode in the linear regime. There is also a symmetry breaking effect observed in the nonlinear regime. We have examined the effect of helical flows on the mode which further confirm these conclusions. We have also done a comparison of the stability of a mode in both single and two fluid regimes and found that mode is more stable in the single fluid regime as compared to the two fluid regime. Comparisons have been done with the NEAR code, which is a toroidal code where there are additional stabilising effects. In **Chapter 5**, we investigate (1,1) kink mode in a single fluid model. We examine the effect of flows in linear and nonlinear regimes. Here, we have extended previous studies on the tearing mode and have found that the kink mode behaves a little differently in the presence of viscosity and flow. We notice that the effect of axial flow depends strongly on the viscosity regime. We notice symmetry breaking in a similar manner as was noticed in the case of the tearing mode but it is stronger. We also see the poloidal flow can be nonlinearly destabilising, which is an unexpected conclusion. In **Chapter 6**, we investigate the (1,1) kink mode using a two fluid model and the effects of flows thereon. We have found considerable differences from the single fluid results in the two fluid regime. We find that poloidal flow can be destabilising both linearly and nonlinearly. We have studied the diamagnetic drift frequency $\omega*$ with viscosity and found a variation in its behaviour in different viscosity regimes. Finally, we summarise our findings in **Chapter 7**.

2

Resistive Modes in a Tokamak

In this chapter, we will describe the FKR[20] analysis, which stands for Furth, Killeen and Rosenbluth, the authors of the cited paper, of resistive MHD modes, particularly the tearing modes where resistive MHD modes are those which occur in a plasma when there is a finite resistivity present. This enables magnetic field lines to move within the plasma. In this chapter, we would like to explain resistive MHD modes further, which are the subject of study in this thesis.

Kink modes

The kink mode is a transverse displacement of a plasma column's cross section from its centre of mass. It is driven by radial current gradients and occurs if the Kruskal-Shafranov limit [1] is exceeded, that is the safety factor, $q = \frac{rB_t}{RB_p} < 1$, where $r =$minor radius, $R =$major radius,B_t =axial magnetic field and B_p =poloidal magnetic field. It is quite dangerous for a plasma, and it is sought to be avoided by keeping $q > 1$ at all points in the tokamak so that there is no rational surface for the $m = 1$, $n = 1$ internal kink mode present inside the plasma. However, within the core region, $q < 1$ is typically the case due to the profile of the safety factor present. The presence of resistivity allows magnetic field lines to move, allowing magnetic reconnection to occur. We have studied $m = 1, n = 1$ visco-resistive internal kink modes in this thesis. These are suspected to be initiating sawtooth oscillations and lot of work has been devoted in the past to study this connection[21–25]. The mode can also couple to other MHD modes like the (2,1) mode, and a lot of work has been performed on this[26–28]. Work in this area began with Kadomtsev's theory[22], according to which complete resistive reconnection takes place in the core which leads to a loss of temperature confinement. This theory could not however completely explain experiments due to various reasons, among which it is not understood why experimentally how complete core reconnection is prevented. Simulation work has been done to understand the connection of the internal kink mode and sawtooth oscillations[29, 30]. However, it has not been proven clearly as to what is the role of the internal kink mode on sawtooth oscillations. There are older review papers[31, 32] which have presented an overview of the understanding we have regarding the relationship of the internal kink mode and sawtooth oscillations and their effect on tokamak oscillations. To attempt a complete understanding of the dynamics of the internal kink mode, we would require a full three dimensional toroidal simulation which includes nonlinear coupling between various helical modes and kinetic corrections. This is beyond the scope of our efforts and we have attempted to understand both in a single and two fluid model, what is the effect of flows and viscosity on the internal kink mode, with possible extensions to sawtooth oscillations in the future.

Tearing modes

In our thesis we have worked on classical tearing modes ignoring neoclassical effects. These are driven by gradients of current in a plasma, which is their source of free energy. They grow on the mode rational surfaces, i.e., where the magnetic field has made a integer number of poloidal and toroidal turns. There occurs a resonance between the helicity of this perturbed mode and the equilibrium magnetic field. These modes are characterised by a parameter Δ' which measures the discontinuity in the magnetic field across the mode rational surface. There is a rearrangement of magnetic field topology here which is possible if resistivity is non zero. This can lead to the formation of magnetic islands, which alter transport in a tokamak and can lead to disruptions if they become big enough. It is possible to avoid these modes by ensuring that Δ' is negative. Since we do not deal with neoclassical tearing modes, in which case this is not generally true, this condition is adequate for our purposes.

In the following, we will describe briefly the FKR[20] analysis, of resistive MHD modes, particularly the tearing modes where resistive MHD modes are those which occur in a plasma when there is a finite resistivity present, whose presence enables magnetic field lines to move within the plasma. They have made their calculations in a slab geometry. It will serve as a springboard for further investigations of the kink and tearing modes, which are the subject matter of this thesis. Generally resistivity damps out perturbations in plasmas, however it can actually be destabilising factor in certain situations. As we have indicated, the presence of resistivity enables magnetic field lines to change their topology to form a configuration of lower energy. This process can lead to a destabilisation of the plasma. It is also to be emphasised that resistive MHD modes are quite fast growing, and they play a role in disruptions and sawteeth phenomena. This could be possibly be due to the fact that resistive diffusion of plasma across the magnetic field occurs on a scale length in space, which is lesser than the size of the plasma, and could still release large amounts of energy relatively. The diffusion itself occurs quickly as it has a short distance to traverse. We have summarised the following expressions related to MHD stability as given in Fitzpatrick[33].

Let the equilibrium magnetic field be,

$$\mathbf{B_0} = B_{0y}(x)\hat{y} \tag{2.1}$$

assuming symmetry about origin and assuming no equilibrium flow.

The MHD equations we have are,

$$\mathbf{E} + \mathbf{v_0} \times \mathbf{B} = \eta \mathbf{J_0}$$

$$\rho_0 \frac{\partial \mathbf{v_0}}{\partial t} = -\nabla p + \mathbf{J_0} \times \mathbf{B}$$

Perturbing and linearising these equations, and solving them enables us to derive a dispersion relation

Here, (redefining symbols for our convenience), ρ_0 is the equilibrium plasma density, B the perturbed magnetic field, V the perturbed plasma velocity, and p the perturbed plasma pressure.

Let us suppose all perturbed quantities vary as,

$$A(x,y,z,t) = A(x)\exp(iky + \gamma t) \tag{2.2}$$

Here γ is the growth rate of the tearing mode.

We define the Alfven time-scale,

$$\tau_A = \frac{a}{V_A} \tag{2.3}$$

where $V_A = \frac{B_0}{\sqrt{\mu_0 \rho_0}}$ is the Alfven velocity, and the resistive diffusion time-scale,

$$\tau_R = \frac{\mu_0 a^2}{\eta} \tag{2.4}$$

We additionally define the Lundquist number,

$$S = \frac{\tau_R}{\tau_A} \tag{2.5}$$

Let $\psi = \frac{B_x}{B_0}, \phi = \frac{ikV_y}{\gamma}, \bar{x} = \frac{x}{a}, F = \frac{B_{0y}}{B_0}, F' \equiv \frac{dF}{d\bar{x}}, \bar{\gamma} = \gamma\tau_A, \bar{k} = ka.$

We assume the tearing instability grows on a hybrid time-scale which is much less than τ_R but much greater than τ_A. We must solve the outer equations which are ideal MHD equations and

$$\tau_H = \frac{\tau_A}{kaF'(0)} \tag{2.6}$$

τ_H is known as the hydromagnetic time scale. We have to match the two solutions at the boundary, there being a discontinuity given by,

$$\Delta' = \left[\frac{1}{\psi}\frac{d\psi}{d\bar{x}}\right]_{\bar{x}=0_-}^{\bar{x}=0_+} \tag{2.7}$$

An unstable tearing mode would be characterised by $Q > 0$, where, $Q = \gamma\tau_H^{2/3}\tau_R^{1/3}$
We shall further assume that,

$$Q \ll 1 \tag{2.8}$$

This is termed as the constant ψ approximation. The growth rate of the tearing mode is given by,

$$\gamma = \left[\frac{\Gamma(\frac{1}{4})}{2\pi\Gamma(\frac{3}{4})}\right]^{\frac{4}{5}} \frac{(\Delta')^{\frac{4}{5}}}{\tau_H^{\frac{2}{5}}\tau_R^{\frac{3}{5}}} \tag{2.9}$$

or,

$$\gamma\tau_A = \left[\frac{\Gamma(\frac{1}{4})}{2\pi\Gamma(\frac{3}{4})}\right]^{\frac{4}{5}} \frac{(\Delta')^{\frac{4}{5}} kaF'(0)}{S^{\frac{3}{5}}} \tag{2.10}$$

Thus we see that , $\gamma\tau_A$ scales as $S^{-3/5}$ and $\Delta'^{4/5}$ in a slab geometry.

Militello[34] has provided corrections for the aforementioned dispersion relation, viz the relation between growth rate and delta prime. The dispersion relation then gets modified for moderate values of the electrical resistivity and of the tearing stability parameter, Δ'. The measure of resistivity is via the inverse of the Lundquist number which is the ratio of alfvenic time scale to the diffusive time scale.

The relation obtained above 2.10, in terms of the unnormalised growth rate, γ and η can be rewritten as

$$\gamma = \Delta'^{-4/5} \alpha_1^{-4/5} k^{-2/10} \eta^{-3/5} \tag{2.11}$$

Where, $\alpha_1 = 2.1$ and k is the perturbation mode number normalised to a macroscopic length.

Also, 2.11 can be written in terms of Δ'

$$\Delta' = \alpha_1 k^{1/2} \gamma^{5/4} \eta^{-3/4} \tag{2.12}$$

The above relation 2.11 is modified for high η and in a cylindrical geometry, obtained by Militello[34] and is the following,

$$\gamma = \frac{(\Delta' + \alpha_1 F\delta)\,\eta}{\alpha_1 \delta} \tag{2.13}$$

,

also,

$$\Delta' = \alpha_1 \gamma\delta/\eta + \alpha_1 F\delta \tag{2.14}$$

where,

$$\alpha_1 = 2.1, \gamma = growth\ rate, \delta = \left(\frac{\gamma\eta}{k_c^2}\right)^{\frac{1}{4}}$$

$$F = [(aA/2) + a^2 log(\delta) - a^2(\alpha_2 + \pi)/\alpha_1 + b]$$

and,

$$a = \left(-\frac{m}{r_s}\frac{dJ_{eq}}{dr} \bigg/ \frac{n}{R}\frac{q'_{eq}}{q_{eq}}\right) \tag{2.15}$$

,

$$b = \left[a\left(\frac{q''_{eq}n}{2q_{eq}R}\right) - \frac{d}{dr}\left(\frac{m}{r}\frac{dJ_{eq}}{dr}\right)\right] \bigg/ \frac{n}{R}\frac{q'_{eq}}{q_{eq}}\Bigg) \tag{2.16}$$

The above relation 2.13 extends the result obtained in slab geometry to a cylindrical geometry, and is important in the case of low S, or high η. We have obtained this behaviour in our results shown in the subsequent chapters.

3

CUTIE code and its implementation

In this chapter, we will describe the CUTIE code[35, 36], its background and its implementation in IPR. To begin with, CUTIE stands for Culham Transporter of Ions and Electrons. It was conceived as plasma fluid initial value code, and has the following attributes. It is nonlinear, global, electromagnetic, quasi neutral i.e, $n_e \approx n_i$, and very importantly has been used for profile turbulence interaction studies in the past.

In our description, we would like to clarify the geometry and scale in which we solve our equations, before proceeding to a description of the fundamental equations of CUTIE. This will be followed by a description of the implementation of CUTIE in IPR for our studies. The geometry we employ in CUTIE is a periodic cylinder geometry. This is topologically equivalent to a torus but without the curvature. In the code, the curvature effect is taken care of by introducing the toroidal coupling effect externally[37]. However, in the case of a single mode study, such coupling is not necessary. In this geometry, magnetic flux surfaces are concentric cylinders. This geometry is used as an approximation for large aspect ratio tokamaks, i.e., the aspect ratio, $R/a \gg 1$, where R is the major radius of the tokamak and a is the minor radius of the tokamak. We solve our equations on the “mesoscale”, which is defined as an intermediate scale between the device size and the ion gyroradius. We incorporate approximations for the underlying transport effects. Kinetic effects have been neglected, except for some classical and neoclassical transport coefficients[38]. We operate on scales much larger than the ion gyroradius therefore the fluid approximation is valid in our studies.

In our studies, we treat plasma fields in the following manner. We split the fields into mean and fluctuating fields, denoted by the subscript 0 and δ respectively. The mean quantities are averaged over each flux surface as shown

$$n_0(r;t) = \frac{1}{4\pi^2}\int_0^{2\pi}\int_0^{2\pi} n(r,\theta,\zeta;t)d\theta d\zeta \tag{3.1}$$

and the total quantities are shown below

$$n(r,\theta,\zeta;t) = n_0(r,t) + \delta n(r,\theta,\zeta;t) \tag{3.2}$$

The mean quantities have a spatial dependence only on r, and evolve slowly with time. The fluctuating quantities on the other hand vary over all spatial coordinates and evolve much faster with time. These fields interact with each other in a self-consistent manner.

We evolve the following fields evolved in the CUTIE code, the magnetic field, $\mathbf{B}$, electrostatic potential, ϕ,and additionally in the two fluid case, density, n, plasma flow velocity, $\mathbf{v}$, and the ion and electron temperatures, T_i and T_e respectively. We have assumed that plasma flow velocity is well represented by the ion's velocity, $\mathbf{v_i}$, as ions are much heavier than electrons. The current density is given by,

$$\mathbf{J} = ne(\mathbf{v_i} - \mathbf{v_e}) \tag{3.3}$$

We have split the magnetic field as,

$$\mathbf{B} = \nabla\psi \times \mathbf{b_{tor}} + B_{tor}\mathbf{b_{tor}} \tag{3.4}$$

in terms of a scalar magnetic potential ψ and toroidal direction vector $\mathbf{b_{tor}}$. Due to the fact that mean fields only have a radial variation, we only have a mean poloidal field generated by this potential. The toroidal component is unaffected.

It can be mentioned here that CUTIE equations contain a lot of physics in themselves, in particular tearing modes, kink modes, ballooning modes, drift Alfvén among others. We will here restrict our attention to the kink and tearing modes. We have adapted the full CUTIE model to our studies. In this process we have neglected some physics present in the full model, for instance curvature, and the evolution of temperature in the system, which is held constant.

CUTIE model

We here present the governing equations of CUTIE [36]. Additionally, we note that these are non-relativistic equations. The equations are as follows:

- Ampère's law,

$$\nabla \times \mathbf{B} = \frac{4\pi}{c}\mathbf{J} \tag{3.5}$$

  Here, $\mathbf{B} = \nabla\psi \times \mathbf{b_t} + B_0\mathbf{b_t}$ where $\mathbf{b_t}$ the unit vector in the toroidal direction, ψ is the magnetic potential and B_0 the mean toroidal magnetic field strength. The current density is defined as $\mathbf{J} = ne(\mathbf{v_i} - \mathbf{v_e})$ for singly charged ions, where $\mathbf{v_i}$ and $\mathbf{v_e}$ are the ions and electron fluid velocities respectively.

- Continuity equation for particles,

$$\frac{\partial n}{\partial t} + \nabla \cdot (n\mathbf{v}) = S_p \tag{3.6}$$

  where density, $n = n_e \approx n_i$, plasma fluid velocity $\mathbf{v} = \frac{m_i\mathbf{v_i} + m_e\mathbf{v_e}}{m_i + m_e} \approx \mathbf{v_i}$ and the external particle source is S_p.

- The momentum equation is as follows,

$$m_i n \frac{d\mathbf{v}}{dt} = -\nabla p + \frac{1}{c}\mathbf{j} \times \mathbf{B} + \mathbf{F_{eff}} \tag{3.7}$$

  where $p = p_i + p_e = n(T_e + T_i)$ is the total pressure, and $\mathbf{F_{eff}}$ is the effective force on the plasma.

- Energy equations for ion and electron species,

$$\frac{3}{2}\frac{dp_{i,e}}{dt} + p_{\{i,e\}}\nabla \cdot \mathbf{v_{e,i}} = -\nabla \cdot \mathbf{q_{i,e}} + P_{i,e} \tag{3.8}$$

  where $\mathbf{q_{i,e}}$ are the respective heat flux vectors.

- Ohm's law

$$\mathrm{E} + \frac{1}{c}\mathbf{v_e} \times \mathbf{B} = -\frac{1}{en}\nabla p_e + \mathbf{R}_e \tag{3.9}$$

where R_e is the electron-ion friction force. The plasma fields **B**,**E**,**v**, n and $p_{i,e}$ are written as the sum of a flux surface averaged mean[35].

Fluctuating equations of Full CUTIE model

As described in the introduction, we use Fourier analysis to split the equations into 'mean' and 'fluctuating' components, where the mean parts are the (0,0) components in the fourier sum. Although in principle, the mean and fluctuating quantities need not be different in their relative size, in practice the fluctuating components are smaller than the mean quantities. In this section, we describe the full nonlinear fluctuating equations for the sake of completeness, they have been discussed in detail in earlier literature of CUTIE[35, 38]. Our numerical investigations have been carried out in the framework of a two fluid model in a periodic cylinder geometry (ρ, θ, z),(ρ being the radial coordinate, θ being the azimuthal coordinate, and z being the axial coordinate) defined in terms of the minor radius, a, and the major radius, R_0. Using normalised coordinates, we set $\rho = r/a$, r being the radial distance, namely $0 \leqslant \rho \leqslant 1; 0 \leqslant \theta, \zeta \leqslant 2\pi; \zeta = z/R_0$. The model utilises CGS electrostatic units. The equations in our model are as follows:

$$\tilde{W} = \rho_s^2 \nabla \cdot \left(\frac{n_0(\rho)}{n_0(0)} \nabla_\perp \tilde{\phi} \right) \tag{3.10}$$

$$\begin{aligned}
\frac{\partial \tilde{W}}{\partial t} + \mathbf{v_0} \cdot \nabla \tilde{W} + v_A \nabla_\parallel \rho_s^2 \nabla_\perp^2 \tilde{\psi} = \\
v_A \rho_s \frac{1}{r} \frac{\partial \tilde{\psi}}{\partial \theta} \frac{4\pi \rho_s}{c B_0} j_0' + v_{th} \rho_s \frac{1}{r} \frac{\partial \left(\tilde{\psi}, \rho_s^2 \nabla_\perp^2 \tilde{\psi} \right)}{\partial (r, \theta)} + \\
v_{th} \rho_s \left[\frac{1}{r} \frac{\partial \left(\tilde{W}, \tilde{\phi} \right)}{\partial (r, \theta)} + \left(\frac{n_0(0) T_{i0}}{n_0 T^*} \right) \frac{1}{r} \frac{\partial \left(\tilde{W}, \tilde{n} \right)}{\partial (r, \theta)} \right] - \\
\frac{2 v_{th} \rho_s}{R_0} \left[\frac{\cos\theta}{r} \frac{\partial \tilde{p}}{\partial \theta} + \sin\theta \frac{\partial \tilde{p}}{\partial r} \right] + \frac{\rho_s^2 W_0'}{r} \frac{\partial \tilde{\phi}}{\partial \theta} + \nu \nabla_\perp^2 \tilde{W}
\end{aligned} \tag{3.11}$$

$$\frac{\partial\tilde{\psi}}{\partial t}+\mathbf{v_{e0}}\cdot\nabla\tilde{\psi}+v_A\nabla_{\parallel}\tilde{\phi}=v_A\left(\frac{n_0(0)T_{e0}}{n_0T^*}\right)\nabla_{\parallel}n^*+$$
$$\frac{v_{th}\rho_s}{r}\left[\frac{1}{r}\frac{\partial\left(\tilde{\psi},\tilde{\phi}\right)}{\partial(r,\theta)}+\left(\frac{n_0(0)T_{e0}}{n_0T^*}\right)\frac{1}{r}\frac{\partial\left(\tilde{\psi},\tilde{n}\right)}{\partial(r,\theta)}\right]+\frac{c^2\eta}{4\pi}\nabla_{\perp}^2\tilde{\psi}\quad(3.12)$$

$$\frac{\partial\tilde{n}}{\partial t}+\mathbf{u_{e0}}\cdot\nabla\tilde{n}+v_A\nabla_{\parallel}\rho_s^2\nabla_{\perp}^2\tilde{\psi}=$$
$$v_rho_s\frac{1}{r}\frac{\partial\tilde{\psi}}{\partial\theta}\frac{4\pi\rho_s}{cB_0}j_0^{'}+v_{th}\rho_s\frac{1}{r}\frac{\partial\left(\tilde{\psi},\rho_s^2\nabla_{\perp}^2\tilde{\psi}\right)}{\partial(r,\theta)}+$$
$$v_{th}\rho_s\frac{1}{r}\frac{\partial\left(\tilde{n},\tilde{\phi}\right)}{\partial(r,\theta)}+$$
$$v_{th}\rho_s\left(\frac{n_0^{'}}{N^*}\right)\frac{1}{r}\frac{\partial\tilde{\phi}}{\partial\theta}-\frac{2v_{th}\rho_s}{R_0}\left[\frac{\cos\theta}{r}\frac{\partial\tilde{p}}{\partial\theta}+\sin\theta\frac{\partial\tilde{p}}{\partial r}\right]-$$
$$v_{th}\nabla_{\parallel}\tilde{\xi}+D\nabla_{\perp}^2n^*\quad(3.13)$$

$$\frac{\partial\tilde{\xi}}{\partial t}+\mathbf{u_0}\cdot\nabla\tilde{\xi}+v_{th}\left(\frac{T_{e0}+T_{i0}}{T^*}\right)\nabla_{\parallel}n^*=$$
$$\left(\frac{n_0(r)v_{\parallel 0}^{'}}{n_0(0)}\right)\rho_s\frac{1}{r}\frac{\partial\tilde{\phi}}{\partial\theta}+v_{th}\rho_s\frac{1}{r}\frac{\partial\left(\tilde{\xi},\tilde{\phi}\right)}{\partial(r,\theta)}-$$
$$v_{th}\rho_s\beta^{1/2}\left(\frac{p_0^{'}}{P^*}\right)\frac{1}{r}\frac{\partial\tilde{\psi}}{\partial\theta}-v_{th}\rho_s\beta^{1/2}\frac{1}{r}\frac{\partial\left(\tilde{p},\tilde{\phi}\right)}{\partial(r,\theta)}-$$
$$v_{th}\left(\frac{n_0}{N^*}\right)\nabla_{\parallel}\left(\lambda_i^*+\lambda_e^*\right)+\chi\nabla_{\perp}^2\xi^*\quad(3.14)$$

Equation[3.10] is the Poisson relation for our system. Equation[3.11] is the vorticity equation, where $\tilde{W}$ is the perturbed vorticity. Equation[3.12] describes the evolution of the perturbed poloidal flux function $\tilde{\psi}$. Equation [3.13] describes density evolution and equation [3.14] describes the evolution of parallel momentum. Here, $\mathbf{u_0}=-\frac{cE_{r0}}{B}\mathbf{e}_\theta+\mathbf{b_0}v_{\parallel 0}$ is the equilibrium 'MHD' flow, and $\mathbf{u_{e0}}=-\frac{cE_{r0}}{B}\mathbf{e}_\theta+\mathbf{b_0}\left(v_{\parallel 0}-j_{\parallel 0}/en_0\right)$ is the corresponding electron flow. The ion flow alone is given by $\mathbf{v_0}=\mathbf{u_0}+\frac{c}{en_0B}\frac{\partial p_{io}}{\partial r}\mathbf{e}_\theta$, and $\mathbf{v_{e0}} = -\left[\frac{cE_{r0}}{B} + \frac{c}{en_0B}\frac{\partial p_{e0}}{\partial r}\right]\mathbf{e}_\theta$ is the total electron poloidal flow composed of the electron $\mathbf{E}\times\mathbf{B}$ equilibrium flow and the electron diamagnetic flow. The resistivity η and viscosity ν are specified quantities and are held constant during our calculations. Additionally, $\rho_s = \frac{v_{th}}{\omega_{ci}}$, where, $v_{th}^2 = (T_{0i}+T_{0e})/m_i$, $\omega_{ci} = (eB_0/m_ic)$, with T_{0i}, T_{0e} being ion and electron temperatures respectively. m_i is the ion mass, e is the elementary charge. $\Phi_0(r), \Psi_0(r)$ denote the mean electrostatic and magnetostatic potentials respectively.

Also, we have used fixed boundary conditions, along with a conducting boundary.

This comes from

$$\frac{\delta\mathbf{E}}{B_0} = -\nabla\tilde{\phi} - \frac{1}{c}\frac{\partial\tilde{\phi}}{\partial t}\mathbf{e}_\zeta$$

where, $\mathbf{E}$ is the electric field, ϕ is the electrostatic potential, and $\mathbf{B_0} \simeq B_{0z}\mathbf{e}_\zeta + B_{0\theta}(\rho)\mathbf{e}_\theta$ is the equilibrium field. The fluctuating electric field, δE, is related to $\tilde{\phi}$ [this has dimensions of length]. We use, $\varepsilon = a/R_0$, the inverse aspect ratio, $v_0 = V_{0z}(\rho)\,\mathbf{e}_\zeta + a\rho\Omega(\rho)\,\mathbf{e}_\theta$. The equilibrium axial and poloidal, sub-Alfvénic sheared flows are: $M_z = V_{0z}/v_A$ is the Axial Mach number; $M_\theta(\rho) = \rho\,\Omega\,(1-\rho)^2$ is the poloidal Mach number; $\tau_A = a/v_A$ the Alfvén time; $\tau_\eta = (4\pi a^2/c^2\eta)$ the resistive time; $\tau_\nu = (a^2/\nu)$ the viscous time. We will use in the following the *Lundquist Number*, $S = \frac{\tau_\eta}{\tau_A}$, and the *Prandtl Number*, $Pr = \frac{\tau_\eta}{\tau_\nu}$. We use an equilibrium electron density profile of the form $n_e = n_{0e}exp\{-\alpha * \rho^2\}$. $\alpha = \frac{dn}{dr}$, the electron density gradient of the plasma.

The velocity perturbations are non-dimensionalised relative to the Alfven speed, $v_A = \frac{B_0}{(4\pi m_i n_0)^{1/2}}$. The magnetic field perturbations are normalised by the equilibrium axial magnetic field B_{0z}. The fluctuations of magnetic field and velocity are incompressible in the $(r-\theta)$ plane.

Together, these equations constitute the four field model we use and we solve them using the CUTIE (**CU**lham **T**ransporter of **I**ons and **E**lectrons) code [35, 39], a nonlinear, global, electromagnetic, quasi-neutral, two fluid initial value code. It has been used earlier for studies of kink modes, tearing modes, ELMs, L to H transitions, internal transport barriers and other problems [35, 36, 39–41].

Reduced visco-resistive MHD equations(RMHD model)

In this section, we describe the RMHD model, a reduced description we have employed to study the kink and tearing modes. It is derived from the full model described in the previous section. They are given as follows: The periodic cylinder geometry is defined in terms of a, the minor radius and R_0 the major radius. We set, $\rho = r/a$ and we use the non-dimensional coordinates, $0 \leqslant \rho \leqslant 1; 0 \leqslant \theta, \zeta \leqslant 2\pi; \zeta = z/R_0$. The fluctuating electric field, $\delta\mathbf{E}$, is related to the fluctuating potentials $\widetilde{\psi}\widetilde{\phi}$ (these have dimensions of length in Gaussian CGS units which are used throughout this paper) according to, $\frac{\delta\mathbf{E}}{B_0} = -\nabla\widetilde{\phi} - \frac{1}{c}\frac{\partial\widetilde{\phi}}{\partial t}\mathbf{e}_\zeta$, where, $B_0 \simeq B_{0z}$ is the equilibrium field. Furthermore, we have the following expressions (obtained from the definitions of the various quantities and $\nabla z \equiv \mathbf{e}_\zeta$) relating these potential perturbations to the (non-dimensional) velocity and magnetic and field perturbations:

$$-\left(\frac{c}{v_A}\right)\nabla\widetilde{\phi} \times \mathbf{e}_\zeta = \tilde{\mathbf{v}}_* = v_{*r}\mathbf{e}_r + v_{*\theta}\mathbf{e}_\theta = \left(\frac{c}{v_A}\right)\left[-\frac{1}{r}\frac{\partial\widetilde{\phi}}{\partial\theta}, \frac{\partial\widetilde{\phi}}{\partial r}\right] \tag{3.15}$$

$$\nabla\widetilde{\psi} \times \mathbf{e}_\zeta = \frac{\tilde{\mathbf{B}}}{B_0} = \frac{\tilde{B}_r}{B_0}\mathbf{e}_r + \frac{\tilde{B}_\theta}{B_0}\mathbf{e}_\theta = \left[\frac{1}{r}\frac{\partial\widetilde{\psi}}{\partial\theta}, \frac{\partial\widetilde{\psi}}{\partial r}\right] \tag{3.16}$$

Thus, we velocity perturbations are non-dimensionalized relative to the Alfven speed, $v_a = \frac{B_0}{(4\pi m_i n_0)^{1/2}}$. The magnetic field perturbations are typical of 'shear-Alfven' perturbations and are normalized by the equilibrium axial/toroidal field[NB:$B_{0z} \simeq B_0$ in the present model]. The fluctuations of the magnetic field and velocity are incompressible in the $'r-\theta'$- plane. The corresponding 'mean' quantities are assumed constant in time and are denoted by, $\Phi_0(r), \Psi_0(r)$.

The reduced visco-resistive magnetohydrodynamic(RMHD) equations are then written (in CGS units for intuitive clarity) as

$$\begin{aligned}\frac{\partial\tilde{W}}{\partial t} + \mathbf{v_0}\cdot\nabla\tilde{W} + v_A\nabla_\parallel\rho_s^2\nabla_\perp^2\tilde{\psi} = v_A\rho_s\frac{1}{r}\frac{\partial\tilde{\psi}}{\partial\theta}\frac{4\pi\rho_s}{cB_0}j_0' + \frac{v_{th}\rho_s}{r}\left\{\tilde{\psi}, \rho_s^2\nabla_\perp^2\tilde{\psi}\right\} \\ + \frac{v_{th}\rho_s}{r}\left\{\tilde{W}, \tilde{\phi}\right\} + \frac{\rho_s^2 W_0'}{r}\frac{\partial\tilde{\phi}}{\partial\theta} + \nu\nabla_\perp^2\tilde{W}\end{aligned} \tag{3.17}$$

$$\frac{\partial\tilde{\psi}}{\partial t} + \mathbf{v_{e0}}\cdot\nabla\tilde{\psi} + v_A\nabla_\parallel\tilde{\phi} = \frac{v_{th}\rho_s}{r}\left\{\tilde{\psi}, \tilde{\phi}\right\} + \frac{c^2\eta}{4\pi}\nabla_\perp^2\tilde{\psi} \tag{3.18}$$

where, $\tilde{W} = \rho_s^2 \nabla \cdot \left(\frac{n_0}{n_0(0)} \nabla_\perp \tilde{\phi} \right)$. Here, $\{F, G\} \equiv \frac{\partial(F,G)}{\partial(r,\theta)}$, for any pair of functions, F, G. Note that, $\nabla_\perp^2 = \frac{1}{r}\frac{\partial}{\partial r}\left(r \frac{\partial}{\partial r} \right) + \frac{1}{r^2}\frac{\partial^2}{\partial \theta^2}$ and n_0 is mean density. The resistivity η and the viscosity ν are specified quantities, held constant during the calculations. Note that, $\rho_S = \frac{v_{th}}{\omega_{ci}}; v_{th}^2 = (T_{0i} + T_{0e})/m_i; \omega_{ci} = (eB_0/m_i c)$. We repeat from the earlier section, that, here, $\mathbf{u_0} = -\frac{cE_{r0}}{B}\mathbf{e}_\theta + \mathbf{b_0} v_{\parallel 0}$ is the equilibrium 'MHD' flow, and $\mathbf{u_{e0}} = -\frac{cE_{r0}}{B}\mathbf{e}_\theta + \mathbf{b_0}\left(v_{\parallel 0} - j_{\parallel 0}/en_0 \right)$ is the corresponding electron flow. The ion flow alone is given by $\mathbf{v_0} = \mathbf{u_0} + \frac{c}{en_0 B}\frac{\partial p_{io}}{\partial r}\mathbf{e}_\theta$, and $\mathbf{v_{e0}} = -\left[\frac{cE_{r0}}{B} + \frac{c}{en_0 B}\frac{\partial p_{e0}}{\partial r} \right]\mathbf{e}_\theta$ is the total electron poloidal flow composed of the electron $\mathbf{E} \times \mathbf{B}$ equilibrium flow and the electron diamagnetic flow.

Two fluid model used for simulations

In this section, we describe the two fluid model used by us for our two fluid simulations. It is a subset of the full CUTIE model stated earlier.

$$\tilde{W} = \rho_s^2 \nabla \cdot \left(\frac{n_0(\rho)}{n_0(0)} \nabla_\perp \tilde{\phi} \right) \tag{3.19}$$

$$\begin{aligned}
\frac{\partial \tilde{W}}{\partial t} + \mathbf{v_0} \cdot \nabla \tilde{W} + v_A \nabla_\parallel \rho_s^2 \nabla_\perp^2 \tilde{\psi} = \\
v_A \rho_s \frac{1}{r}\frac{\partial \tilde{\psi}}{\partial \theta}\frac{4\pi\rho_s}{cB_0} j_0^{\prime} + v_{th}\rho_s \frac{1}{r}\frac{\partial\left(\tilde{\psi}, \rho_s^2 \nabla_\perp^2 \tilde{\psi}\right)}{\partial(r,\theta)} + \\
v_{th}\rho_s \left[\frac{1}{r}\frac{\partial\left(\tilde{W},\tilde{\phi}\right)}{\partial(r,\theta)} + \left(\frac{n_0(0)}{2n_0} \right) \frac{1}{r}\frac{\partial\left(\tilde{W},\tilde{n}\right)}{\partial(r,\theta)} \right] - \\
\frac{\rho_s^2 W_0^{\prime}}{r}\frac{\partial \tilde{\phi}}{\partial \theta} + \nu \nabla_\perp^2 \tilde{W}
\end{aligned} \tag{3.20}$$

$$\begin{aligned}
\frac{\partial \tilde{\psi}}{\partial t} + \mathbf{v_{e0}} \cdot \nabla \tilde{\psi} + v_A \nabla_\parallel \tilde{\phi} = v_A \left(\frac{n_0(0)\, T_{e0}}{n_0 T^*} \right) \nabla_\parallel n^* + \\
\frac{v_{th}\rho_s}{r}\left[\frac{1}{r}\frac{\partial\left(\tilde{\psi},\tilde{\phi}\right)}{\partial(r,\theta)} + \left(\frac{n_0(0)}{2n_0} \right) \frac{1}{r}\frac{\partial\left(\tilde{\psi},\tilde{n}\right)}{\partial(r,\theta)} \right] + \frac{c^2\eta}{4\pi}\nabla_\perp^2 \tilde{\psi}
\end{aligned} \tag{3.21}$$

$$\frac{\partial \tilde{n}}{\partial t}+\mathbf{u_{e0}}\cdot\nabla\tilde{n}+v_A\nabla_{\parallel}\rho_s^2\nabla_{\perp}^2\tilde{\psi}=$$
$$v_{\rho s}\frac{1}{r}\frac{\partial\tilde{\psi}}{\partial\theta}\frac{4\pi\rho_s}{cB_0}j_0^{'}+v_{th}\rho_s\frac{1}{r}\frac{\partial\left(\tilde{\psi},\rho_s^2\nabla_{\perp}^2\tilde{\psi}\right)}{\partial\left(r,\theta\right)}+$$
$$v_{th}\rho_s\frac{1}{r}\frac{\partial\left(\tilde{n},\tilde{\phi}\right)}{\partial\left(r,\theta\right)}+$$
$$v_{th}\rho_s\left(\frac{n_0^{'}}{N^*}\right)\frac{1}{r}\frac{\partial\tilde{\phi}}{\partial\theta}-$$
$$v_{th}\nabla_{\parallel}\tilde{\xi}+D\nabla_{\perp}^2 n^* \tag{3.22}$$

$$\frac{\partial\tilde{\xi}}{\partial t}+\mathbf{u_0}\cdot\nabla\tilde{\xi}+v_{th}\nabla_{\parallel}\tilde{n}=$$
$$\left(\frac{n_0(r)v_{\parallel 0}^{'}}{n_0(0)}\right)\rho_s\frac{1}{r}\frac{\partial\tilde{\phi}}{\partial\theta}+v_{th}\rho_s\frac{1}{r}\frac{\partial\left(\tilde{\xi},\tilde{\phi}\right)}{\partial\left(r,\theta\right)}-$$
$$v_{th}\rho_s\beta^{1/2}\left(\frac{p_0^{'}}{P^*}\right)\frac{1}{r}\frac{\partial\tilde{\psi}}{\partial\theta}-v_{th}\rho_s\beta^{1/2}\frac{1}{r}\frac{\partial\left(\tilde{p},\tilde{\phi}\right)}{\partial\left(r,\theta\right)}-$$
$$v_{th}\left(\frac{n_0}{N^*}\right)+\chi\nabla_{\perp}^2\tilde{\xi} \tag{3.23}$$

Equation[3.19] is the Poisson relation for our system. Equation[3.20] is the vorticity equation, where $\tilde{W}$ is the perturbed vorticity. Equation[3.21] describes the evolution of the perturbed poloidal flux function $\tilde{\psi}$. Equation [3.22] describes density evolution and equation [3.23] describes the evolution of parallel momentum. Here, $\mathbf{u_0} = -\frac{cE_{r0}}{B}\mathbf{e}_\theta+\mathbf{b_0}v_{\parallel 0}$ is the equilibrium 'MHD' flow, and $\mathbf{u_{e0}} = -\frac{cE_{r0}}{B}\mathbf{e}_\theta+\mathbf{b_0}\left(v_{\parallel 0}-j_{\parallel 0}/en_0\right)$ is the corresponding electron flow. The ion flow alone is given by $\mathbf{v_0}=\mathbf{u_0}+\frac{c}{en_0B}T\frac{\partial n_{io}}{\partial r}\mathbf{e}_\theta$, here due to quasi-neutrality $n_{i0}\sim n_{e0}$ and $\mathbf{v_{e0}}=-\left[\frac{cE_{r0}}{B}+\frac{c}{en_0B}T\frac{\partial n_{e0}}{\partial r}\right]\mathbf{e}_\theta$ is the total electron poloidal flow composed of the electron $\mathbf{E}\times\mathbf{B}$ equilibrium flow and the electron diamagnetic flow. Also, we have $N^*=n_e\left(0,t\right)$, $T^*=T_e\left(0,t\right)+T_i\left(0,t\right)$, $\tilde{\xi}=N^*V_{TH}$. The resistivity η and viscosity ν are specified quantities and are held constant during our calculations. In particular, we use the self-consistent formulation whereby $\eta(r)\text{æ}_{0z}(r)\equiv E_{0z}\equiv\frac{V_{loop}}{2\pi R_0}$, where the specified q profile and B_0 are used to get j_{0z} initial profile. After this, we hold the profile and the value of $\eta(0)$ fixed throughout both linear and nonlinear calculations. We also have, $D_{res} = \frac{c^2\eta(r)}{4\pi}$,$\nu \equiv D_{visc} \equiv Pr.D_{res}$, therefore,

$$Pr \equiv \frac{D_{visc}}{D_{res}} \tag{3.24}$$

is the Prandtl number, which we have introduced earlier. We can therefore we see that kinematic viscosity ν and η share the same radial profile and are invariant in time.

This comes from

$$\frac{\delta \mathbf{E}}{B_0} = -\nabla\tilde{\phi} - \frac{1}{c}\frac{\partial\tilde{\phi}}{\partial t}\mathbf{e}_\zeta$$

where, $\mathbf{E}$ is the electric field, ϕ is the electrostatic potential, and $\mathbf{B_0} \simeq B_{0z}\mathbf{e}_\zeta + B_{0\theta}(\rho)\mathbf{e}_\theta$ is the equilibrium field. The fluctuating electric field, δE, is related to $\tilde{\phi}$ [this has dimensions of length]. We use, $\varepsilon = a/R_0$, the inverse aspect ratio, $v_0 = V_{0z}(\rho)\,\mathbf{e}_\zeta + a\rho\Omega(\rho)\,\mathbf{e}_\theta$. For clarity, we restate that, here, $\mathbf{u_0} = -\frac{cE_{r0}}{B}\mathbf{e}_\theta + \mathbf{b_0}v_{\|0}$ is the equilibrium 'MHD' flow, and $\mathbf{u_{e0}} = -\frac{cE_{r0}}{B}\mathbf{e}_\theta + \mathbf{b_0}\left(v_{\|0} - j_{\|0}/en_0\right)$ is the corresponding electron flow. The ion flow alone is given by $\mathbf{v_0} = \mathbf{u_0} + \frac{c}{en_0 B}\frac{\partial p_{io}}{\partial r}\mathbf{e}_\theta$, and $\mathbf{v_{e0}} = -\left[\frac{cE_{r0}}{B} + \frac{c}{en_0 B}\frac{\partial p_{e0}}{\partial r}\right]\mathbf{e}_\theta$ is the total electron poloidal flow composed of the electron $\mathbf{E}\times\mathbf{B}$ equilibrium flow and the electron diamagnetic flow.

The magnetic field perturbations are normalised by the equilibrium axial magnetic field B_{0z}. The fluctuations of magnetic field and velocity are incompressible in the $(r-\theta)$ plane. The temperatures are measured in energy units, i.e, electron volts. Also, we have used fixed boundary conditions, along with a conducting boundary, which means that all the variables are zero at $\rho = 1$. Additionally, regularity considerations mean that at $\rho = 0$, the fluctuations approach zero, and we have set the plasma edge at $\rho = 0.95$. We have used the Fourier representation for the purpose of periodicity of the angular coordinates.

Together, these equations constitute the four field model we use and we solve them using the CUTIE (**CU**lham **T**ransporter of **I**ons and **E**lectrons) code [35, 39], a nonlinear, global, electromagnetic, quasi-neutral, two fluid initial value code. It has been used earlier for studies of kink modes, tearing modes, ELMs, L to H transitions, internal transport barriers and other problems [35, 36, 39–41].

Method of solution

The CUTIE code has two versions, as follows,

- Evolutionary code: In this version, the physical quantities in the equation are evolved with time. Both linear and nonlinear calculations are carried out in this version.
- Resolvent code: In this version, we solve for the eigenvalue of the equations. By its nature, it is a linear code.

The two versions of the code solve the same linear equations, and thus agree for linear calculations. The slight difference as mentioned is due to the approach we employ in solving the equations, as nonlinear time dependent calculations can only be done by evolving our equations with time.

In the evolutionary code, we use the TDMA(Tri diagonal matrix)[35] method to solve the equations. This method involves reformulating the coefficient matrix of the equation in the form of a tridiagonal, and solving for the quantities thus involved by using the procedure of gaussian elimination to arrive at the final answer. In the case of the resolvent code[39], we look for the response of the quantity $1/(A-\lambda I)$ where the original equation is of the form $Ax = \lambda x$.

CUTIE implementation

The CUTIE code as used for our studies has undergone development according to our needs. CUTIE code was originally an initial value code, evolving in time. A linear eigenvalue solver version of CUTIE has been developed[39] and it is termed as the resolvent code. In the linear regime, when we can ignore the nonlinear terms, it is full agreement with the initial value code, as only the method of solution is different, with the physics kept the same. In addition, it is also able to give us a number of other eigenvalues, which we could not see in the initial value code, as it only picks up the fastest growing eigenmode. Therefore, the resolvent code is useful both as a check on the linear results we obtain from the initial value code, and also revealing to us the eigenspectrum of a particular mode. The CUTIE code is of two types in our usage, one is a Reduced MHD code, which uses single fluid equations only, and the other which uses the full nonlinear CUTIE equations. There are corresponding resolvent versions of the CUTIE code, namely a single fluid and two fluid code. However, an important difference is that the resolvent is essentially a linear code, and also it is able to reveal the eigenspectrum of a mode, which the evolutionary version does not, as it evolves only the fastest growing modes.

In our implementation, I have noticed that CUTIE is a code which is highly customisable in terms of the parameters it employs. We have changed some of the default for the running CUTIE, CUTIE gives us the ability to change a large number of parameters like density profile, resistivity profile etc. We have first studied the tearing mode using the CUTIE code. Subsequently, we were able to study other other modes like the kink mode using the CUTIE code.

4

Studies of (2,1) Tearing modes

The work described in this chapter has been published in the paper [39]. We describe in detail our studied on the effect of flow on the (2,1) tearing modes in a tokamak.

Introduction

Neoclassical tearing modes (NTMs) pose a serious threat to the operation of long pulse tokamak devices like ITER as they can severely degrade plasma confinement and thus prevent the achievement of high values of β (where β is the ratio of plasma pressure to magnetic field pressure). A great deal of theoretical and experimental effort is being devoted to exploring various means of controlling this instability either directly by use of localized radio frequency current drive/heating or indirectly by preventing the occurrence of seed magnetic islands that can act as triggers for NTMs. Recent experimental observations from some tokamaks indicate that equilibrium sheared-toroidal flows have a beneficial influence on NTMs. More specifically, an increase in the equilibrium flow [with shear] leads to an increase of the NTM excitation threshold and also decreases the size of the saturated island [42, 43]. A sound theoretical understanding of these experimental observations is still lacking and a proper identification of the underlying physical mechanisms would greatly facilitate development of additional strategies for the control of NTMs. Our present work is motivated by such a consideration.

Equilibrium flows can influence the stability of tearing modes through a variety of physical effects arising from the dynamical characteristics of the plasma as well as the confinement geometry, as studied extensively in the past [12, 44]. To understand and assess systematically the roles played by these effects, we have carried out a series of numerical and analytic studies on the stability of the $(2,1)$ tearing mode, using a number of model systems that progressively incorporate various effects of changes in geometry and more detailed physics. We begin, in section 4.5, with a simple reduced MHD description of the plasma in a cylindrical geometry and present a series of numerical computation results carried out with the code CUTIE [45]. The cases include purely axial sheared flows, purely poloidal sheared flows and helical flows that are a combination of the axial and poloidal flows leading to different flow helicities. In section 4.6, we present CUTIE simulations using a two fluid model and discuss the differences observed from the single fluid simulations. Section 4.3 contains a discussion of a new and powerful technique (called the "resolvent method") for obtaining the full eigen-spectrum that is applicable to non-self-adjoint problems. The growth rate and real frequencies obtained through the use of this method confirm and further validate our results from the CUTIE code. In section 4.7 we examine the equilibrium modifications arising in a toroidal geometry due to the presence of toroidal flows and their impact on the stability of the $(2,1)$ mode. The numerical results were obtained using the codes NEAR (stability) and TOQ (equilibrium) [46–48] and the stabilizing influence of the flow induced shift in the current profile is analytically estimated from an approximate calculation of the Δ' parameter and the saturated island size W. A brief summary of our results and a discussion on future directions of research are provided in section 4.8.

Model equations

We repeat the details of the model equations for convenience.They have been used in our study are described in several publications [45–48]. In the following, the periodic cylinder geometry is defined in terms of a, the minor radius and R_0 the major radius. We set, $\rho = r/a$ and we use the non-dimensional coordinates, $0 \leqslant \rho \leqslant 1; 0 \leqslant \theta, \zeta \leqslant 2\pi; \zeta = z/R_0$. The fluctuating electric field, $\delta\mathbf{E}$, is related to the fluctuating potentials $\widetilde{\psi}\widetilde{\phi}$ (these have dimensions of length in Gaussian CGS units which are used throughout this thesis) according to, $\frac{\delta\mathbf{E}}{B_0} = -\nabla\widetilde{\phi} - \frac{1}{c}\frac{\partial\widetilde{\phi}}{\partial t}\mathbf{e}_\zeta$, where, $B_0 \simeq B_{0z}$ is the equilibrium field. Furthermore, we have the following expressions (obtained from the definitions of the various quantities and $\nabla z \equiv \mathbf{e}_\zeta$) relating these potential perturbations to the (non-dimensional) velocity and magnetic and field perturbations:

$$-\left(\frac{c}{v_A}\right)\nabla\tilde{\phi}\times\mathbf{e}_\zeta=\tilde{\mathbf{v}}_*=v_{*r}\mathbf{e}_r+v_{*\theta}\mathbf{e}_\theta=\left(\frac{c}{v_A}\right)\left\{-\frac{1}{r}\frac{\partial\widetilde{\phi}}{\partial\theta},\frac{\partial\widetilde{\phi}}{\partial r}\right\} \tag{4.1}$$

$$\nabla\tilde{\psi}\times\mathbf{e}_\zeta=\frac{\tilde{\mathbf{B}}}{B_0}=\frac{\tilde{B}_r}{B_0}\mathbf{e}_r+\frac{\tilde{B}_\theta}{B_0}\mathbf{e}_\theta=\left\{\frac{1}{r}\frac{\partial\widetilde{\psi}}{\partial\theta},\frac{\partial\widetilde{\psi}}{\partial r}\right\} \tag{4.2}$$

Here, $\{F,G\}\equiv\frac{\partial(F,G)}{\partial(r,\theta)}$, for any pair of functions, F, G. Thus, the velocity perturbations are non-dimensionalized relative to the Alfven speed, $v_a=\frac{B_0}{(4\pi m_i n_0)^{1/2}}$. The magnetic field perturbations are typical of 'shear-Alfven' perturbations and are normalized by the equilibrium axial/toroidal field[NB:$B_{0z}\simeq B_0$ in the present model]. The fluctuations of the magnetic field and velocity are incompressible in the $'r-\theta'$- plane. The corresponding 'mean' quantities are assumed constant in time and are denoted by, $\Phi_0(r),\Psi_0(r)$.

The reduced visco-resistive magnetohydrodynamic(RMHD) equations are then written (in CGS units for intuitive clarity) as

$$\begin{aligned}\frac{\partial\tilde{W}}{\partial t}+\mathbf{v_0}\cdot\nabla\tilde{W}+v_A\nabla_\parallel\rho_s^2\nabla_\perp^2\tilde{\psi}=v_A\rho_s\frac{1}{r}\frac{\partial\tilde{\psi}}{\partial\theta}\frac{4\pi\rho_s}{cB_0}j_0'+\frac{v_{th}\rho_s}{r}\left\{\tilde{\psi},\rho_s^2\nabla_\perp^2\tilde{\psi}\right\}\\+\frac{v_{th}\rho_s}{r}\left\{\tilde{W},\tilde{\phi}\right\}+\frac{\rho_s^2W_0'}{r}\frac{\partial\tilde{\phi}}{\partial\theta}+\nu\nabla_\perp^2\tilde{W}\end{aligned} \tag{4.3}$$

$$\frac{\partial\tilde{\psi}}{\partial t}+\mathbf{v_{e0}}\cdot\nabla\tilde{\psi}+v_A\nabla_\parallel\tilde{\phi}=\frac{v_{th}\rho_s}{r}\left\{\tilde{\psi},\tilde{\phi}\right\}+\frac{c^2\eta}{4\pi}\nabla_\perp^2\tilde{\psi} \tag{4.4}$$

where, $\tilde{W}=\rho_s^2\nabla\cdot\left(\frac{n_0}{n_0(0)}\nabla_\perp\tilde{\phi}\right)$. Note that, $\nabla_\perp^2=\frac{1}{r}\frac{\partial}{\partial r}\left(r\frac{\partial}{\partial r}\right)+\frac{1}{r^2}\frac{\partial^2}{\partial\theta^2}$ and n_0 is mean density. The resistivity η and the viscosity ν are specified quantities, held constant during the calculations. Note that, $\rho_S=\frac{v_{th}}{\omega_{ci}};v_{th}^2=(T_{0i}+T_{0e})/m_i;\omega_{ci}=(eB_0/m_ic)$.

Resolvent methods

Here we have used the 'resolvent method' of calculating the full eigen-spectrum, applicable to non-self-adjoint problems and have used it in conjunction with an initial value approach [49]. In this method, one essentially solves [using a suitably modified resolvent code derived from CUTIE] the inhomogeneous differential equations for the amplitudes of fluctuating quantities varying like $e^{\Gamma t}\hat{f}(r,m,n)$ for an assumed complex frequency $\Gamma = \gamma + i\omega_r$. This amounts to calculating the Green's function for the system as a function of the complex variable Γ. The poles of this solution are sought in the complex $\Gamma-$plane. The poles in the upper half plane correspond to unstable modes with real frequency given by ω_r and growth rate, γ, whereas those in the lower half plane correspond similarly to stable modes.
Let us consider the eigenvalues and eigenvectors of a matrix A which satisfy the following equation,

$$(A - \lambda I)\mathbf{x} = 0 \tag{4.5}$$

where I is the $n \times n$ identity matrix. In case of resolvent method, we solve the following system for the vector $\mathbf{x}^*$,

$$(A - \lambda^* I)\mathbf{x}^* = \mathbf{g} \tag{4.6}$$

where λ^* is the initial guess for the eigen value and $\mathbf{g}$ is some nonzero vector of same dimension of vector $\mathbf{x}^*$. Then the solution of the equation (4.6) is achieved using TDMA for given values of λ^* and $\mathbf{g}$. Now solving it for a range of λ^*, we can write a $D(\lambda^*) = \sum_{i=1}^{n} \frac{1}{x_i^*(\lambda^*)}$. As λ^* approaches the true eigenvalue λ then left hand side of the equation (4.6) will approach zero, so one or more elements of the solution vector $\mathbf{x}^*$ will tend to blow up. So $D(\lambda^*) = 0$ for $\lambda^* = \lambda$, eigenvalue of the system.
The method has been tested systematically in single and two fluid versions. The growth rates match the ones obtained with the "evolutionary method" perfectly. The two-fluid application of the method shows that the real frequency matches correctly with the electron drift frequency, $\omega_{*e} = \frac{T_e}{eB_0}(\frac{m}{r})[\frac{1}{n_e}\frac{dn_e}{dr}]; n_e \sim e^{-k_*(r/a)^2}$. Further details and many examples of this method can be found in the PhD thesis of J. Douglas [50]. The resolvent technique is very much more efficient in obtaining the eigenvalues and the eigenfunctions than the evolutionary method and gives accurate eigenfunctions for any given discretization.

Benchmarking of CUTIE in visco-resistive regime

The simulations have been carried out in a reduced version of the CUTIE (CUlham Transporter of Ions and Electrons) code. CUTIE is a nonlinear, global, electromagnetic, quasi neutral, two fluid initial value code that has been sucessfully used in the past to gain insight into a number of experimental phenomena in tokamaks, such as the formation of internal transport barriers, L to H transitions, formation of ELMs, sawteeth oscillations etc. However, a comprehensive linear benchmarking (some results are documented in [[45] ,[50]] of tearing mode simulations using the CUTIE code for wide ranges of resistivity and viscosity are incomplete. Such benchmarking is important becuase there are different existing theories of tearing modes that predict distinct behaviour of the modes for different viscous and resistive regimes. The benchmarking results are presented in the figures Fig. 4.1, Fig. 4.2, Fig. 4.3 and Fig. 4.4.

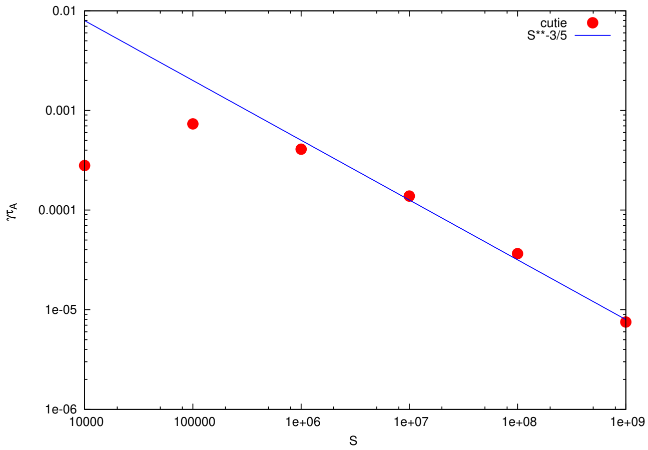

Figure 4.1: Linear growth rate vs Lundquist number of the (2,1) mode in low viscosity regime

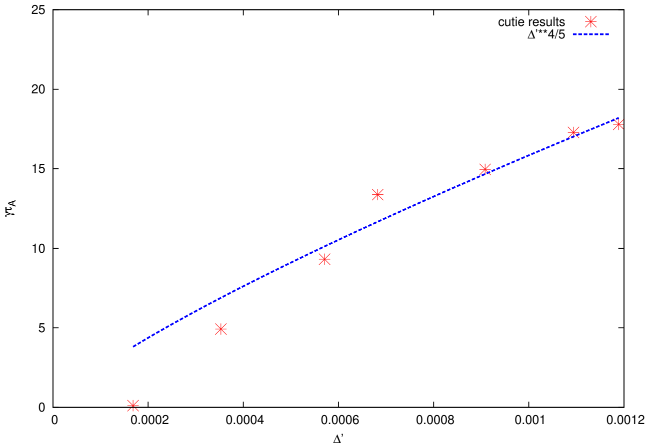

Figure 4.2: Linear growth rate vs stability index of the (2,1) mode in low viscosity regime

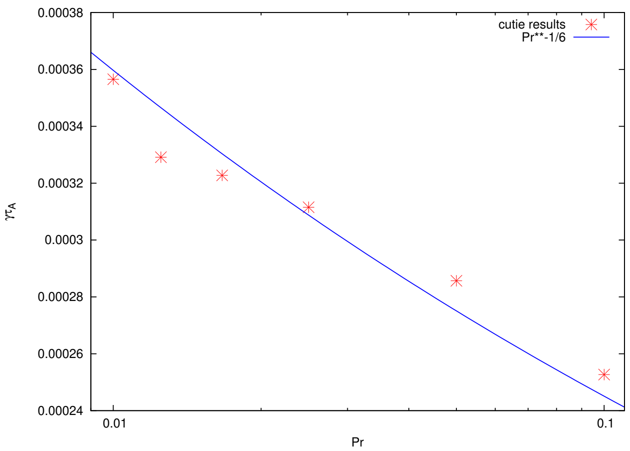

Figure 4.3: Linear growth rate vs Prandtl number of the (2,1) mode

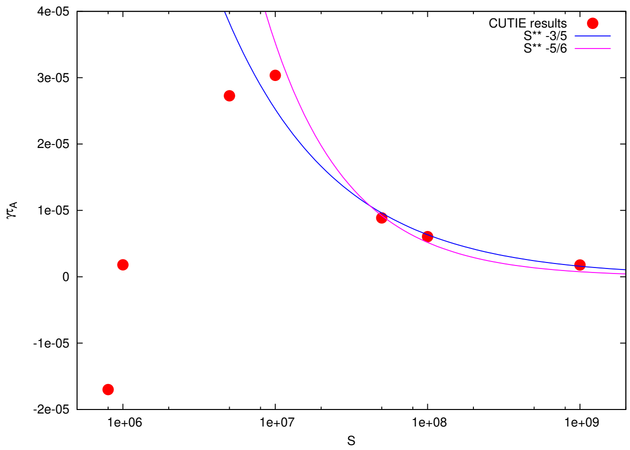

Figure 4.4: Linear growth rate vs Lundquist number of the (2,1) mode in higher viscosity regime

Visco-resistive MHD in a cylindrical geometry

In this section we present simulation results carried out with a simple reduced MHD model in a periodic cylindrical geometry to study the stability of the $(2,1)$ tearing mode in the presence of equilibrium flows. To separate the two fluid effects from basic MHD effects our initial simulations have been done by using a subset of the original CUTIE model equations that represent a reduced MHD model. The equilibrium flow profile for the axial flow is chosen to be of the form $V_{0z}/V_A = M_A \tanh[\lambda(x-x_s)]$ where x_s is the location of the mode resonant surface, $V_A = \frac{B_0}{(\mu_0 m_i n_e)^{1/2}}$ is the Alfven velocity, M_A is the toroidal Mach number indicating the strength of the flow and the parameter λ is a measure of the flow shear. The poloidal flow profile is taken to be of the form $V_{0\theta}/V_A = M_\theta x(1+kx)$ where M_θ is the poloidal Mach number and k measures the shear in the flow. For all our linear and nonlinear runs we have taken a q profile of the form $q = q_0[1+(x/x_0)^{2\lambda_1}]^{1/\lambda_1}$ with $q_0 = 1.5504$, $x_0 = 0.598552$ and $\lambda_1 = 1.208$. Other parameters that are held constant for all the runs are the Lundquist number $S = 10^6$ and the Prandtl number $P_r = (S/Re) = 1$, where $Re = aV_A/\nu$ is the Reynolds number, ν being the kinematic viscosity. We also assume a large aspect ratio ($R = 1m, a = 0.1m$) configuration that is appropriate for the periodic cylinder model and further assume flat profiles for the resistivity (η) and the kinematic viscosity (ν).

Effects of sheared axial flow

First we have studied scaling laws in presence of sheared axial flow. Fig. 4.5 show the linear growth rate changes with $S^{-1/3}$ scaling in presence of sheared axial flow. This is consistent with our analytical arguments given in section 4.5.3. Fig. 4.6 shows the scaling fo the growth rate with Prandtl number in presence of flow. At low Prandtl number the growth rate becomes independent of viscosity since the latter is negligibly small.

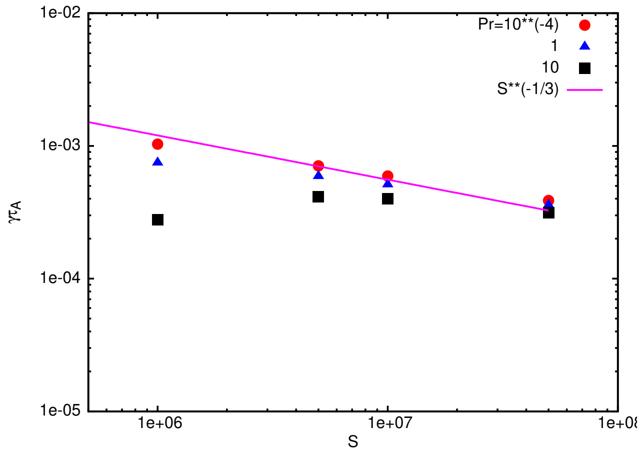

Figure 4.5: Linear growth rate vs Lundquist number S of the (2,1) mode in the presence of sheared axial flow for $M_z = 0.05$ and $M_\theta = 0$

Our numerical results for the linear growth rates in the presence and absence of a pure axial sheared flow are shown in Fig. 4.7 for $M_A = 0.05$ and $\lambda = \pm 10$. Evidently the axial flow has a destabilizing influence on the tearing mode. The dotted curve shows the value of the linear growth rate for non-zero flow rates; the solid curve shows the growth rate in the reference zero-flow case. The value of the growth rate remains the same for positive or negative values of M_A [for fixed λ]. These results are consistent with the theoretical findings of Gimblett *et al* [51].

The nonlinear evolution of the mode with and without imposed axial flow is shown in Figure 4.8. The same destabilizing trend of the axial sheared flow is seen to extend to nonlinear regimes. However, unlike the linear case, the saturated final state depends on the sign of flow shear. The saturation level of the $(2,1)$ magnetic island is higher for a positive sheared axial flow than that of a negative sheared axial flow and both are higher

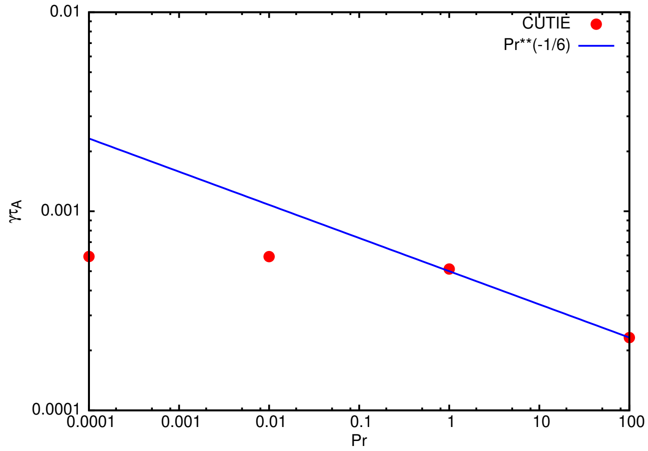

Figure 4.6: Linear growth rate versus Prandtl number Pr of the (2,1) mode in the presence of sheared axial flow for $M_z = 0.05$ and $M_\theta = 0$

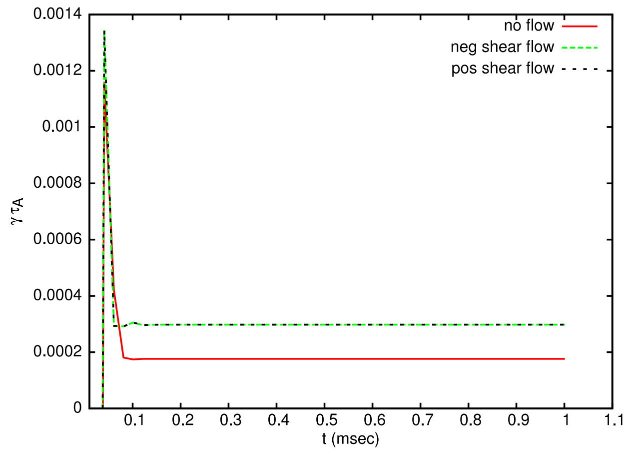

Figure 4.7: Linear growth rate (asymptotic value) vs time of the (2,1) mode in the presence of sheared axial flow.

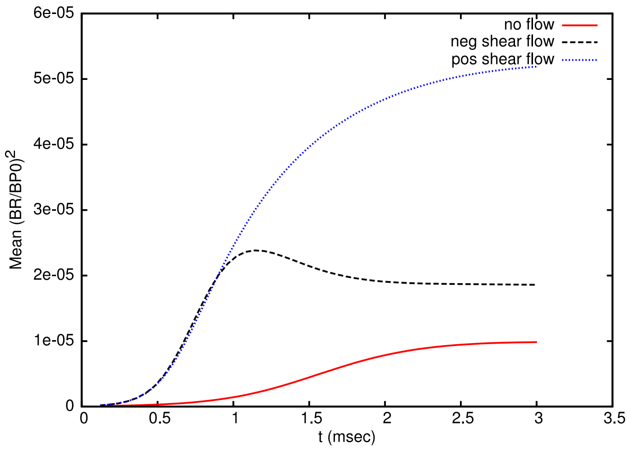

Figure 4.8: Nonlinear evolution of the (2,1) mode in the presence of sheared axial flow.

than the no flow reference case. Such dependence of nonlinear saturation level with the sign of sheared flow may be related to the fact that the nonlinear generation of poloidal flow component makes the flow helical. In section 4.5.3, it is shown that tearing mode stability depends on flow helicity sign, relative to the field helicity.

Effects of sheared poloidal flow

A purely poloidal sheared flow exerts a stabilizing influence on the $(2,1)$ tearing mode. Figs. show the results of the variation of the growth rate, Re($\gamma\tau_A$) and the real mode frequency, Im($\gamma\tau_A$) as functions of $\Omega\tau_A$ obtained using the resolvent method. Fig. clearly shows that the real mode frequency is linearly proportional to M_θ from Doppler shift considerations. The growth rate is clearly seen to be decreasing starting with $M_\theta = 0$.

Numerical results from CUTIE simulations are shown in Fig. 4.9, Fig. 4.10, and Fig. 4.11. The plot shows the nonlinear evolution of the mode for $M_\theta = 0.005$(the dotted and dashed curves) and for $M_\theta = 0$(the solid curve). In the linear regime the slopes of the dotted and dashed curves are smaller than the solid curve indicating stabilizing effects of the flow. Furthermore, the curves for positive shear(dotted) and negative shear(dashed) initially overlap displaying symmetry of the linear growth with respect to the sign of the flow. In the nonlinear regime however, the sign of the shear is important with the positive shear flow showing a higher saturation level than the negative shear. Both these

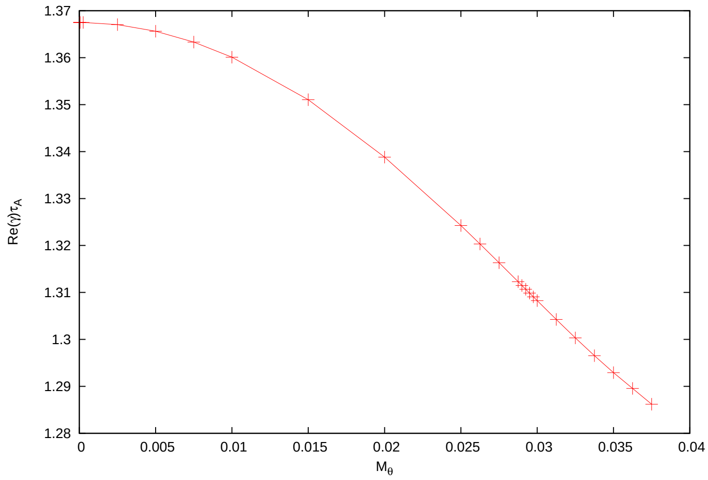

Figure 4.9: Linear growth rate versus M_θ of the (2,1) tearing mode in the presence of sheared poloidal flow at $S = 10^6$ and $Pr = 1$ for $M_z = 0$

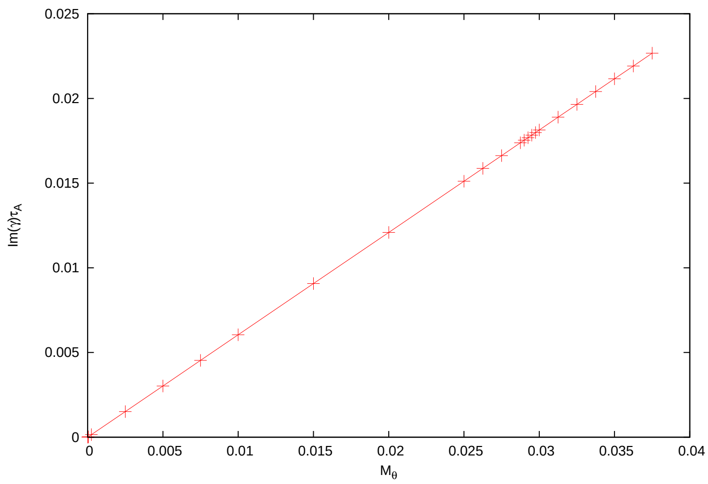

Figure 4.10: Mode frequency versus M_θ of the (2,1) tearing mode in the presence of sheared poloidal flow at $S = 10^6$ and $Pr = 1$ for $M_z = 0$

levels are lower than the no flow case saturation level.

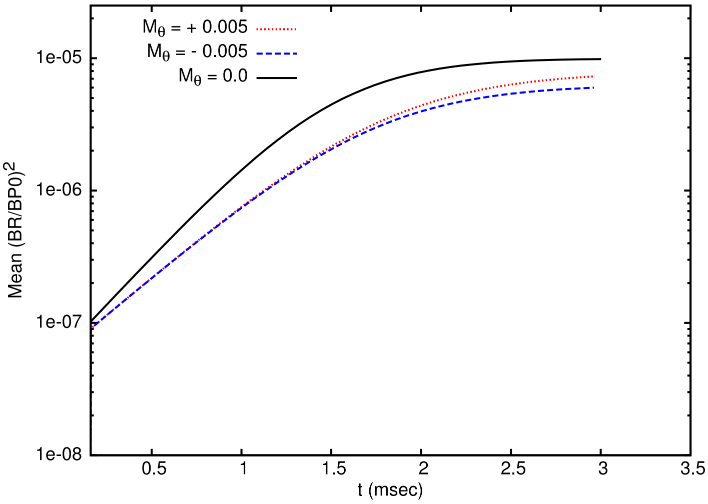

Figure 4.11: Nonlinear evolution of the (2,1) tearing mode in the presence of sheared poloidal flow.

Effects of helical flow

We have next considered a combination of the axial and poloidal flows leading to flows with different flow helicities (the equilibrium magnetic fields are kept fixed) and studied their influence on the (2,1) tearing mode. Figure 4.12 shows the linear growth rate of the mode for different combinations of the axial and poloidal flows with $M_A = 0.05$ and $M_\theta = 0.005$. We find that keeping the direction of the poloidal flow fixed if we change the sign of the axial flow then the linear growth rate of the mode either increases or decreases with respect to that of the no poloidal flow case. However if we change the sign of both the axial and the poloidal flow simultaneously then the linear growth rate remains unchanged. Thus, the sign of shear in the helical flow matters for the linear stability of the tearing mode. The nonlinear evolution of the mode as shown in Fig. 4.13 shows a similar behaviour as regards the dependence of the stability on the sign of the helical flow shear. However the nonlinear saturation level shows a further fine splitting in that it depends on the individual signs of the axial and poloidal flow for a given helical flow. We have also used Gaussian axial flow profiles (i.e. $V_{0z} = M_z v_A \exp(-C\rho^2)$ to study profile effects and the results are qualitatively the same.

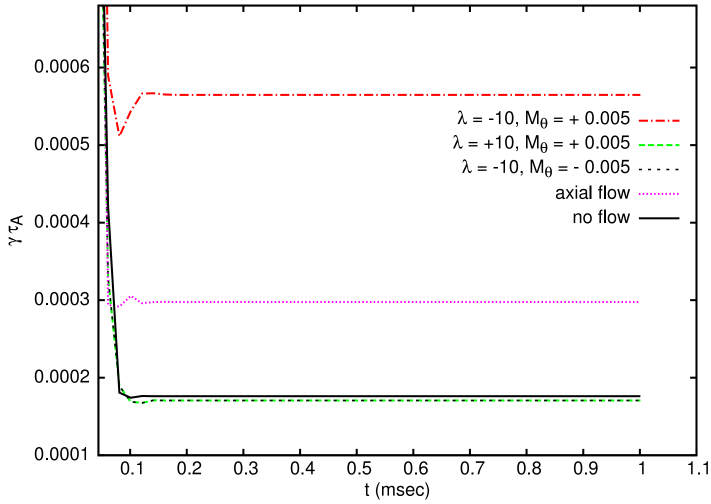

Figure 4.12: Linear growth rate versus time of the (2,1) tearing mode in the presence of helical flow for $M_z = 0.05$ and $M_\theta = 0.005$

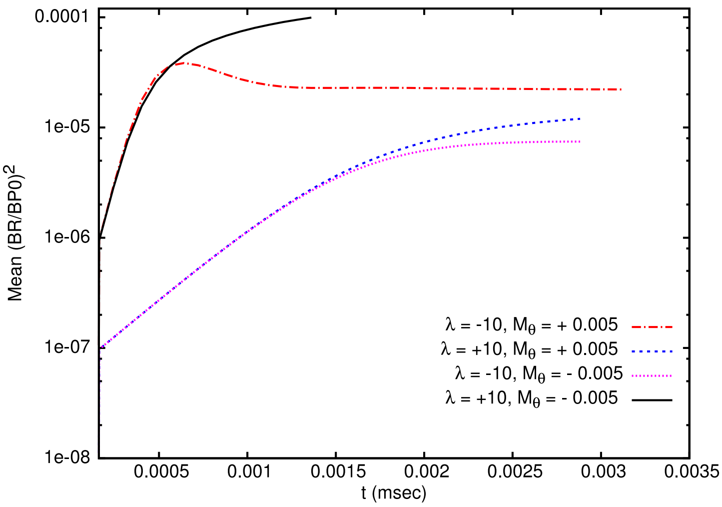

Figure 4.13: Nonlinear growth rate versus time of the (2,1) tearing mode in the presence of helical flow for $M_z = 0.05$ and $M_\theta = 0.005$

We can understand these results from the symmetry of the linearized versions of equations (4.3) and (4.4) of as follows,

$$\gamma\tilde{W} + \left(\frac{v_{0z}}{R_0}in + \Omega im\right)\tilde{W} + v_A ik_{\parallel}\rho_s^2\nabla_{\perp}^2\tilde{\psi} = \frac{v_A\rho_s}{r}im\tilde{\psi}\frac{4\pi\rho_s}{cB_0}j_0' + \rho_s^2\frac{\Omega im}{r}\tilde{\phi} + \nu\nabla_{\perp}^2\tilde{W} \tag{4.7}$$

$$\gamma\tilde{\psi} + \left(\frac{v_{0z}}{R_0}in + \Omega im\right)\tilde{\psi} + v_A ik_{\parallel}\tilde{\phi} = \frac{c^2\eta}{4\pi}\nabla_{\perp}^2\tilde{\psi} \tag{4.8}$$

To understand the symmetry of the equations relative to flow, we have examined the conjugate equation by putting $\gamma \to \gamma*$, $\tilde{W} \to \tilde{W}^*$, $\tilde{\phi} \to \tilde{\phi}^*$, $\tilde{\psi} \to \tilde{\psi}^*$ and $i \to -i$. As ψ can always be chosen to be real because outer solutions are always real and inner solution need to be matched with it, so we can write $\tilde{\psi}^* = \tilde{\psi}$ which leads to $\tilde{\phi}^* = -\tilde{\phi}$ and $\tilde{W}^* = -\tilde{W}$. After substituting these relations the conjugate equations can be written as,

$$\gamma^*\tilde{W} - \left(\frac{v_{0z}}{R_0}in + \Omega im\right)\tilde{W} + v_A ik_{\parallel}\rho_s^2\nabla_{\perp}^2\tilde{\psi} = \frac{v_A\rho_s}{r}im\tilde{\psi}\frac{4\pi\rho_s}{cB_0}j_0' - \rho_s^2\frac{\Omega im}{r}\tilde{\phi} + \nu\nabla_{\perp}^2\tilde{W} \tag{4.9}$$

$$\gamma^*\tilde{\psi} - \left(\frac{v_{0z}}{R_0}in + \Omega im\right)\tilde{\psi} + v_A ik_{\parallel}\tilde{\phi} = \frac{c^2\eta}{4\pi}\nabla_{\perp}^2\tilde{\psi} \tag{4.10}$$

Now, if we change the sign of v_{0z} and Ω simultaneously or change the sign of either of them but keeping the other one to zero then the conjugate equations (4.9) and (4.10) can be mapped exactly to the original equations (4.7) and (4.8) except that $\gamma \to \gamma*$ so real part of them i.e. growth rate will remain same but imaginary part i.e. rotation frequency will change the sign. However if we change the sign for only one of them keeping other one with same sign but finite eg. $v_{0z} \to -v_{0z}$, $\Omega \to \Omega$ then no such mapping is feasible, so γ and γ^* will be different.

Two fluid visco-resistive model

We have repeated some of the simulations reported in the previous section with the full set of model equations in the CUTIE code in order to assess the impact of two fluid effects on the stability of the tearing modes in the presence of sheared flows. In addition to the equations (4.3) and (4.4) used in RMHD calculations, here we have used the following linear equations,

$$\begin{aligned}\frac{\partial \tilde{n}}{\partial t} + \mathbf{u_{e0}} \cdot \nabla \tilde{n} + v_A \nabla_{\parallel} \rho_s^2 \nabla_{\perp}^2 \tilde{\psi} + v_{th} \frac{n_0}{n_0(0)} \nabla_{\parallel} \tilde{v_{\parallel}} &= \frac{v_A \rho_s}{r} \frac{\partial \tilde{\psi}}{\partial \theta} \frac{4\pi\rho_s}{cB_0} j_0' \\ &+ \frac{v_{th}\rho_s}{r} \left(\frac{n_0'}{n_0(0)} \right) \frac{\partial \tilde{\phi}}{\partial \theta} + D\nabla_{\perp}^2 \tilde{n}\end{aligned} \tag{4.11}$$

$$\begin{aligned}\frac{\partial \tilde{v_{\parallel}}}{\partial t} + \mathbf{u_0} \cdot \nabla \tilde{v_{\parallel}} + v_{th} \frac{n_0(0)}{n_0} \frac{T_{e0} + T_{i0}}{T_{e0}(0) + T_{i0}(0)} \nabla_{\parallel} \tilde{n} &= \frac{v_{\parallel 0}' \rho_s}{r} \frac{\partial \tilde{\phi}}{\partial \theta} \\ &- v_{th} \rho_s \beta^{1/2} \frac{n_0(0)}{n_0} \frac{p_0'}{p_0(0)} \frac{\partial \tilde{\psi}}{\partial \theta} + \chi D \nabla_{\perp}^2 \tilde{v_{\parallel}}\end{aligned} \tag{4.12}$$

We have also added the $v_A \left(\frac{n_0(0)T_{e0}}{n_0(T_{e0}(0)+T_{i0}(0))} \right) \nabla_{\parallel} \tilde{n}$ term in Ohm's law. Regarding the simulation results, Fig. 4.14 show a comparison of the linear stability results of the mode for the single and two fluid models in the presence of an axial flow. As can be seen two fluid effects tend to have a stabilizing influence on the tearing mode. In the absence of flow, the linear mode is more stable in a two fluid model as compared to a single fluid model. In the presence of sheared axial flows a negative sheared flow is more destabilizing while a positive sheared flow is more stabilizing compared to the single fluid results discussed in 4.5.1. This is similar to the results one obtains in the presence of helical flows as discussed in section 4.5.3 and may have its origin in the excitation of self consistent poloidal flows due to two fluid effects. A closer investigation of the physical mechanism underlying the stabilization effects arising in a two fluid model is currently in progress and will be reported elsewhere. We have also used Gaussian axial flow profile for the same study but the nature of results do change significantly in these cases with the change in axial flow profile. Figure 4.15 shows how the linear growth rate of the modes change with the Gaussian axial flows.

Visco-resistive MHD in a toroidal geometry

To complement the cylindrical studies mentioned above, we have simultaneously carried out systematic studies on the tearing mode stability in a toroidal geometry using the code NEAR [46]. This code solves the generalized reduced MHD equations and incorporates visco-resistive effects as well as toroidal mode coupling, flow induced centrifugal effects and neoclassical contributions. The equilibrium configurations for its stability runs are generated by a Grad-Shafranov solver (TOQ) incorporating toroidal flows in the equilibrium. In contrast to the cylindrical results, our simulations on NEAR for a toroidal flow show stabilizing effects on the evolution of a single $(2,1)$ tearing mode both in the linear stage as well as in the nonlinear saturated state as shown in Fig. 4.16. This stabilizing influence is seen to persist even when flow term contributions in NEAR are switched off. The stabilizing influence therefore appears to come from equilibrium modifications brought about by toroidal flow. To test this idea we generated several equilibria from TOQ using different magnitudes of the toroidal flow while keeping the total current constant. As is well known the presence of a toroidal flow modifies the pressure profile due to centripetal force effects. TOQ uses the Mashke-Perrin expression for the pressure given by, $p_0 = p_{nf}(\psi_0)exp[\Gamma M_s^2(\psi_0)(\hat{R}^2 - \hat{R}_{axis}^2)/2]$ where p_{nf} is the pressure profile in the absence of flow, M_s is the normalized Mach number, Γ is the adiabatic constant, $\hat{R} = R/R_0$ and $\hat{R}_{axis} = R_{axis}/R_0$.

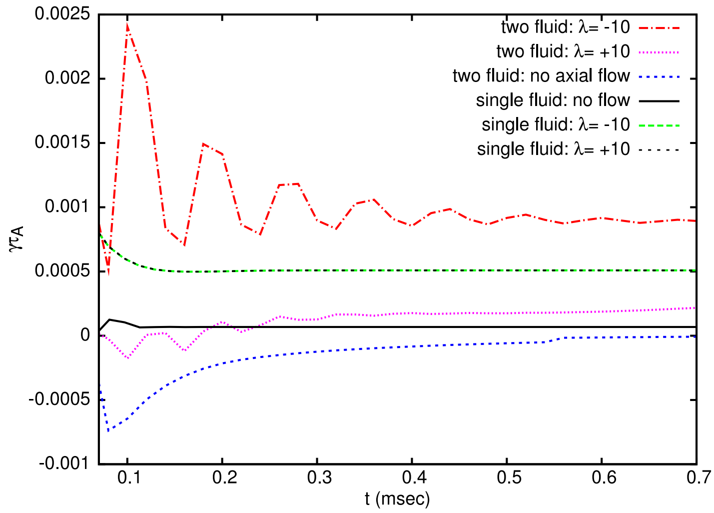

Figure 4.14: Linear growth rate v/s time in presence of sheared axial flow using the two fluid model

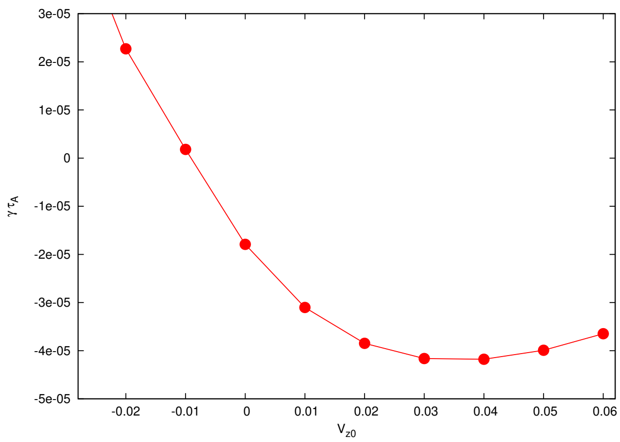

Figure 4.15: Linear growth rate v/s axial flow (at r=0) with a Gaussian flow profile using the two fluid model

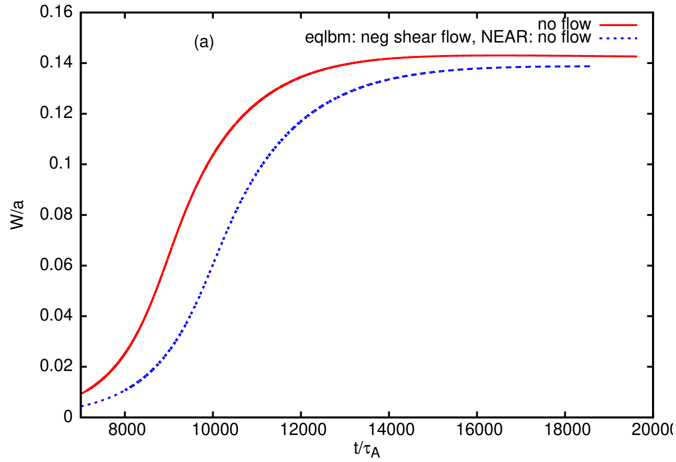

Figure 4.16: NEAR/TOQ: Island width vs time in presence of equillibrium toroidal flow

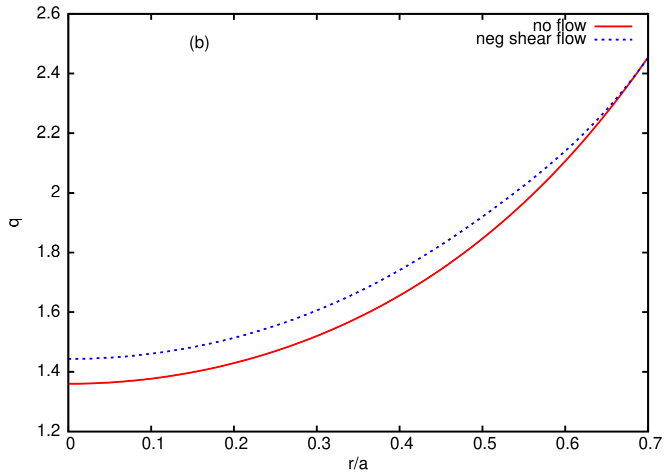

Figure 4.17: NEAR/TOQ: change in q profile due to equilibrium toroidal flow.

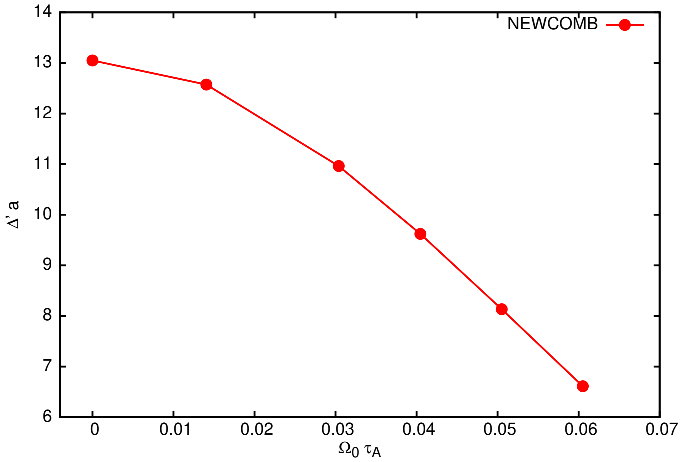

Figure 4.18: NEWCOMB: Δ' vs equilibrium toroidal flow

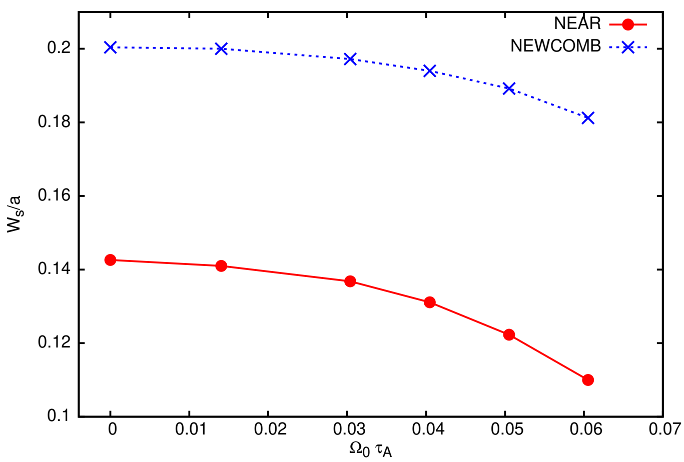

Figure 4.19: W_{sat} vs equilibrium toroidal flow.

In addition to keeping the current constant we have also kept p_{nf} the same while generating equilibria for various values of M_s. We find that flow introduces changes in the profiles of the current density, pressure and the safety factor q by inducing a sort of 'Shafranov' like shift. This is shown in Fig. 4.16, Fig. 4.17, Fig. 4.18 and Fig. 4.19 in terms of the flow induced modifications in the q profile. It should be noted that this effect is purely due to magnitude of the flow (proportional to M_s^2) and flow shear does not play a role here. To assess the influence of this shift on the stability of the tearing mode we have calculated the stability index Δ' for various flow modified q profiles obtained from the code TOQ. These analytic estimates are obtained by using the q profiles in a cylindrical Newcomb equation. As shown in Fig. 4.18 the value of Δ' decreases with increasing toroidal flow indicating the stabilizing influence of the 'Shafranov' like shift. To understand the decrease in nonlinear saturation level with flow we have also carried out an approximate estimate of the island width by using the nonlinear definition of the stability index as given Carreras *et al*[52] and Thyagaraja [53]. The basic idea is to define Δ' across the width of the island instead of across the infinitesimal tearing layer. Accordingly the nonlinear stability index is now given by the expression,

$$\Delta'(W) = \frac{1}{\psi_{2,1}(r_s)} \left(\frac{d\psi_{2,1}}{dr}\Big|_{r^+} - \frac{d\psi_{2,1}}{dr}\Big|_{r^-} \right) \tag{4.13}$$

where $r^{\pm} = r_s \pm W/2$, r_s is the mode resonant surface and W is the width of the island. Using this approximate formula we have calculated the island width for the different flow modified equilibrium q profiles and the results are displayed in Fig. 4.17. For comparison we have also given the island widths obtained directly from the nonlinear simulations on NEAR. It is seen that both curves show a similar trend, namely a stabilizing influence of the toroidal flow leading to a decrease in the island size with increasing flow. The quantitative difference between the two curves can be attributed to the additional stabilizing influences inherent in NEAR from mode coupling and other effects and the errors arising from the approximate nature of expression (4.13).

Summary and Discussions

To summarize, we have carried out extensive numerical studies to examine the influence of equilibrium sheared flows on the stability of a $(2,1)$ tearing mode. Our cylindrical geometry investigations, using a RMHD version of the code CUTIE, show that in the linear regime pure axial sheared flows have a destabilizing influence while pure sheared poloidal flows tend to stabilize the mode. These effects are independent of the sign of the flows. However for a helical flow the sign of the helicity matters with positive helicity providing a stabilizing influence. In the nonlinear regime the independence from the sign of the flow no longer exists (even for purely axial or poloidal flows) and is an important finding of our investigations. The inclusion of two fluid effects provides a further stabilizing effect on the mode presumably due to self consistent excitation of poloidal flows. Our toroidal geometry stability studies have identified a stabilizing influence of toroidal flows that is not dependent on the flow shear but is purely due to the modification in the q profile arising from centripetal force induced shift in the flux surfaces. To gain further understanding of the physical mechanism responsible for the

Table 4.1: Effect of sheared axial flows on Δ' in presence of positive poloidal flow

M_A	-0.05	-0.03	0	+0.03	+0.05
$\Delta' a$	-1.998	-0.680	2.216	2.304	2.464

symmetry breaking phenomena observed in CUTIE simulations, we have calculated the stability index Δ' in cylindrical geometry using the generalized Newcomb equation in presence of helical flow. The method of calculations are similar to that given in Ref [54]. The table 4.1 shows that how Δ' changes when direction of sheared axial flow changes without any change in the sign of poloidal flows. Here the profile of the axial flow has been taken as Gaussian, $V_{0z} = M_A e^{-x^2}$. So these results are in agreement to our single fluid CUTIE simulation results showing symmetry breakingin presence of helical flows. We have noticed in case of earlier study [54] the stability index is very sensitive to nature of poloidal flow. In case of two fluid CUTIE runs, the self generated diamagnetic poloidal flow changes significantly depending on the axial flow profile which is not the case for single fluid runs. So it is possible that two fluid stability results are very sensitive to the nature of axial flow profiles unlike single fluid results. In future, We like to incorporate additional physics features in our future CUTIE simulations by evolving the electron and temperature equations and by retaining parallel transport.

5

VRMHD studies of (1,1) mode

Introduction

The $m = 1, n = 1$ internal kink instability is of great importance in tokamaks and has beeen extensively studied in the past by several authors, notably[21–25]. The (1,1) mode arises within the q=1 rational surface (where q is the safety factor), when the q at the axis is smaller than 1. It can trigger sawtooth oscillations which can influence plasma quality and confinement[21, 22]. Monticello et. al. [25] have given an overview of the research on the (1,1) mode and its importance, particularly in the context of research on the sawtooth oscillations.

It is well known that flows are a common occurence in a tokamak, which can be generated intrinsically[55] or induced externally e.g. by unbalanced NBI injection [56, 57]. Experiments on NSTX have shown a significant increase of sawtooth period that is attributed to a fast rotation of the plasma[56, 57]. Experimental studies on sawteeth phenomena in presence of NBI in JET [58, 59], MAST [15], and TEXTOR [60] have further shown that there is an asymmetry in sawtooth period depending on the direction of the NBI. The sawtooth period increases with an increase in co-NBI power, and decreases with an increase in counter-NBI power. Thus, these experiments have shown that flow can have a stabilising or destabilising effect on the kink mode depending on the direction of flow.

However, there still does not exist a full understanding of the effect of flows on the $m = 1, n = 1$ kink instability. A number of past studies have addressed this question. In one of the earliest such studies carried out in a slab geometry, Ofman et. al.[12] have shown that small flow shear has a stabilising influence on the $m = 1$ resistive mode.

Numerical studies by Kleva and Guzdar[13] show that toroidal sheared flow close to the sound speed can completely stabilise the (1,1) mode. Shumlak et al.[61] have also found a similar stabilising effect due to a sheared axial flow on the (1,1) mode in a cylindrical Z-pinch. On the other hand, Gatto et. al. [62] have found sheared axial flows to have a destabilising effect on the $m = 1$ mode in a reverse field pinch configuration. Naitou et al. [63] have studied the effect of poloidal flow on the kink mode in kinetic and two fluid regimes, and noted a stabilisation of the kink mode that can possibly be related to sawtooth stabilisation. Studies by Mikhailovskii et. al.[64], Wahlberg et. al.[14] and Waelbrock[65] show that toroidal and poloidal rotations are a stabilising factor for the internal kink mode. Chapman et. al.[15] have explained the asymmetry in sawtooth period in terms of the relative direction of the plasma flow with respect to the diamagnetic drift. They postulated that the toroidal component of the diamagnetic drift adds to the toroidal rotation for co-current flow but it reduces the toroidal rotation for counter current flow. Therefore, there are conflicting results in the literature regarding the nature of stabilisation due to flows depending on the parameter regime of the studies. Recent analytic calculations by Brunetti et. al.[66] have found that small flow shear has a destabilising effect on the (1,1) mode, but a large flow shear can stabilise it.

It may be noted that most of the past flow studies have been done in the low viscosity regime. However, viscosity can be high in tokamak operations, particularly due to enhancements from turbulent effects and could therefore significantly influence the effect of flow shear on the internal kink mode. For example, Maget et. al.[17], Wang et. al.[18], Tala et. al.[16] and Takeda et. al.[19] have shown that Magnetic Prandtl number in advanced tokamak scenarios can be as high as 100, and stability results in the high viscosity regime can be significantly different from results of the low viscosity regime. Chen et. al.[44] and Ofman et. al.[67] have given detailed analytical calculations as to how viscosity can modify shear flow effects for constant-ψ and nonconstant-ψ for the resistive tearing mode instability. Wang et. al.[18] have also reported from their simulation studies of (2,1) tearing modes in the presence of flows, which showed a destabilisation at lower viscosity and stabilisation at higher viscosity. They predict that this is due to the distortion of magnetic island structures at higher viscosity as reported by Ren et. al.[68] and La Haye et. al.[69].

Thus, viscosity is an important contributing factor and can change the nature of the effect of flows significantly. In this chapter we have addressed this issue and investigated the stability of the (1,1) mode in the presence of sheared flows over a range of viscosity regimes. We indeed find that the high viscosity results are often very different from the low viscosity results. In our study, we have systematically examined the effects of several kinds of sheared flows on the (1,1) mode, namely axial, poloidal and combinations of both kinds of flows in the linear as well as nonlinear regimes.Various non-dimensional parameters are used to characterise our results, such as **S** (the Lundquist number, which measures resistivity), **Pr** (Prandtl Number, which measures viscosity), **M** (Alfvén Mach number) and λ(a measure of the equilibrium flow shear). These linear and nonlinear studies on the (1,1) mode were obtained using the CUTIE code [35].

Our principal findings are as follows. To begin with, we have done the linear scaling studies of the $m = 1, n = 1$ mode in the absence of flow. Here, the variation of linear growth rates have been studied for different S and Pr values. The obtained scalings are in agreement with past analytic theory results in the no flow case[70]. With the application of sheared axial flows, a significant change in the scaling of the growth rates is observed. However, in the presence of poloidal flow, there is no such change in scaling as compared to the no flow case. In our linear studies we have noticed that axial flows destabilise the mode in the low viscosity regime, but it stabilises in the high viscosity regime as compared to the no flow case. On the other hand, poloidal flow always tends to stabilise the linear growth rate. For pure axial and poloidal flows, the results do not change if we change the direction of the flow. This symmetry is broken for helical flows where the time evolution of the modes show a significant dependence on the helicity of the flows even in the linear regime. In the nonlinear regime, there is mostly a reduction of the nonlinear saturation level of the (1,1) mode for both sheared axial and poloidal flows in the high viscosity regime, while in the low viscosity regime, the poloidal and axial flows are destabilising in nature. Helical flows show a strong stabilisation for positive helicity and in most cases, weak stabilisation for negative helicity in the high viscosity regime. In the low viscosity regime, this symmetry breaking of helical flow results gets significantly diminished.

This chapter is organised in the following manner. We have In section 5.2, we have studied the (1,1) mode in the linear regime. Here, we have described studies of the growth rate scaling in the absence of flow, and compared our results with analytical results from the literature. Then we have repeated these studies in the presence of flow. We have done these studies both in the low and high viscosity regimes. In section 5.3 we have studied the (1,1) mode in the nonlinear regime in the absence of flow as well as in presence of axial, poloidal and helical flows. Section 5.4 provides a brief summary and a discussion of the results.

Linear Results

In this section we describe the results of our linear studies carried out for a q profile of the following form:

$$q(\rho) = q_0 \left(1 + \left(\frac{\rho}{\rho_0}\right)^{2\Lambda}\right)^{\frac{1}{\Lambda}} \tag{5.1}$$

with the safety factor, $q(\rho) = \frac{\varepsilon \rho B_{0z}}{B_{0\theta}(\rho)}$, $q_0 = 0.9$, $\Lambda = 1$, $\rho_0 = 0.6a$, $a =$ radius of the cylinder.

Fig. 5.1 shows the q profile used in the simulations and the q=1 surface.

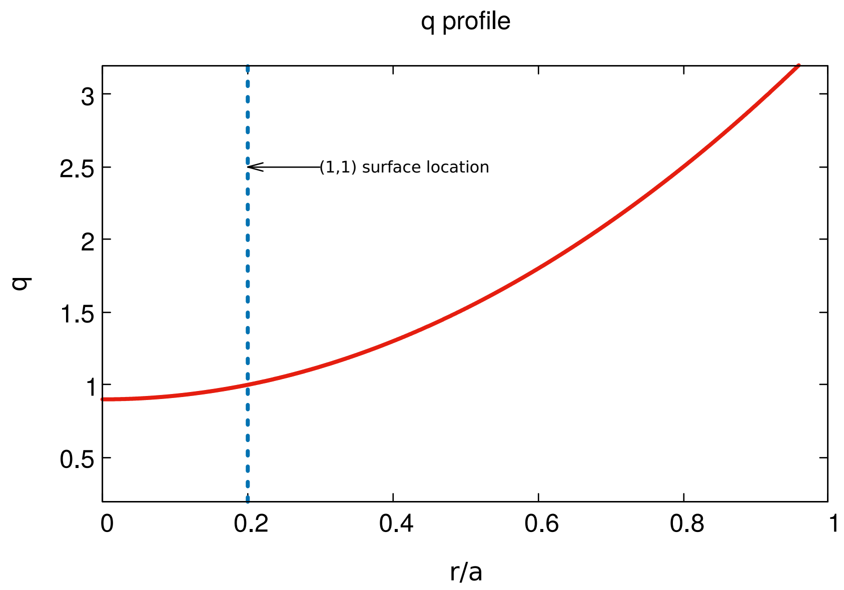

Figure 5.1: q profile

Scaling with S and Pr

At first, we have studied the scaling of the growth rate of the (1,1) mode with S(Lundquist number) and Pr(Prandtl Number). For most of our simulations we have used a flat η profile but we get similar results when we use a self-consistent η such that $E_{0z} = \eta j_{0z}; E_{0z} =$

$V/(2\pi R_0)$, where V is the constant loop-voltage. In Fig. 5.2, we have plotted the normalised growth rate $\gamma\tau_A$ with S, at a fixed Pr of 0.1. We have found a scaling of the variation of $\gamma\tau_A$ with S to be of the form $S^{-1/3}$. These results are similar to those obtained by Porcelli[70] for the resistive internal kink mode. At low S, we notice a deviation from the scaling that can be attributed to local asymmetries of the equilibrium current density[34].

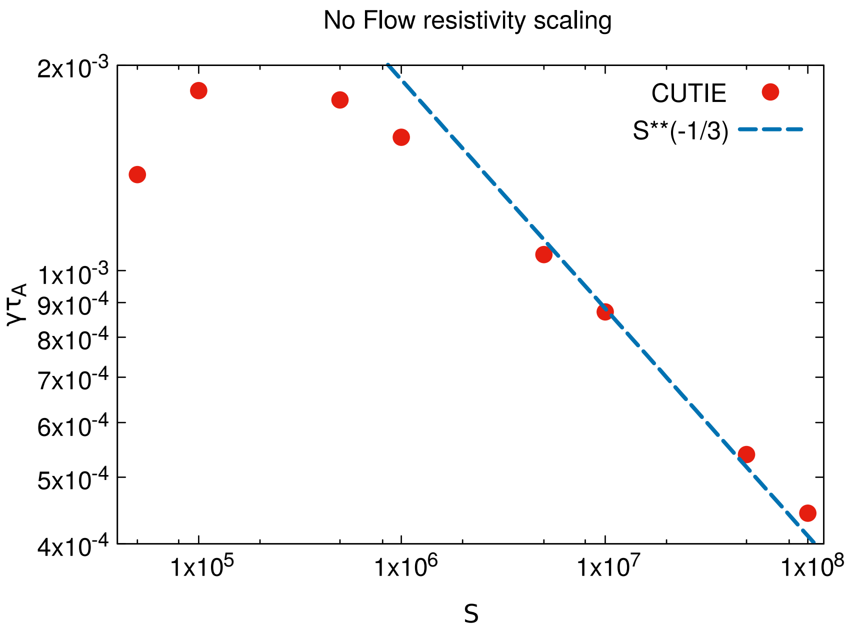

Figure 5.2: Linear Resistivity scaling without flow for the m=1, n=1 mode at $Pr = 0.1$

In Fig. 5.3, we observe a $Pr^{-1/3}$ scaling of $\gamma\tau_A$ as we vary Pr by keeping S fixed. This scaling agrees with that reported earlier by Porcelli[70]. However, as we increase the viscosity further, the growth rate scaling changes to $Pr^{-5/6}$, which is a new result that has not been reported earlier. It shows that high viscosity can strongly influence the linear growth rate of the modes. These results can be qualitatively understood by a standard dominant balance analysis of the dynamical equations of the mode in the inner layer. From the set of model equations given below one can obtain the following set of linear inner layer equations 5.5:

$$\begin{aligned}
&\frac{\partial \tilde{W}}{\partial t} + \mathbf{v_0}\cdot\nabla\tilde{W} + v_A\nabla_\parallel \rho_s^2\nabla_\perp^2\tilde{\psi} \\
=& v_A\rho_s\frac{1}{r}\frac{\partial\tilde{\psi}}{\partial\theta}\frac{4\pi\rho_s}{cB_0}j_0' + \frac{v_{th}\rho_s}{r}\left\{\tilde{\psi},\rho_s^2\nabla_\perp^2\tilde{\psi}\right\} + \frac{v_{th}\rho_s}{r}\left\{\tilde{W},\tilde{\phi}\right\} \\
&+\frac{\rho_s^2 W_0'}{r}\frac{\partial\tilde{\phi}}{\partial\theta} + \nu\nabla_\perp^2\tilde{W}
\end{aligned} \tag{5.2}$$

$$\frac{\partial\tilde{\psi}}{\partial t} + \mathbf{v_0}\cdot\nabla\tilde{\psi} + v_A\nabla_\parallel\tilde{\phi} = \frac{v_{th}\rho_s}{r}\left\{\tilde{\psi},\tilde{\phi}\right\} + \frac{c^2\eta}{4\pi}\nabla_\perp^2\tilde{\psi} \tag{5.3}$$

where,

$$\tilde{W} = \rho_s^2\nabla\cdot\left(\frac{n_0(\rho)}{n_0(0)}\nabla_\perp\tilde{\phi}\right)$$

Equation[5.2] is the vorticity equation, where $\tilde{W}$ is the perturbed vorticity. Equation[5.3] describes the evolution of the perturbed poloidal flux function $\tilde{\psi}$. The resistivity η and viscosity ν are specified quantities and are held constant during our calculations. Additionally, $\rho_s = \frac{v_{th}}{\omega_{ci}}$, where, $v_{th}^2 = (T_{0i}+T_{0e})/m_i$, $\omega_{ci} = (eB_0/m_i c)$, with T_{0i}, T_{0e} being ion and electron temperatures respectively. m_i is the ion mass, e is the elementary charge. $\Phi_0(r), \Psi_0(r)$ denote the mean electrostatic and magnetostatic potentials respectively.

$$\begin{aligned}
(\gamma + i v_{0,res}' x)\frac{d^2\phi}{dx^2} + i\frac{q_{res}'}{q_{res}}x\frac{d^2\psi}{dx^2} &= \nu\frac{d^4\phi}{dx^4} \qquad (5.4)\\
(\gamma + i v_{0,res}' x)\psi + i\frac{q_{res}'}{q_{res}}x\phi &= \eta\frac{d^2\psi}{dx^2} \qquad (5.5)
\end{aligned}$$

where all quantities are suitably made non-dimensional and where ν, η are non-dimensional viscous and resistive diffusivities respectively. $v_{0,res}'$ and q_{res}' are the derivatives of the flow terms and q profile respectively at the resonant surface and γ is the normalized growth rate. In the absence of flow and in the regime where both the viscous and resistive contributions are important, the term proportional to ν with the highest derivative dominates over the term proportional to γ in (5.4), while in (5.5) all terms contribute equally. Using the dominant balance argument one then gets,

$$\gamma \sim \eta^{2/3}\nu^{-1/3} \sim \eta^{2/3}\eta^{-1/3}\frac{\nu^{-1/3}}{\eta^{-1/3}} \sim Pr^{-1/3}$$

(η here is held constant)

and the layer width goes as

$$x \sim \eta^{1/6}\nu^{1/6}$$

This agrees with the numerical scaling obtained in Fig. 3 for moderate values of Pr and is also in accordance with the scaling discussed by Porcelli [70]. For higher values of viscosity, when viscous effects dominate over resistive contributions, the term on the R.H.S. of (5.5) may be ignored in the dominant balance calculation. In this limit the layer width also has a very weak dependence on viscosity and can be nearly taken to be a constant. The balance arguments then lead to $\gamma\nu \sim x^4$ and hence $\gamma \sim \nu^{-1}$. This scaling is close to the $\gamma \sim Pr^{-5/6}$ obtained from our numerical solutions. Such a scaling has also been alluded to by Porcelli [70] for the so-called visco-ideal limit. The growth rate becomes nearly constant in the low Pr regime, as we would expect the plasma to be nearly inviscid. We next consider the effect of flows on the linear growth rates.

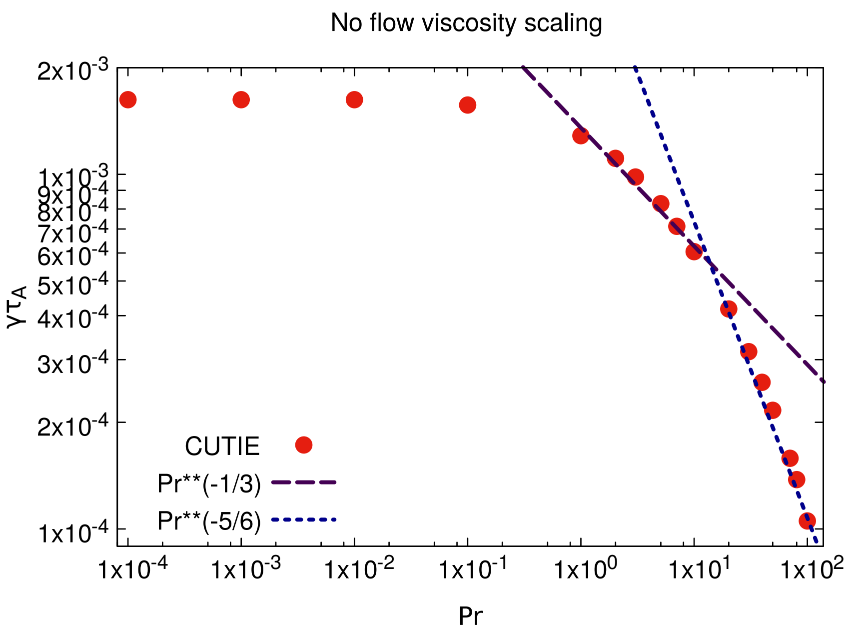

Figure 5.3: Linear Viscosity scaling without flow for the m=1, n=1 mode at $S = 10^6$

Axial Flow

We next present scaling results in the presence of a sheared axial flow. We have used an axial flow profile of the form:

$$\frac{V_{0z}}{v_A} = M_z \tanh[\lambda(\rho - \rho_{res})] \tag{5.6}$$

where, V_{0z} is the equilibrium axial flow, M_z is the axial Mach number, λ is the shear parameter and ρ_{res} is the location of the mode resonant surface. The flow profile is shown in Fig. 5.4

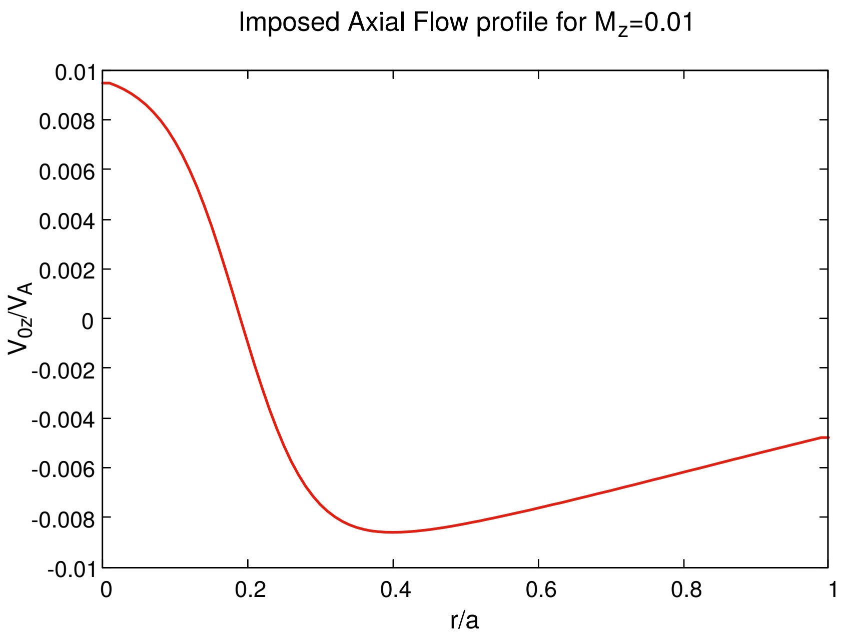

Figure 5.4: Axial flow profile(tanh profile)

This profile has the property that it has zero flow and non-zero shear at the resonant surface and hence is a useful profile to study the effect of shear on the mode. It has been used in the past to understand the effect of flow shear on tearing modes[39, 67]. For our linear scaling studies we have taken several different values $M_z = 0.05$ that are within a physically reasonable range of values for experimental observations. In general, the presence of an axial sheared flow has a destabilizing influence on the $m = 1$ resistive kink mode, as has been noted before [51] and is due to the additional ideal free energy arising from the nature of the flow profile. A principal consequence of this is an increase in the growth rate of the kink mode compared to the no flow case. This is clearly seen in Fig. 5.5 where we have marked the values of the growth rate for the no flow case and for several different finite values of the axial flow (and correspondingly different velocity shears) in a single plot. It is also seen that there is a near independence of the growth rate on S for higher values of S. This can be physically understood as follows: as the resistivity decreases (S increases) the growth rate of the classical resistive kink mode decreases and the growth is dominated by the ideal driving term of the flow shear. This term is independent of S and hence at higher values of S the growth rate becomes independent of S. In Fig. (5.5) we thus see how an increase in M_z progressively changes the $S^{-1/3}$ scaling in the "no-flow" case to one independent of S.

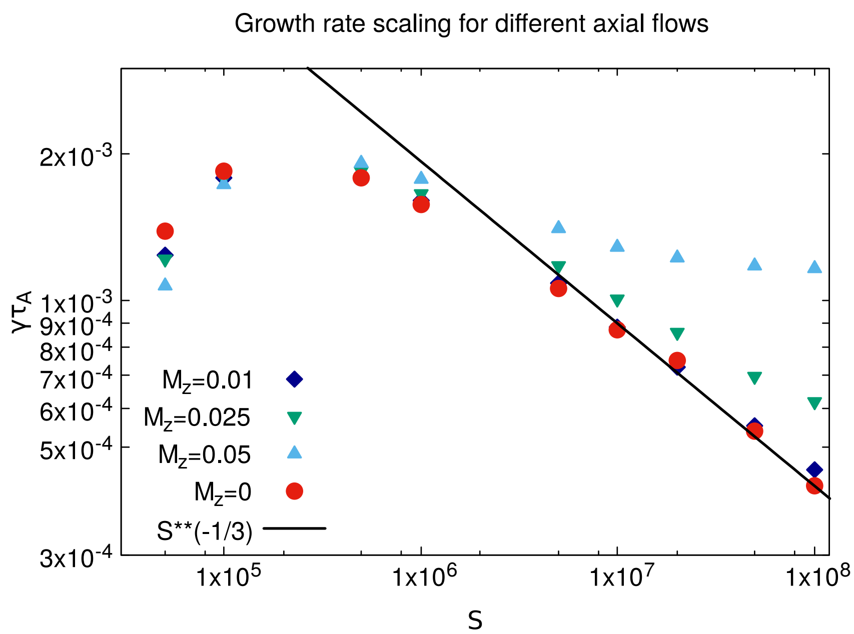

Figure 5.5: Linear Resistivity scaling with axial flow for the m=1, n=1 mode at $Pr = 0.1$ with $M_z = (0.0, 0.01, 0.025, 0.05)$

We have similarly observed a change in the viscosity scaling due to the presence of axial flow and this is shown in Fig. 5.6. As we go from $Pr = 1$ to $Pr = 10$, the scaling of the linear growth rate gradually changes from $Pr^{-1/5}$ to $Pr^{-3/5}$ and beyond $Pr = 10$, the growth rate becomes negative. If we compare it with the no flow case, there the scaling goes as $Pr^{-1/3}$ up to $Pr = 10$, beyond which it changes to $Pr^{-5/6}$. Thus in the presence of an axial flow, the stabilising influence of viscosity is enhanced and can lead to complete stabilisation of the $m = 1$ visco-resistive mode at high Pr numbers.

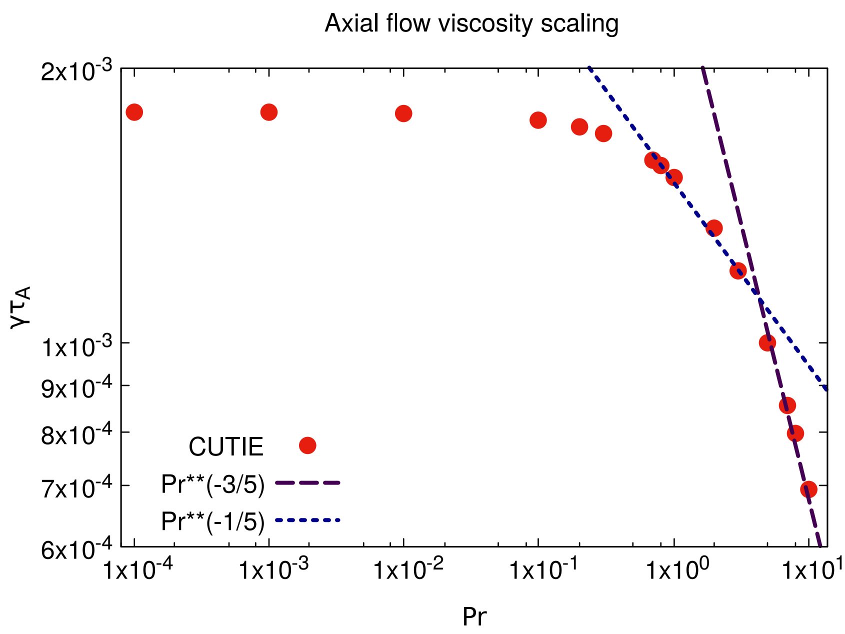

Figure 5.6: Linear Viscosity scaling with axial flow for the m=1, n=1 mode at $S = 10^6$, $M_z = 0.05$

Poloidal flow

For our poloidal flow studies, we have used the following flow profile,

$$\frac{V_{0\theta}}{v_A} = M_\theta(\rho) \tag{5.7}$$

where,

$$M_\theta(\rho) = \Omega\tau_A\, \rho\, (1 + k\rho)$$

Here, $V_{0\theta}$ is the equilibrium poloidal flow, and Ω is the poloidal angular frequency and k measures the shear in the flow.

The profile is plotted in Fig. 5.7

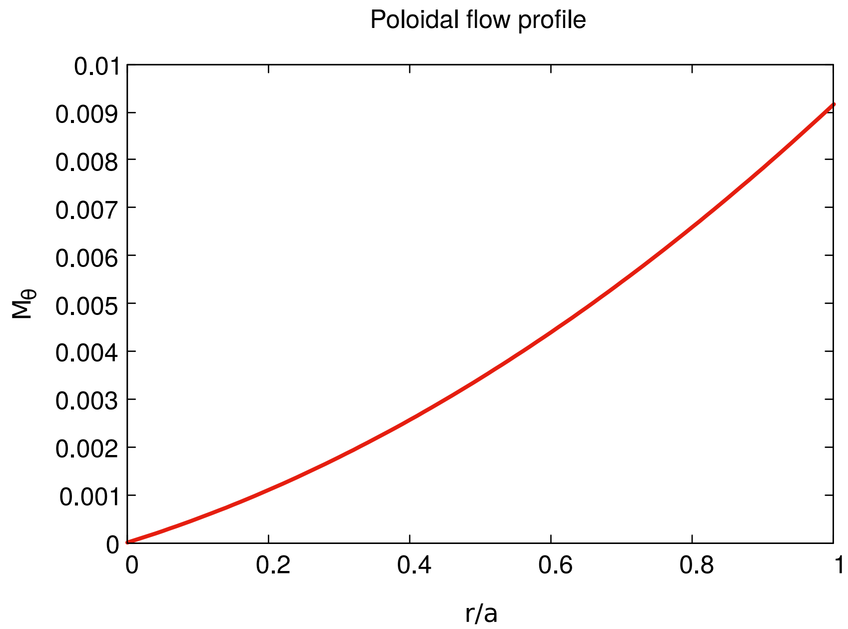

Figure 5.7: Poloidal flow profile

We have obtained the growth rates for several different values of M_θ and the results are plotted in Fig. (5.8). In contrast to the sheared axial flow the sheared poloidal flow has a stabilizing influence on the resistive kink mode so that it decreases the value of the growth rate. This stabilizing influence is independent of S and hence the net effect is a shift in the value of the growth rate without a change in the scaling dependence on S which remains the same as the no-flow case, namely $\gamma\tau_A \propto S^{-1/3}$. As seen in Fig. (5.8) as the poloidal Mach number is increased from zero, the scaling curve shifts downwards without changing shape. For very low values of M_θ, the curve almost coincides with the no-flow case, as expected.

In Fig. 5.9 we have displayed the scaling of the growth rate with viscosity for a fixed value of the resistivity. We find that the scaling is similar to the no flow case, namely $\gamma\tau_A \propto Pr^{-1/3}$ at a lower viscosity and $\gamma\tau_A \propto Pr^{-5/6}$ at a higher viscosity.

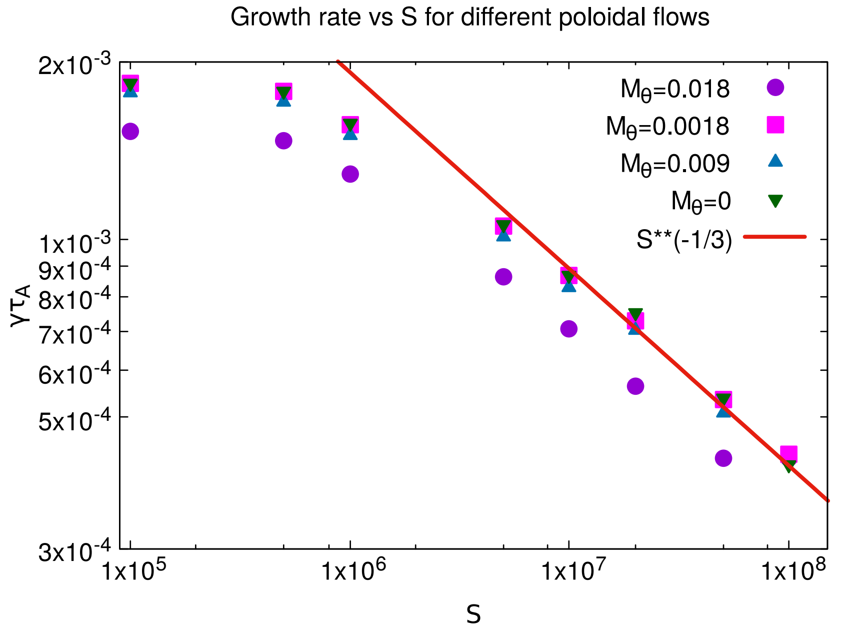

Figure 5.8: Linear Resistivity scaling with poloidal flow for the m=1,n=1 mode at $Pr = 0.1$, $M_\theta = (0.0, 0.0018, 0.009, 0.018)$

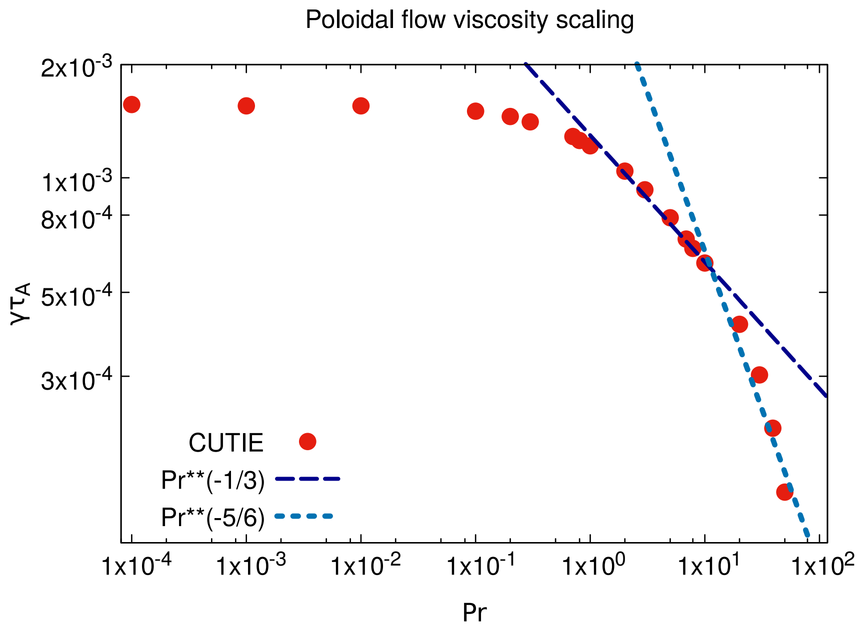

Figure 5.9: Linear Viscosity scaling with poloidal flow for the m=1,n=1 mode at $S = 10^6$, $M_\theta = 0.009$

Effect of flows in different viscosity regimes

We begin by showing the effect of various kinds of flows and frequencies on the (1,1) mode. In the following, we see the effect of axial flow on the growth rate and frequency of the (1,1) mode in Fig. 5.10 and in Fig. 5.11 respectively. The symmetry of the growth rate curves as a function of the sign of flow is expected from our previous study of the RMHD equations.

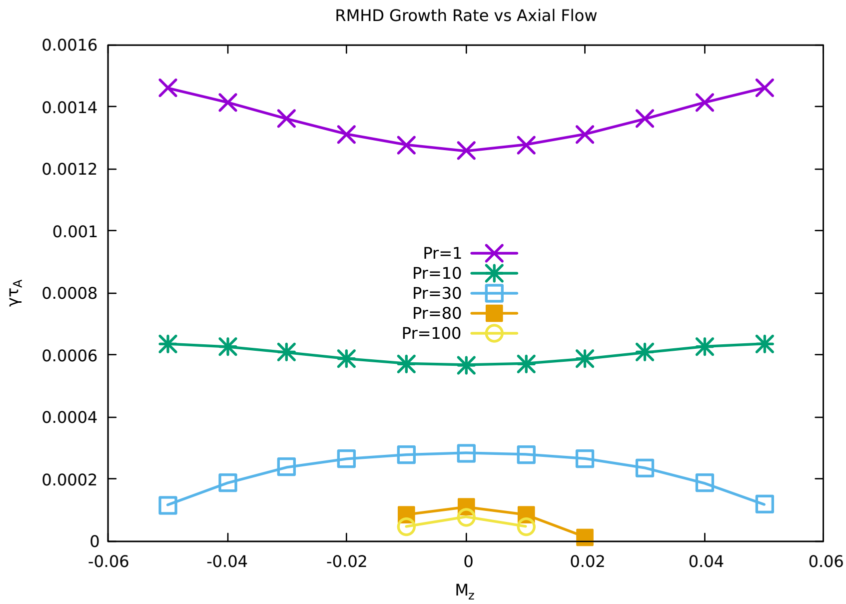

Figure 5.10: Growth rate vs Axial Mach Number

In the next figures, we describe the behaviour of the poloidal flow curves in the presence of flow. In Fig.5.12 we describe the variation of growth rate with poloidal flow. We observe a similar symmetry as in the case of axial flow. In the next Fig. 5.13 we describe the corresponding variation of frequency with flow. We notice it is a linear relationship.

After this, we describe the variation of the growth rates and frequencies in the presence of helical flow. In Fig. 5.14, we describe the growth rate of the (1,1) mode in the presence of helical flows. We see that the symmetry of the curves observed in the case of axial flows is broken in the presence of helical flow. In the next Fig. 5.15, we see that the frequency curve in the helical flow case is parallel to that in the axial flow case, and in fact the difference is equal to the amount of poloidal flow in the system.

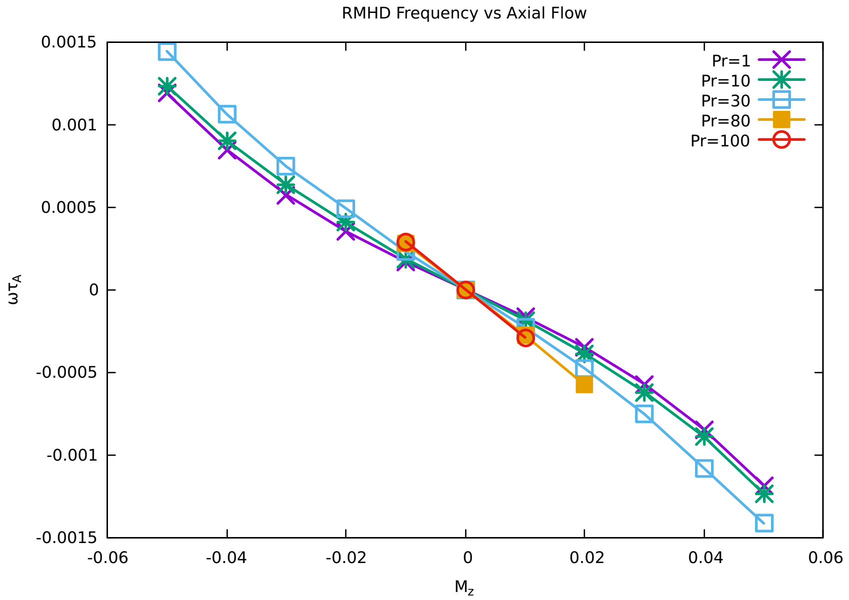

Figure 5.11: Frequency vs Axial Mach Number

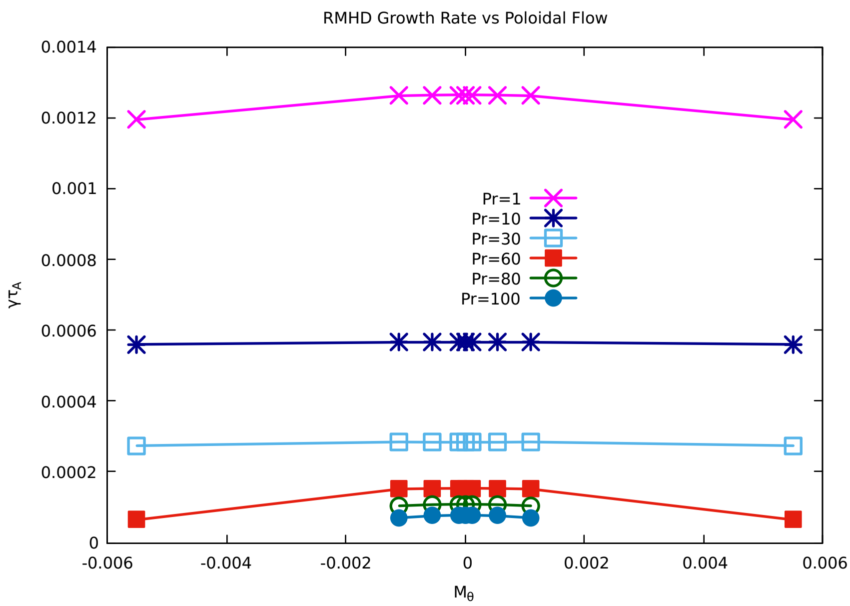

Figure 5.12: Growth rate vs Poloidal Mach Number

In Fig. 5.16, we compare the linear growth rate changes of the $m = 1, n = 1$ mode with axial and poloidal flows as we go from low to high viscosity. We note that the

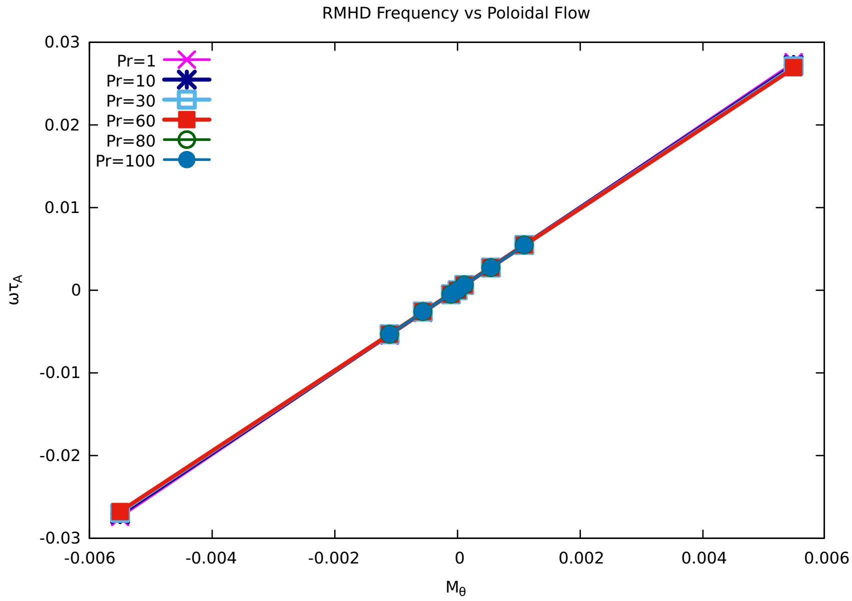

Figure 5.13: Frequency vs Poloidal Mach Number

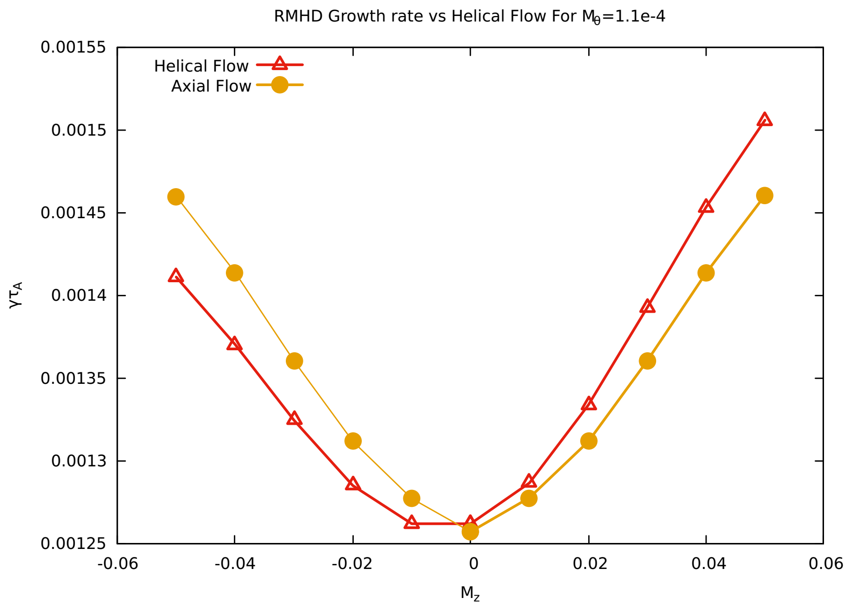

Figure 5.14: Growth rate vs Helical Mach Number

nature of stabilisation for axial flows changes as we increase the viscosity. While axial flows *destabilise* the mode at low viscosity, they *stabilise* it at higher viscosities. On the

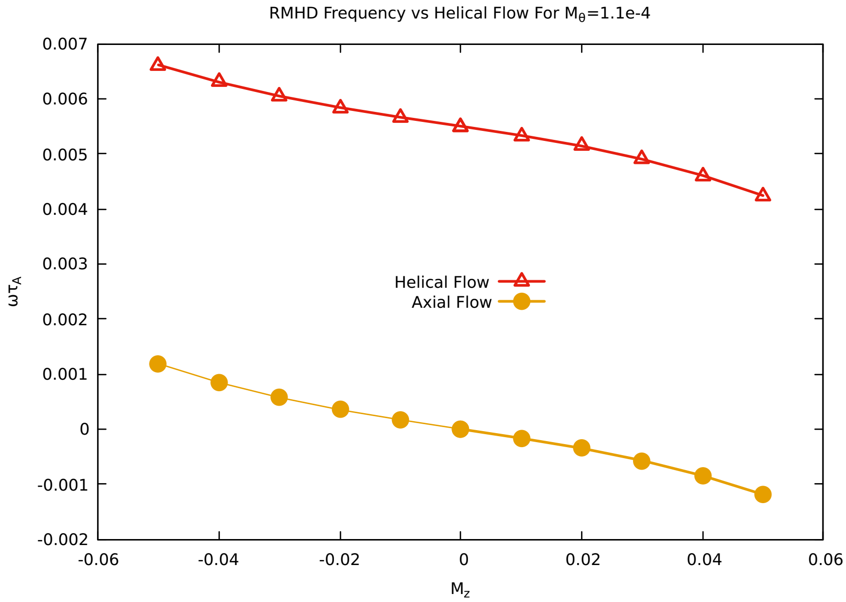

Figure 5.15: Frequency vs Helical Mach Number

other hand, we find the poloidal flow to be always stabilising in contrast to the no-flow case.

In Fig. 5.17, we have shown how the linear growth rate of the $m = 1, n = 1$ mode changes as we go from low to high axial flow shear, $\frac{a}{V_a}\frac{dv_{0z}}{dr}$, for different viscosity regimes. We see that for a fixed Pr, the nature of stabilisation of flow does not change with the amount of flow shear. However, the nature of stabilisation changes depending on the viscosity regime irrespective of the amount of flow shear.

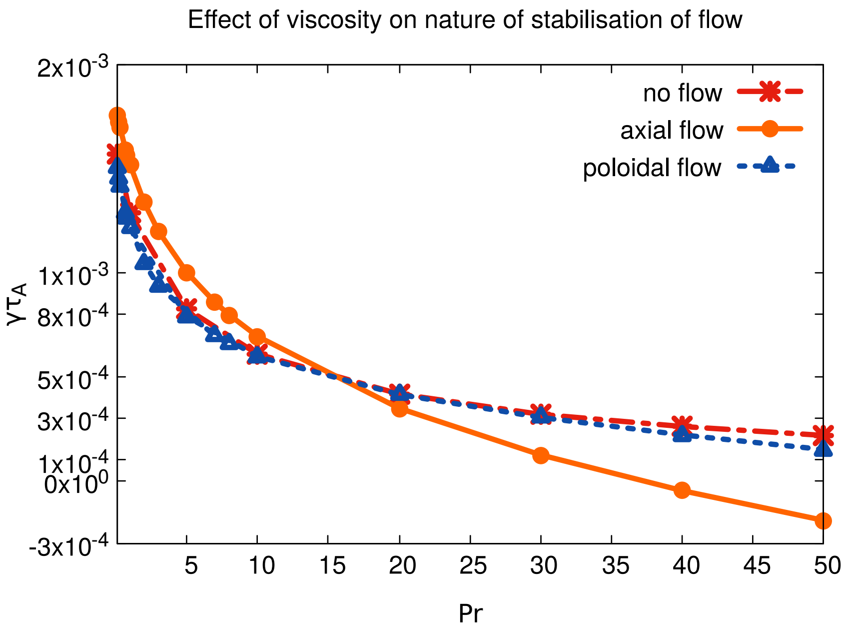

Figure 5.16: Effect of viscosity on the linear growth rate of the m=1, n=1 mode with and without axial flow at $S = 10^6$

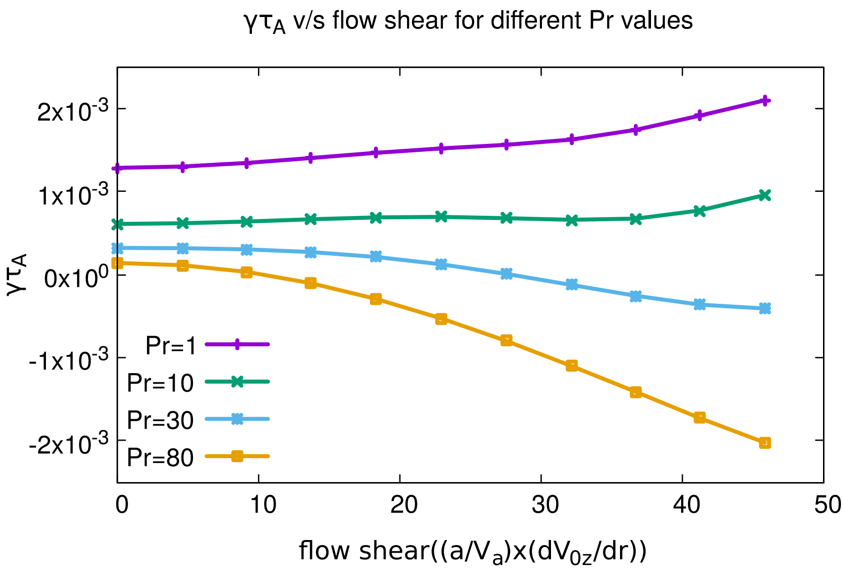

Figure 5.17: Linear growth rate of (1,1) mode v/s axial flow shear for different Pr values and $S = 10^6$

Nonlinear Results

Next we report on our nonlinear results for the (1,1) mode in the absence and presence of flows. We have continued with the same parameters and related profiles that we have used for the linear runs. Here, we have a slight difference in the method of calculation as compared to the linear case. We set up an equilibrium from the given initial parameters and in every iteration we solve both the mean, i.e., (0,0) Fourier components and the perturbed components. As a result, the equilibrium evolves with time, while in the linear case, the equilibrium was held fixed.

Axial flow

In this section, we describe the nonlinear evolution of (1,1) modes in the presence of axial flows. Here, two different flow profiles are employed to elucidate the dependence of the results on the profile. At first, to understand the effect of flow shear we have used a tanh flow profile. The form of the tanh profile has been described in section 5.2.1.1, but here we have used $M_z = 0.01$

Next, we use a Gaussian flow profile which is more realistic from an experimental point of view. This profile has the form (illustrated in Fig. 5.18) :

$$V_{0z}/V_A = M_z e^{-\rho^2} \tag{5.8}$$

where, ρ_{res} is the location of the mode resonant surface and $M_z = 0.05$.

The Figs. 5.19 and 5.20 illustrate the time evolution of $|\tilde{\psi}|_{max}$ with a tanh flow profile for $Pr = 100$ and $Pr = 30$ respectively. For the high viscosity case, we notice a strong stabilisation of the (1,1) mode in the presence of axial flow both in the linear growth rate as well as in the nonlinear saturation level. However, for the low viscosity case, there is a slight increase of nonlinear saturation level of the modes in the presence of axial flow. Similar to the linear runs, the nonlinear evolution runs also show the destabilising trend of the mode for lower viscosity and a stabilising influence for higher viscosity compared to the no flow case.

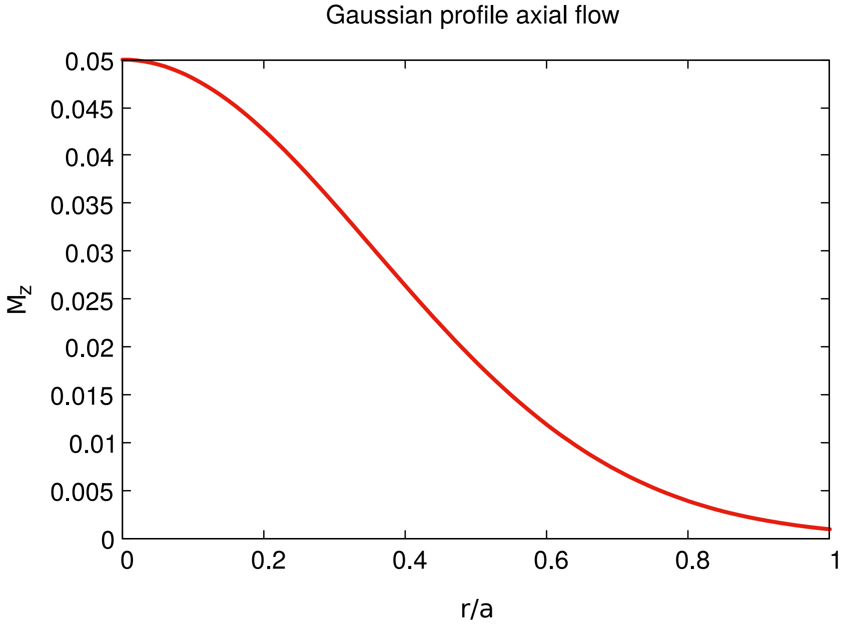

Figure 5.18: Axial flow profile(Gaussian profile)

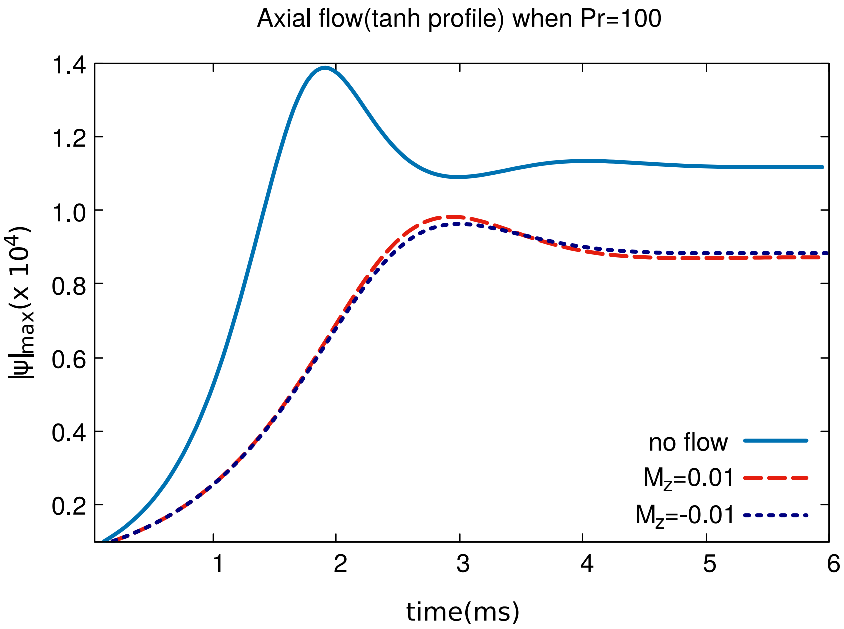

Figure 5.19: $|\tilde{\psi}|_{max}$ evolution with axial flow with tanh profile, $M_z = 0.01$, $Pr = 100$ and $S = 10^6$.

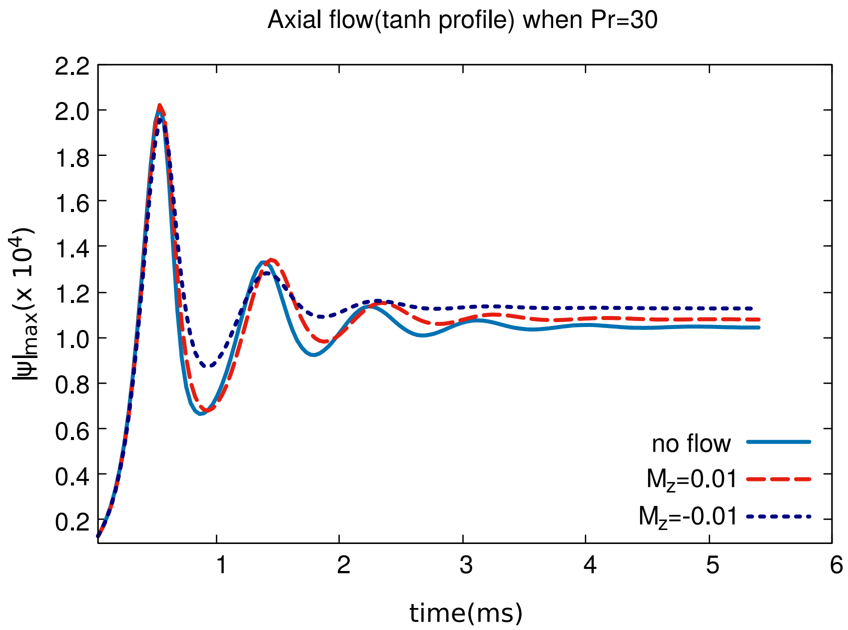

Figure 5.20: $|\tilde{\psi}|_{max}$ evolution with axial flow with tanh profile, $M_z = 0.01$, $Pr = 30$ and $S = 10^6$.

Figs. 5.21 and 5.22 show the nonlinear evolution of the mode with a Gaussian flow profile for $Pr = 100$ and $Pr = 30$ respectively. In this case, the nature of the effects is qualitatively similar to that of the tanh flow case. However, the changes in the growth rates compared to the no flow case are smaller even if the amount of flow is higher in this case. We have seen that even if the linear evolution does not depend on the sign of the flow, the nonlinear saturation levels of $|\tilde{\psi}|_{max}$ are different for different signs of flows except for the $Pr = 100$ tanh flow profile case(cf. Fig. 5.19), where the difference is very small.

Poloidal Flow

In Fig. 5.23, we display the effects of poloidal flow upon the nonlinear evolution of the amplitude of the (1,1) mode. Here, we notice that the poloidal flow stabilises the mode, and the final saturation levels are nearly equal for such small amounts of flow. For higher values of M_θ the saturation levels do differ significantly as a function of the direction of flow.

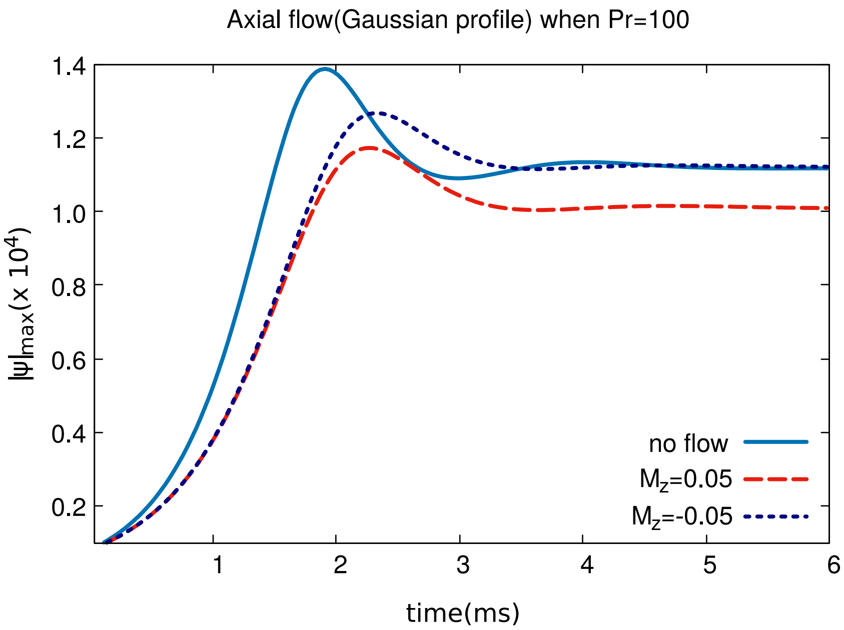

Figure 5.21: $|\tilde{\psi}|_{max}$ evolution with axial flow with gaussian profile, $M_z = 0.05$, $Pr = 100$ and $S = 10^6$.

We have repeated this study with a $Pr = 30$ in Fig. 5.24, and we notice here that the nonlinear saturated levels show a different behaviour from that at a higher Pr, in that poloidal flow now slightly destabilises the mode. The implication of this effect is clearly reflected for helical flows which we will discuss next.

Helical Flow

In this subsection we discuss the combined effect of axial and poloidal flows on the stability of the (1,1) mode. We have considered all four sign combinations of the axial and poloidal flows to understand the effect of flow helicity on the evolution of the mode. In Fig. 5.25, we show the effect of a sheared axial flow with a tanh profile combined with a sheared poloidal flow for $Pr = 100$. Here we can have two types of flow helicity depending on the signs of the axial flow and the poloidal flow. We find that although both the flow helicity cases impart a stabilising effect compared to the no flow case, the

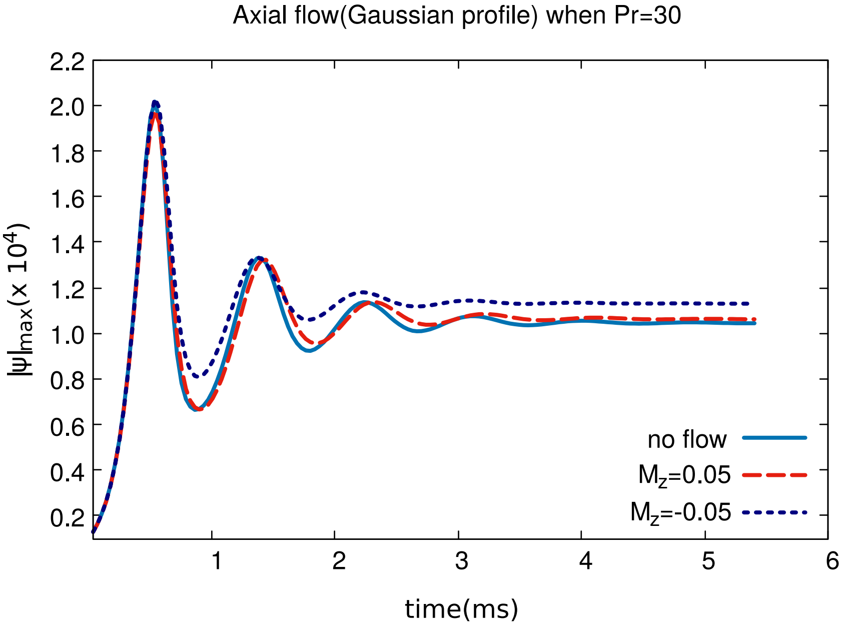

Figure 5.22: $|\tilde{\psi}|_{max}$ evolution with axial flow with gaussian profile, $M_z = 0.05$, $Pr = 30$ and $S = 10^6$

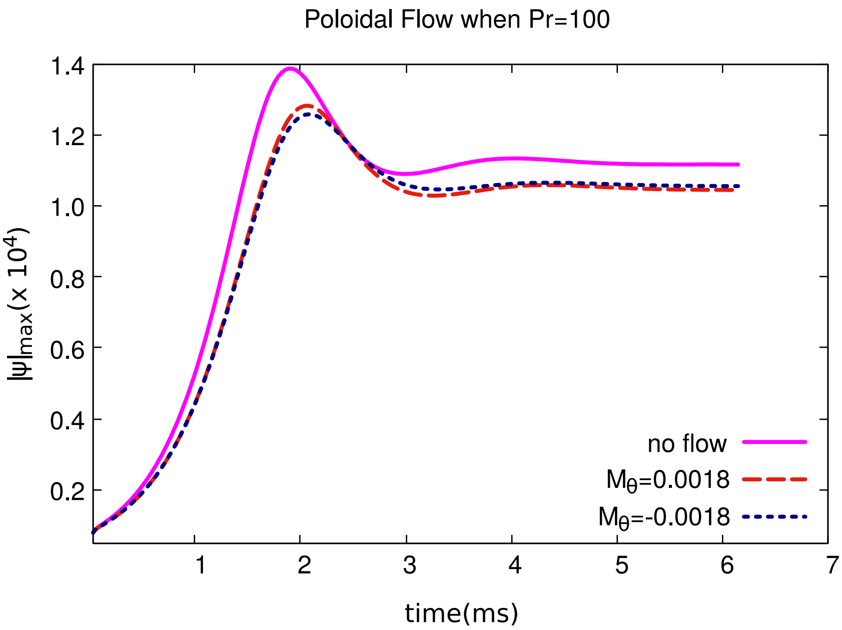

Figure 5.23: $|\tilde{\psi}|_{max}$ evolution with poloidal flow, $M_\theta = 0.0018$ $Pr = 100$ and $S = 10^6$.

degree of stabilisation is very different for different flow helicities. For example, having

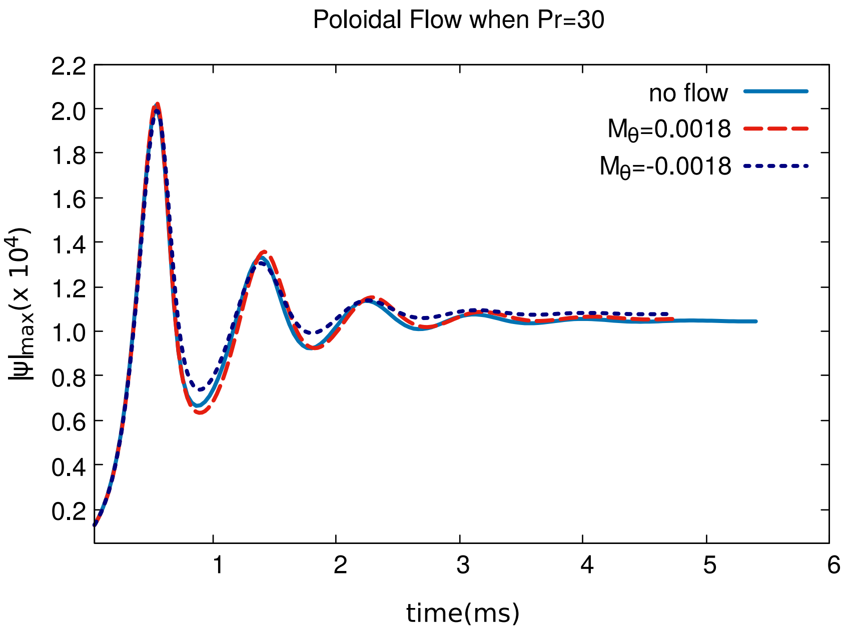

Figure 5.24: $|\tilde{\psi}|_{max}$ evolution with poloidal flow, $M_\theta = 0.0018$, $Pr = 30$ and $S = 10^6$.

kept the poloidal flow sign to be positive but changing the direction of the axial flow from positive to negative, both the linear growth rates and the nonlinear saturation levels have increased significantly to a much higher value. Thus, we find an asymmetry in the nature of the stabilisation of the (1,1) mode in the presence of helical flows that depends on the type of flow helicity. The change in the degree of stabilization for different helicities arises from the relationship between the flow direction and the direction of the magnetic field which essentially changes the relative sign between q'_{res} (the magnetic shear) and $v'_{0,res}$ (the flow shear) near the mode resonant surface [69].

We have carried out a similar study at a lower viscosity of $Pr = 30$ as shown in Fig. 5.26. Here, the nonlinear saturation levels in all flow cases are slightly higher compared to the no flow case. Also, the symmetry breaking for two different flow helicities are so small both in the linear and nonlinear regime that it cannot be distinguished from the figure, but can be distinguished from numerical values of the linear growth rates and nonlinear saturation levels. In fact, the symmetry breaking effect begins to manifest itself in the linear stage itself as can be clearly seen in the difference of the slopes of the time evolution of $|\psi|_{max}$ for the two helicities of the flow. A comparison of Figs. (5.25)

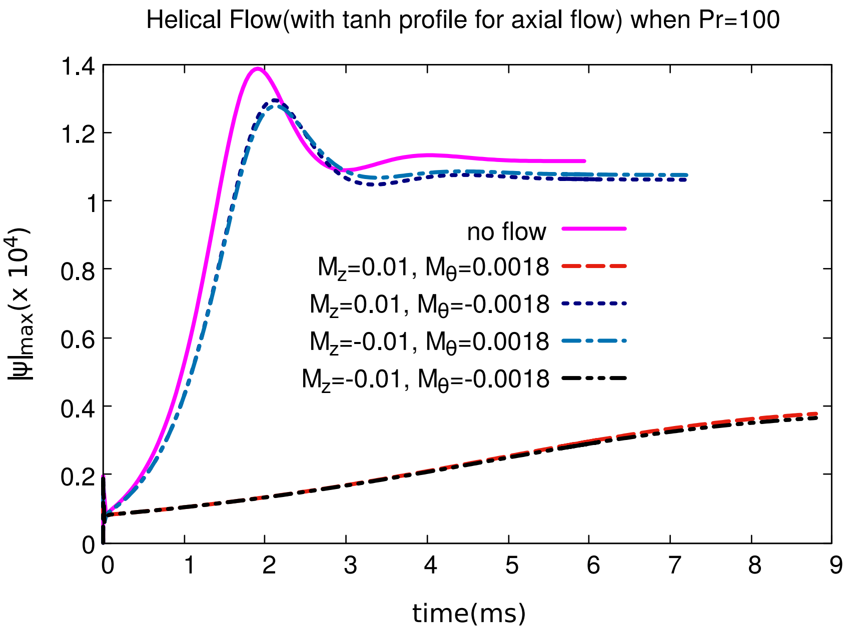

Figure 5.25: $|\tilde{\psi}|_{max}$ evolution with helical flow using tanh profile, $M_z = 0.01$, $M_\theta = 0.0018$, $Pr = 100$ and $S = 10^6$.

and (5.26) also raises the interesting question whether there occurs a “bifurcation” of the saturated states at some value of the Prandtl number between 30 and 100. To check this interesting question we have numerically determined the linear growth rates for a number of different magnitudes of the helical flow and plotted their values for two different helicities in Fig. (5.27). As can be clearly seen there is a continuous transition in the behaviour as a function of Pr that is indicative of an absence of any bifurcation phenomenon.

In Fig. 5.28 and Fig. 5.29, we have shown the effect of a sheared axial flow with a Gaussian profile combined with a sheared poloidal flow for $Pr = 100$ and $Pr = 30$ respectively. Here, we notice that the effects are very similar to the tanh flow case, but the changes in the linear growth rates and nonlinear saturation levels are relatively smaller.

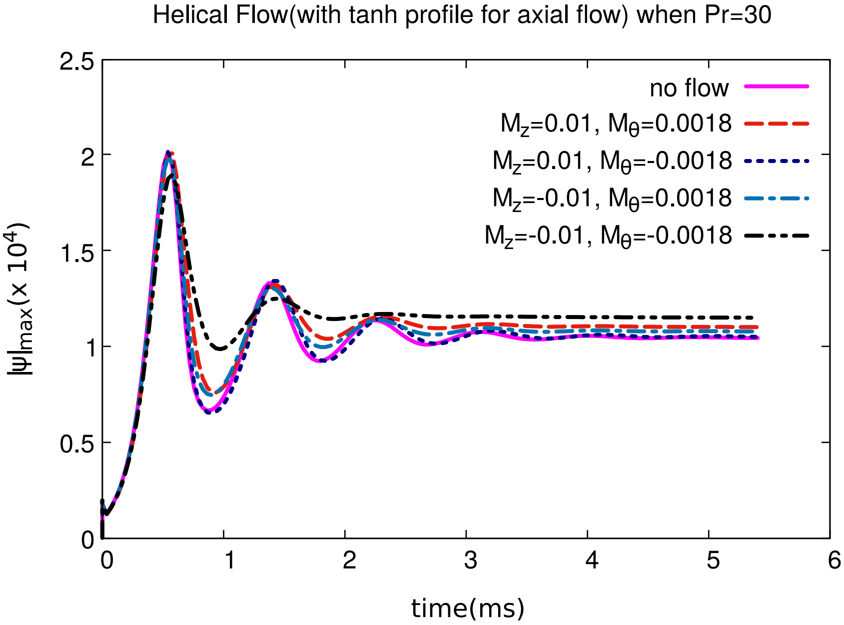

Figure 5.26: $|\tilde{\psi}|_{max}$ evolution with helical flow using tanh profile, $M_z = 0.01$, $M_\theta = 0.0018$, $Pr = 30$ and $S = 10^6$.

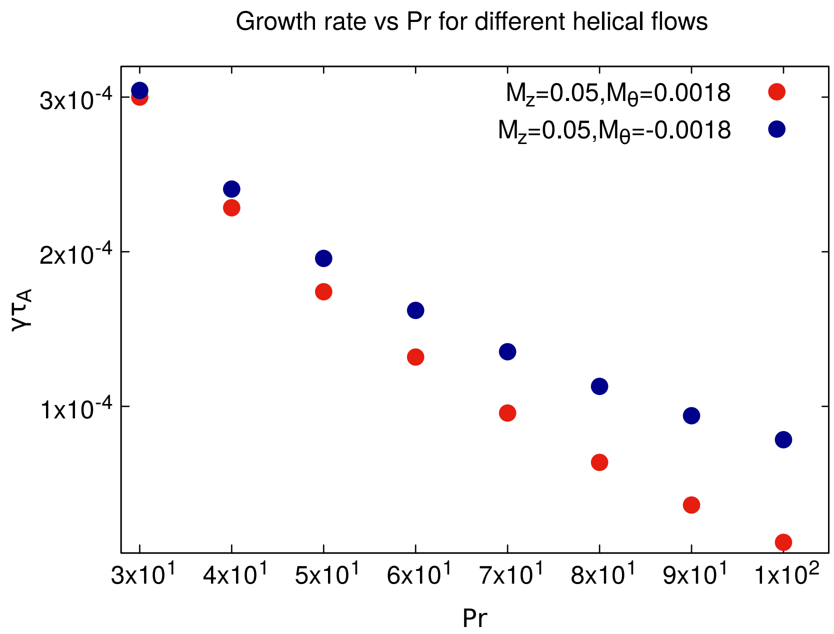

Figure 5.27: $|\tilde{\psi}|_{max}$ Linear growth rates with helical flows for different Prandtl numbers using tanh profile and $S = 10^6$.

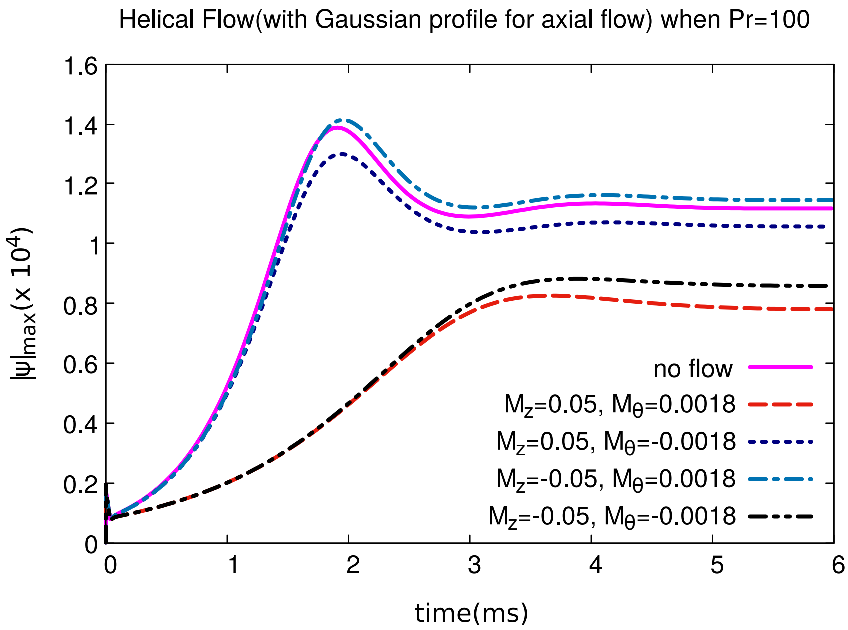

Figure 5.28: $|\tilde{\psi}|_{max}$ evolution with Helical flow using gaussian profile, $M_z = 0.05$,$M_\theta = 0.0018$, $Pr = 100$ and $S = 10^6$.

On comparison of the helical flow results obtained here with those using pure axial and poloidal flows, as discussed in the previous sections, there is no symmetry breaking in the linear growth rates of the (1,1) mode if we change the direction of the flow. However, there is a difference in the nonlinear saturation levels even for those cases where we use a pure axial or poloidal flow. This is due to the self-generation of nonlinear helical terms even if we start with pure flows, as discussed in Chandra et. al. [39].

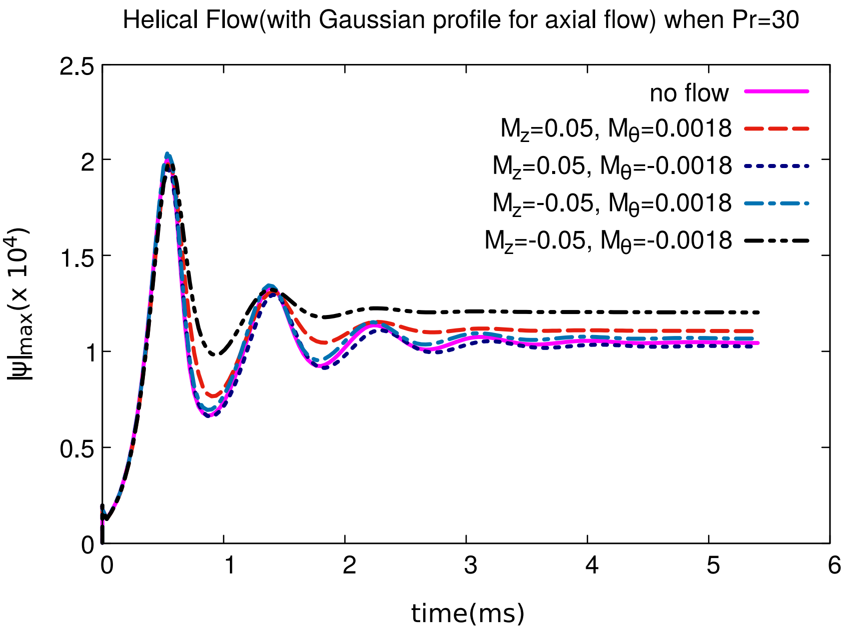

Figure 5.29: $|\tilde{\psi}|_{max}$ evolution with helical flow using gaussian profile, $M_z = 0.05$,$M_\theta = 0.0018$, $Pr = 30$ and $S = 10^6$.

Summary and Discussion

To summarise, we have carried out linear and nonlinear studies of the (1,1) resistive internal kink mode using a V-RMHD version of the CUTIE code, in a cylindrical geometry with periodic boundary conditions. We have studied the effect of equilibrium sheared flows on the (1,1) mode and the role of viscosity in modifying the effect of flows. Viscosity can be significantly enhanced due to turbulence in tokamaks and it is expected that the *Prandtl number* can be as high as 100 [17, 19] in advanced scenarios for JET and ITER.

Our results can be summarised as follows. In the linear regime our scaling studies in the absence of flow agree with analytical results in the literature[70]. The presence of poloidal flow does not change the linear scaling results but axial flows do bring about a significant change. We further find that the effect of viscosity on the growth rate of the mode can be significantly altered by the presence of flows. Helical flows exhibit a strong symmetry breaking with respect to the direction of the flow at high Pr but such an effect weakens at low Pr. In the nonlinear regime, for axial flows the saturation level of the mode decreases at a higher viscosity compared to the case of no flow but slightly increases at lower viscosity. Similar results are found for the poloidal flow case. In the case of helical flows at high viscosity, there is a significant change in the nonlinear saturation level depending on the flow helicity. Such an asymmetry effect is much weaker in the low viscosity case. It might be worth mentioning that similar asymmetric effects in the sawteeth time period have been observed in tokamak experiments with a change in the direction of the equilibrium flow induced by neutral beam injections[15, 58–60]. Our results can prove useful in developing appropriate theoretical models for sawteeth behaviour in the presence of sheared flows and high viscosity.

6

Two fluid studies of (1,1) mode

Introduction

In an advanced tokamak with high temperature plasma, sawtooth is a frequently observed phenomena. As core temperature increases, resistivity goes down which results in a higher current density in the core region. Simultaneously, the safety factor, q becomes less than one which triggers $m = 1$, $n = 1$ internal kink modes. As sawtooth has the capability to degrade the confinement of the plasma, so it is very important to understand its dynamics and how to control it. To do that, first we need to understand the $m = 1$, $n = 1$ mode, as it is closely associated with sawtooth, so it has been extensively studied in the past to understand its physics. Plasma rotation also is very common in a tokamak which gets generated either internally or gets induced externally, such as by NBI injection. It is also well known that plasma rotation can modify sawtooth dynamics[36, 39, 41, 47, 71]. There are several experiments such as NSTX [56, 57], JET [58, 59], MAST [15], TEXTOR[60] etc. which indicate there is a relation between sawtooth behaviour with the change of plasma rotation in a tokamak. Those experiments indicate that the flow, particularly the direction of the flow can either increase or decrease the sawtooth period, that is the stability of the kink mode can change depending on the direction of the flow. There are several past studies which have focused on the stability of the $m = 1$,$n = 1$ mode in the presence of flow. such as Guzdar et al[13] who have shown that toroidal sheared flow which is close to the acoustic speed in plasma can completely stabilise the (1,1) mode. In the work of Shumlak et al.[61], a stabilising effect due to a sheared axial flow on the (1,1) mode in a cylindrical Z-pinch has been found. Most of the past studies found stabilising effects of flow on the (1,1)

mode, but there are a few studies such as Gatto et al[62] and Brunetti et al [66], Crombe et al[72] which found that flow shear can have destabilising effect. Chapman et al[15] have suggested that sawteeth period asymmetry is related to the plasma flow direction with respect to the diamagnetic drift. In our earlier study, using a single fluid model we have observed that there is a similar symmetry breaking in the presence of helical flows. However, those single fluid studies do not include the diamagnetic flows which require a two fluid model. Diamagnetic flows can alter the dynamics of the mode, particularly in the presence of flows, for example, it can change the stability of the modes as well as change the mode rotation frequency of the system.
There has thus been intense research on two fluid models in the study of tokamak instabilities, particularly of the tearing and kink instabilities [73–77]. One of the earliest works in this topic has been by Thyagaraja et al[78], in which they have elucidated the necessary and sufficient conditions required for the existence of a nonlinearly saturated m = 1 tearing mode in tokamaks. In the paper of Barkov et al[73], they have studied the drift-kink instabilities using two fluid simulations and compared their accuracy to that of PIC methods and find good agreement. Zakharov et al[74] have studied the internal kink mode in the context of tokamaks. They study a scenario with a finite β and find that they have good agreement with kinetic studies. A validation study done using the NIMROD code has been carried out by Akcay et al[77]. Though we have several interesting results on the effect of flows on the dynamics of the $m = 1, n = 1$ internal kink modes with flows using a single fluid model, but those results can get modified in the two fluid regime. These motivate the extension of our earlier single fluid study[41] to a two fluid regime to understand the dynamics of the internal kink mode more deeply.

In this work, we have addressed this issue and investigated the stability of the (1,1) mode in the presence of sheared flows over a range of viscosity regimes using the CUTIE[35] code in the two fluid regime. Here we have taken a wide range of viscosity as it can be high in tokamak operations, possibly due to turbulent effects and could therefore modify the effect of flow shear on the stability of the internal kink mode [19, 41, 79] as observed earlier. There is a diamagnetic drift present in the two fluid regime, between the ion and electron fluid whose velocity is denoted by v_d and frequency is denoted by $\omega*$. In the two fluid model, the diamagnetic drift is proportional to the electron density gradient which is depending on α in our model where we have used a density profile of the form $n = n_0 exp(-\alpha \frac{r^2}{a^2})$, where n stands for density and r is the radial coordinate.

We have begun with linear studies which we have carried out using the Resolvent method, a method of finding eigenvalues, explained in the paper[39]. We have observed the modification of growth rate and the rotation frequency of the $m = 1$,$n = 1$ with different diamagnetic flow frequencies over a range of viscosities. Then we have applied pure axial, pure poloidal and helical flows, and studied the same for different combinations of flow magnitudes and directions. In all cases we have seen symmetry breaking with a reversal of flow direction. This symmetry breaking happens either in the presence of diamagnetic flow or by including parallel dynamics or both. However, these dynamics are significantly modified depending upon the viscosity regime. Then we have extended our work in the nonlinear regime and observed a nonlinear saturation level also getting similarly modified with diamagnetic flows, imposed flows, as well as viscosity. Both the linear and nonlinear results are very different as compared to similar studies in the RMHD regime [41]. We also notice that the poloidal flow is destabilising nonlinearly and linearly in some cases.

This paper is organised in the following manner. In section 6.2, we have described the two fluid model of plasma in a cylindrical geometry. In section 6.3, we have studied the effect of diamagnetic flows (1,1) mode in the linear regime without any imposed flows initially. After that, we have studied the behaviour of the mode with different types of flows We have done these studies both in the low and high viscosity regimes. In section 6.4 we have studied the (1,1) mode in the nonlinear regime in the absence of flow as well as in presence of axial, poloidal and helical flows. Section 6.5 provides a brief summary and a discussion of the results.

Model

We have previously published our investigations using a single-fluid incompressible version of the CUTIE code [41]. In the present version, our numerical investigations have been carried out in the framework of a two fluid model, containing a continuity equation for electron density and parallel momentum equation. We use a periodic cylinder geometry (ρ, θ, z),(ρ being the radial coordinate, θ being the azimuthal coordinate, and z being the axial coordinate) defined in terms of the minor radius, a, and the major radius, R_0 as follows: we set $\rho = r/a$, r being the radial distance, $0 \leqslant \rho \leqslant 1; 0 \leqslant \theta, \zeta \leqslant 2\pi$;$\zeta = z/R_0$, is analogous to the toroidal angle. This model thus includes drift effects of two fluid theory, containing density and parallel momentum effects in addition to the single fluid model. We utilise CGS electrostatic units. We have neglected curvature effects as we are using a large aspect ratio, and as in our previous work, toroidal coupling between different (m,n) modes is allowed. We use a constant, uniform axial magnetic field, while the poloidal component of the magnetic field is determined as we evolve the equations. We prescribe and hold fixed imposed equilibrium flows and density profiles. Also, plasma β is assumed to be low and other code parameters are chosen to be consistent with this assumption. A significant difference is that we allow the current profile to evolve in the nonlinear evolution. The equations in our model are as follows[36, 38]:

$$\frac{\partial n}{\partial t}+\nabla\cdot(n\mathbf{v})=S_p \tag{6.1}$$

$$m_i n\frac{d\mathbf{v}}{dt}=-\nabla p+\frac{\mathbf{j}\times\mathbf{B}}{c}+\mathbf{F}_{eff} \tag{6.2}$$

$$\frac{3}{2}\frac{dp_{i,e}}{dt}+p_{i,e}\nabla\cdot\mathbf{v_{i,e}}=-\nabla\cdot\mathbf{q_{i,e}}+P_{i,e} \tag{6.3}$$

$$\mathbf{E}+\frac{\mathbf{v_e}\times\mathbf{B}}{c}=-\frac{\nabla p_e}{en}+\mathbf{R_e} \tag{6.4}$$

$$\nabla\times\mathbf{B}=\frac{4\pi\mathbf{j}}{c} \tag{6.5}$$

$$\nabla\times\mathbf{E}=\frac{\partial\mathbf{B}}{\partial t} \tag{6.6}$$

It must be mentioned that the form of the source terms has been described in earlier papers[36, 38]. We use a reduced model for our present purposes We note here that $T_e=T_i=T_0$. We will introduce the dependent variables here, namely ϕ, the electrostatic potential, ψ, poloidal flux function, n_e, quasi-neutral electron number density, $v_\parallel$, parallel velocity. These are functions of r, θ, z, t, or in the reduced form ρ, θ, ζ and t as introduced above. We can write these by splitting the equilibrium and fluctuation parts, or in other words by Fourier analysing them and keeping the (0,0) component separate. In other words,

$$F(\rho,\theta,\zeta,t)=F_0(\rho,t)+\tilde{f}(\rho,\theta,\zeta,t) \tag{6.7}$$

Here,

$$F_0(\rho,t) = \int_0^{2\pi} \frac{d\theta}{2\pi} \int_0^{2\pi} \frac{d\zeta}{2\pi} F(\rho,\theta,\zeta,t) \tag{6.8}$$

and

$$\tilde{f}(\rho,\theta,\zeta,t) = \sum_m \sum_n \hat{f}_{m,n}(\rho,t)\, e^{i(m\theta+n\zeta)} \tag{6.9}$$

We also introduce the fundamental equilibrium quantities of the model: the axial magnetic field, $B_{tor} = B_\zeta = B_0$(uniform and constant),the safety factor, $q(\rho) = \rho\left(\frac{a}{R_0}\right)\frac{B_0}{B_{0\theta}(\rho)}$, equilibrium quasi-neutral electron density $n_0(\rho)$. They have the following profiles:

$$q(\rho) = q_0\left[1+\left(\frac{\rho}{\rho_0}\right)^{\Lambda}\right]^{1/\Lambda} \tag{6.10}$$

Fig. 6.1 shows the q profile used in the simulations and the q=1 surface.

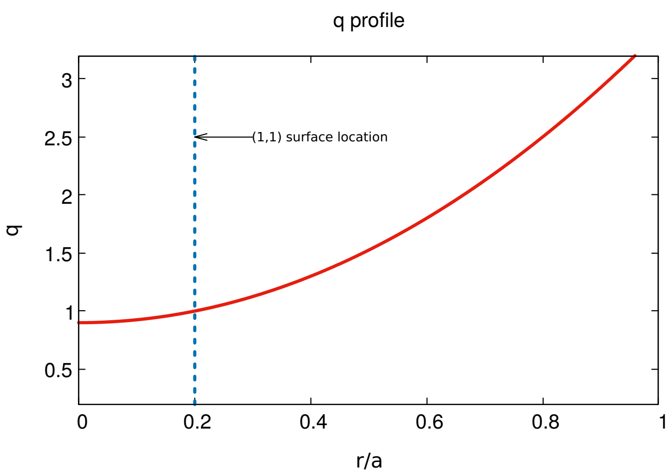

Figure 6.1: q profile

$$n_0(\rho) = n_0(0)\, e^{-\alpha\rho^2} \tag{6.11}$$

The values used for these parameters are as follows: $q_0 = 0.9$, $\Lambda = 1$, $\rho_0 = 0.6$, $T_0 = 275$eV, $B_0 = 2\times10^4$, $I_p = 29.4KA$ The α is proportional to the density gradient, and we vary it from $\alpha = 0$, which is the single fluid case, to $\alpha = 1.5$.

We will now write the equations for the fluctuating quantities. We keep in mind that the following variables are to be evolved:

- The fluctuating quantities, $\tilde{n}$, $\tilde{\phi}$,$\tilde{\psi}$, $\tilde{v}_{\|}$, $\tilde{W}$. Here, $\tilde{W}$ is the linearised 'potential vorticity'. The mean flows are held fixed, namely v_{z0} and $v_{\theta 0}$.
- The mean poloidal field $B_0(r,t)$ in the nonlinear case.

It is convenient to define the following time-scales which are relevant to our work: Alfvén time, Resistive time, Viscous diffusion time, as follows. $\tau_A = a/v_A$ is the Alfvén time; $\tau_\eta = (4\pi a^2/c^2\eta)$ the resistive diffusion time; $\tau_\nu = (a^2/\nu)$ the viscous diffusion time. We will use in the following the *Lundquist Number*, $S = \frac{\tau_\eta}{\tau_A}$, and the *Prandtl Number*, $Pr = \frac{\tau_\eta}{\tau_\nu}$. The velocity perturbations are non-dimensionalised relative to the Alfven speed, $v_A = \frac{B_0}{(4\pi m_i n_0)^{1/2}}$, and thermal velocity, $V_{TH} = \left(\frac{T_e(0,t)+T_i(0,t)}{m_i}\right)^{1/2}$. Additionally, $\rho_s = \frac{v_{th}}{\omega_{ci}}$, where, $v_{th}^2 = (T_{0i}+T_{0e})/m_i$, $\omega_{ci} = (eB_0/m_i c)$, with T_{0i}, T_{0e} being ion and electron temperatures respectively. m_i is the ion mass, e is the elementary charge. $\Phi_0(r), \Psi_0(r)$ denote the mean electrostatic and magnetostatic potentials respectively. The equilibrium axial and poloidal, sub-Alfvénic sheared flows are: $M_z = V_{0z}/v_A$ is the Axial Mach number; $M_\theta(\rho) = \rho\frac{a\Omega(\rho)}{v_A}$ is the poloidal Mach number.

These equations are rewritten in terms of the variables:

$$\tilde{W} = \rho_s^2 \nabla\cdot\left(\frac{n_0(\rho)}{n_0(0)}\nabla_\perp\tilde{\phi}\right) \tag{6.12}$$

$$\begin{aligned}
\frac{\partial\tilde{W}}{\partial t} + \mathbf{v_0}\cdot\nabla\tilde{W} + v_A\nabla_{\|}\rho_s^2\nabla_\perp^2\tilde{\psi} = & \\
& v_A\rho_s\frac{1}{r}\frac{\partial\tilde{\psi}}{\partial\theta}\frac{4\pi\rho_s}{cB_0}j_0' + v_{th}\rho_s\frac{1}{r}\frac{\partial\left(\tilde{\psi},\rho_s^2\nabla_\perp^2\tilde{\psi}\right)}{\partial(r,\theta)} + \\
& v_{th}\rho_s\left[\frac{1}{r}\frac{\partial\left(\tilde{W},\tilde{\phi}\right)}{\partial(r,\theta)} + \left(\frac{n_0(0)}{2n_0}\right)\frac{1}{r}\frac{\partial\left(\tilde{W},\tilde{n}\right)}{\partial(r,\theta)}\right] - \\
& \frac{\rho_s^2 W_0'}{r}\frac{\partial\tilde{\phi}}{\partial\theta} + \nu\nabla_\perp^2\tilde{W}
\end{aligned} \tag{6.13}$$

$$\frac{\partial\tilde{\psi}}{\partial t}+\mathbf{v_{e0}}\cdot\nabla\tilde{\psi}+v_A\nabla_{\|}\tilde{\phi}=v_A\left(\frac{n_0\left(0\right)T_{e0}}{n_0T^*}\right)\nabla_{\|}n^*+$$
$$\frac{v_{th}\rho_s}{r}\left[\frac{1}{r}\frac{\partial\left(\tilde{\psi},\tilde{\phi}\right)}{\partial\left(r,\theta\right)}+\left(\frac{n_0\left(0\right)}{2n_0}\right)\frac{1}{r}\frac{\partial\left(\tilde{\psi},\tilde{n}\right)}{\partial\left(r,\theta\right)}\right]+\frac{c^2\eta}{4\pi}\nabla_{\perp}^2\tilde{\psi} \quad (6.14)$$

$$\frac{\partial\tilde{n}}{\partial t}+\mathbf{u_{e0}}\cdot\nabla\tilde{n}+v_A\nabla_{\|}\rho_s^2\nabla_{\perp}^2\tilde{\psi}=$$
$$v_{\rho s}\frac{1}{r}\frac{\partial\tilde{\psi}}{\partial\theta}\frac{4\pi\rho_s}{cB_0}j_0^{'}+v_{th}\rho_s\frac{1}{r}\frac{\partial\left(\tilde{\psi},\rho_s^2\nabla_{\perp}^2\tilde{\psi}\right)}{\partial\left(r,\theta\right)}+$$
$$v_{th}\rho_s\frac{1}{r}\frac{\partial\left(\tilde{n},\tilde{\phi}\right)}{\partial\left(r,\theta\right)}+$$
$$v_{th}\rho_s\left(\frac{n_0^{'}}{N^*}\right)\frac{1}{r}\frac{\partial\tilde{\phi}}{\partial\theta}-$$
$$v_{th}\nabla_{\|}\tilde{\xi}+D\nabla_{\perp}^2n^* \quad (6.15)$$

$$\frac{\partial\tilde{\xi}}{\partial t}+\mathbf{u_0}\cdot\nabla\tilde{\xi}+v_{th}\nabla_{\|}\tilde{n}=$$
$$\left(\frac{n_0(r)v_{\|0}^{'}}{n_0(0)}\right)\rho_s\frac{1}{r}\frac{\partial\tilde{\phi}}{\partial\theta}+v_{th}\rho_s\frac{1}{r}\frac{\partial\left(\tilde{\xi},\tilde{\phi}\right)}{\partial\left(r,\theta\right)}-$$
$$v_{th}\rho_s\beta^{1/2}\left(\frac{p_0^{'}}{P^*}\right)\frac{1}{r}\frac{\partial\tilde{\psi}}{\partial\theta}-v_{th}\rho_s\beta^{1/2}\frac{1}{r}\frac{\partial\left(\tilde{p},\tilde{\phi}\right)}{\partial\left(r,\theta\right)}-$$
$$v_{th}\left(\frac{n_0}{N^*}\right)+\chi\nabla_{\perp}^2\tilde{\xi} \quad (6.16)$$

Equation[6.12] is the Poisson relation for our system. Equation[6.13] is the vorticity equation, where $\tilde{W}$ is the perturbed vorticity. Equation[6.14] describes the evolution of the perturbed poloidal flux function $\tilde{\psi}$. Equation [6.15] describes density evolution and equation [6.16] describes the evolution of parallel momentum. Here, $\mathbf{u_0}=-\frac{cE_{r0}}{B}\mathbf{e}_\theta+\mathbf{b_0}v_{\|0}$ is the equilibrium 'MHD' flow, and $\mathbf{u_{e0}}=-\frac{cE_{r0}}{B}\mathbf{e}_\theta+\mathbf{b_0}\left(v_{\|0}-j_{\|0}/en_0\right)$ is the corresponding electron flow. The ion flow alone is given by $\mathbf{v_0}=\mathbf{u_0}+\frac{c}{en_0B}T\frac{\partial n_{io}}{\partial r}\mathbf{e}_\theta$, here due to quasi-neutrality $n_{i0} \sim n_{e0}$ and $\mathbf{v_{e0}} = -\left[\frac{cE_{r0}}{B} + \frac{c}{en_0 B} T \frac{\partial n_{e0}}{\partial r}\right] \mathbf{e}_\theta$ is the total electron poloidal flow composed of the electron $\mathbf{E} \times \mathbf{B}$ equilibrium flow and the electron diamagnetic flow. Also, we have $N^* = n_e(0,t)$, $T^* = T_e(0,t) + T_i(0,t)$, $\tilde{\xi} = N^* V_{TH}$. The resistivity η and viscosity ν are specified quantities and are held constant during our calculations. In particular, we use the self-consistent formulation whereby $\eta(r)æ_{0z}(r) \equiv E_{0z} \equiv \frac{V_{loop}}{2\pi R_0}$, where the specified q profile and B_0 are used to get j_{0z} initial profile. After this, we hold the profile and the value of $\eta(0)$ fixed throughout both linear and nonlinear calculations. We also have, $D_{res} = \frac{c^2\eta(r)}{4\pi}, \nu \equiv D_{visc} \equiv Pr.D_{res}$, therefore,

$$Pr \equiv \frac{D_{visc}}{D_{res}} \tag{6.17}$$

is the Prandtl number, which we have introduced earlier. We can therefore we see that kinematic viscosity ν and η share the same radial profile and are invariant in time.

This comes from

$$\frac{\delta \mathbf{E}}{B_0} = -\nabla\tilde{\phi} - \frac{1}{c}\frac{\partial \tilde{\phi}}{\partial t}\mathbf{e}_\zeta$$

where, $\mathbf{E}$ is the electric field, ϕ is the electrostatic potential, and $\mathbf{B_0} \simeq B_{0z}\mathbf{e}_\zeta + B_{0\theta}(\rho)\mathbf{e}_\theta$ is the equilibrium field. The fluctuating electric field, δE, is related to $\tilde{\phi}$ [this has dimensions of length]. We use, $\varepsilon = a/R_0$, the inverse aspect ratio, $v_0 = V_{0z}(\rho)\mathbf{e}_\zeta + a\rho\Omega(\rho)\mathbf{e}_\theta$.

The magnetic field perturbations are normalised by the equilibrium axial magnetic field B_{0z}. The fluctuations of magnetic field and velocity are incompressible in the $(r-\theta)$ plane. The temperatures are measured in energy units, i.e, electron volts. Also, we have used fixed boundary conditions, along with a conducting boundary, which means that all the variables are zero at $\rho = 1$. Additionally, regularity considerations mean that at $\rho = 0$, the fluctuations approach zero, and we have set the plasma edge at $\rho = 0.95$. We have used the Fourier representation for the purpose of periodicity of the angular coordinates.

Together, these equations constitute the four field model we use and we solve them using the CUTIE (**CU**lham **T**ransporter of **I**ons and **E**lectrons) code [35, 39], a nonlinear, global, electromagnetic, quasi-neutral, two fluid initial value code. It has been used earlier for studies of kink modes, tearing modes, ELMs, L to H transitions, internal transport barriers and other problems [35, 36, 39–41].

We briefly describe the numerical details of our investigations. We have used a spatial resolution of 1801 radial grid points, 9 poloidal, 5 toroidal Fourier modes for the linear runs made with the resolvent code[39], a version of CUTIE which is an eigenvalue solver, and is equivalent to the evolutionary version, and helps to find additional eigenvalues, as the evolution version only finds the fastest growing mode. In the nonlinear case, we reduce the radial grid to 101 points, due to limited computational resources. In the nonlinear cases, the error in growth rate thus introduced is not significant as we are more concerned with nonlinear saturated energy levels, a high accuracy in growth rate to many decimal places does not yield any additional information given the approximations in our model.

Results of linear simulations

No flow simulations

We have carried studies without imposed flow,which means that in these runs we have no imposed flows, *i.e.*, $v_{0\theta} \equiv v_{0\zeta} \equiv 0$, in particular, we have studied the variation of mode frequency as a function of Pr, and have compared it against the calculated $\omega*$ frequency for a given density gradient. We have calculated the $\omega*$ frequency using the following formula:

$$\omega* = -\frac{cT}{eB_0}\left[\frac{1}{n_e}\right]\frac{dn_e}{dr}\left[\frac{m}{r}\right](rad/s) \tag{6.18}$$

Here, $T = 275eV$, $B = 2\times10^4 gauss$, $e = 4.8\times10^{-10}$ stat.coul, $c = 3\times10^{10}$ cm/s $\frac{cT}{eB} = 1.37\times10^6 cm^2/s$, $\frac{1}{n_e}\frac{dn_e}{dr} = -2\alpha\left(r/a^2\right)$. Substituting these values, we obtain,

$$\omega * \tau_A = 1.255\times\alpha\times10^{-3} \tag{6.19}$$

We note the values of the following parameters used in our runs: $v_A = 2.18\times10^8$ cm/s, $\beta = 1.6\%$,$\tau_A = 4.58\times10^{-8}$,$\tau_\eta = 4.58\times10^{-2}$ and $\tau_v = Pr\times\tau_\eta$, the value of Pr is specified where used. In the following Fig. 6.2 we have showed a typical profile for D_{res}, and since $D_{visc} = Pr\times D_{res}$, thus it has the same profile because Pr is constant in our model.

The eigenvalue version of CUTIE, called Resolvent-CUTIE was used to compute these linear results[39].

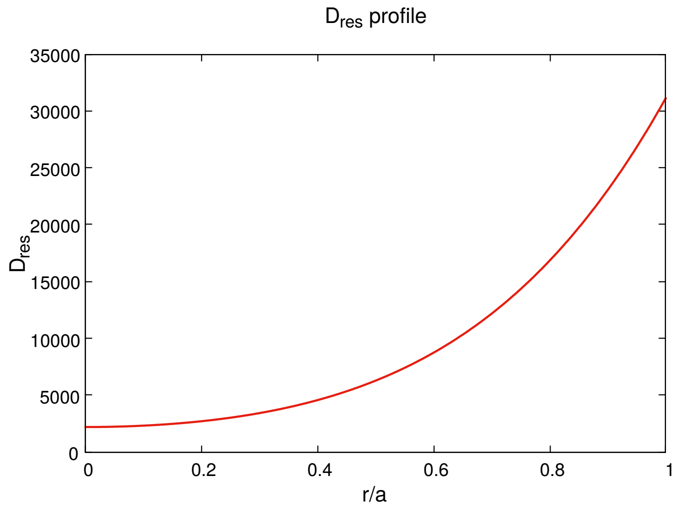

Figure 6.2: D_{res} profile

Our results are plotted as follows in Fig. [6.3] and Fig .[6.4].

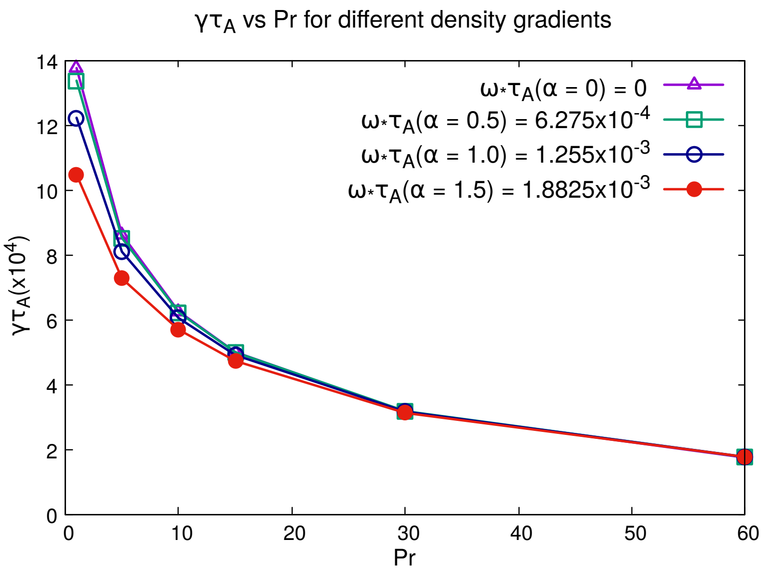

Figure 6.3: Growth rate variation with Pr without flow

In figure [6.3], we notice that the growth rate reduces smoothly with Prandtl number, Pr, as expected that higher viscosity reduces the growth rate. We observe that in the high *Pr* regime, the relative growth rates of the modes change as compared to those at a lower

Pr, that is the growth rate of modes with a higher α is slightly higher than that of those with a lower α.

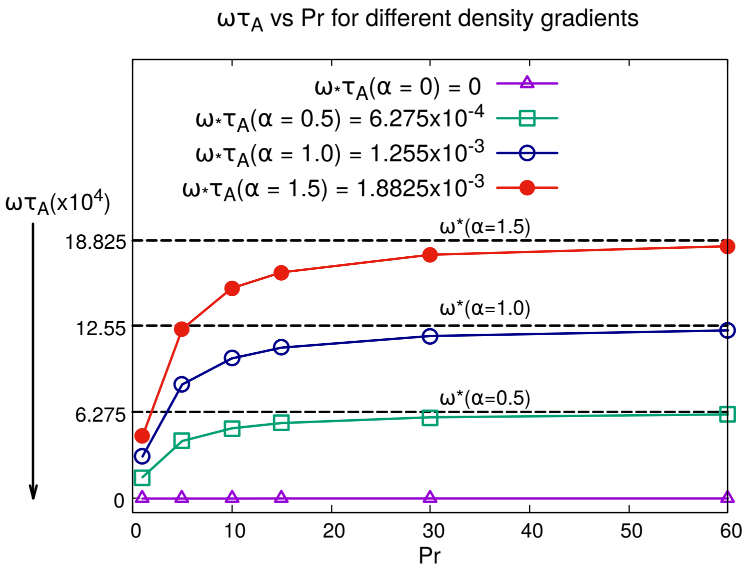

Figure 6.4: Frequency variation with Pr without flow

In figure [6.4] we see that the frequency of the mode approaches the $\omega*$ frequency as we increase Pr asymptotically. An increase in viscosity is correlated with an increase the mode frequency. There is a similar finding over a smaller range of Pr in the paper of Porcelli et al[80]. Also, the frequency increases until it reaches the $\omega*$ frequency. This suggests a complicated relationship between Pr and mode frequency, that the viscosity not only stabilises the mode but also has a reactive component that increases frequency. We also note that the growth rate is almost independent of α once Pr exceeds 15, and for $Pr > 1$ the viscous diffusion layer becomes larger than the resistive layer.

Simulations with imposed flow

Axial Flows

We have used an imposed axial flow profile of the form

$$V_{0z}/V_A = M_z tanh(\rho - \rho_s) \tag{6.20}$$

where, V_{0z} is the imposed axial flow velocity, V_A is the Alfvén velocity, M_z is the axial Mach Number, $\rho = \frac{r}{a}$, is the normalised radial coordinate r being the radial coordinate and a being the minor radius, and $\rho_s = \rho$ when $r = r_s$ is the resonant radius. In this section and henceforth we refer to the $q = 1$ resonant radius as $\rho_{q=1}$.

The following Fig. 6.5 is a typical profile for V_{0z},

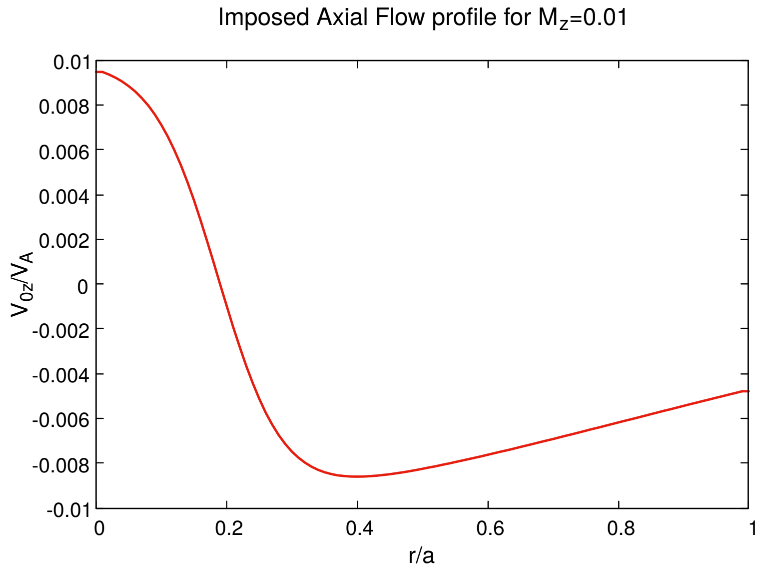

Figure 6.5: Imposed axial flow profile

This profile is chosen to have the property of zero flow at the resonant surface, so we can study the effect of shear alone at the resonant surface on the mode. We state the values of $\omega_*(\alpha)\tau_A$ as a function of α as given in Eqn. 6.19 for convenience:

Table 6.1: Value of $\omega_*(\alpha)\tau_A$

α	$\omega_*(\alpha)\tau_A \times 10^{-4}$
0.5	6.275
1.0	12.25
1.5	18.82

We have studied the reduced growth rate and frequency variation of the internal kink mode in two ways. We have studied the variation of reduced growth rate for different

α values, in Fig. 6.6. In the Fig. 6.6, we observe that the growth curves exhibit a very interesting behaviour, in that, for a pure RMHD case, we obtain symmetry of the reduced growth rate curve about $M_z = 0$, that is changing the sign of M_z does not change the reduced growth rate, but here we see a distinct asymmetry. This is due to the contributions of the parallel momentum and electron continuity equations. We have done a study by eliminating the parallel momentum equations, and setting $\alpha = 0$; in this case, we recover RMHD behaviour.

In a similar manner, in Fig. 6.7, which shows the corresponding variation of real frequency with M_z for different values of α, we observe a similar asymmetry of frequency about $M_z = 0$. This can be attributed to ω_*-related contributions to the frequency of the mode, apart from the rotation caused by the axial flow. However, here all the curves are approximately parallel to each other, unlike in the growth rate case.

In Fig. 6.8 we plot mode reduced growth rate as a function of the axial flow Mach number, M_{0z}, for a given $\omega_*(\alpha = 1.5) = 1.8825 \times 10^{-3}$ for different Pr values, at a fixed α. In the Fig. 6.8, the $\omega * \tau_A$ is fixed and corresponds to $\alpha = 1.5$. It is seen that the curves are qualitatively different for $Pr = 15$ and higher, and upon further investigation, we have found that the behaviour seen for $Pr = 1$ continues upto $Pr = 8$, and after that the curve changes its shape. This suggests a transition in the behaviour of the mode with respect to the viscosity(i.e. Pr alone is changed) when imposed flows exist.

In Fig. 6.9, we plot the real frequencies corresponding to the growth rates shown in Fig. 6.8. It is clearly seen that, as before, $Pr = 1$ frequency variation with M_z is different from those for $Pr = 15$. It is also seen that the real frequencies increase with Pr.

In summary, we see a very strong asymmetry in the reduced growth rates as a function of the sign of M_z.This is because a self consistent poloidal flow is generated by the diamagnetic drift. The frequencies show a similar profile as a function of M_z, which is unlike what we observe for the reduced growth rates. This is probably due to the fact that the ω_* is independent of the axial flow and depends only on the density gradient in the linear regime. We then have the case of varying Pr for a fixed, finite density gradient. In this case, we observe that while low Pr increases the reduced growth rate, high Pr reduces it, consistent with our observations in the RMHD case. The shape of the curves for the $Pr = 1$ case surprisingly is very different than for the other Pr's, which seems to indicate a threshold in Prandtl number after which the behaviour of the mode changes. The frequency also shows similar trends, and it seems to be the case that frequency and viscosity are not directly proportional, contrary to the expectation that viscosity being dissipative in nature should gradually reduce the frequency, but in fact increases it up to a certain limit.

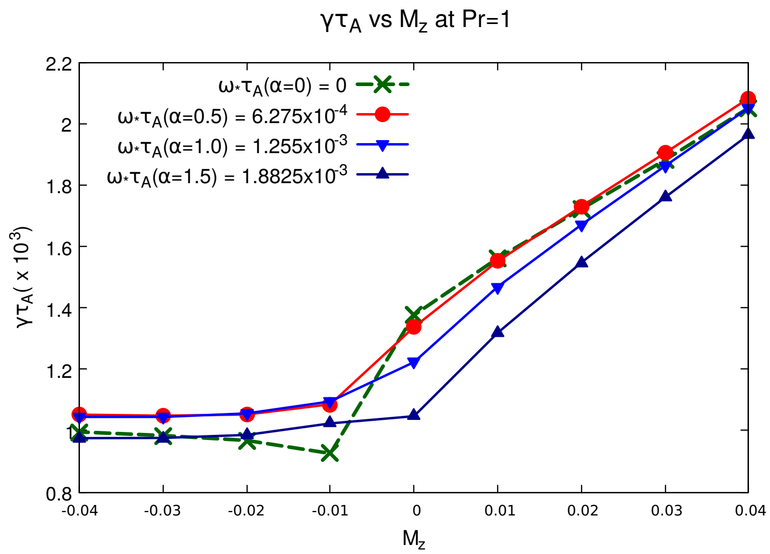

Figure 6.6: Reduced growth rate vs Axial Flow(Axial Mach Number) for different density gradients at a fixed Pr=1

Poloidal flow

We have used the following purely poloidal imposed flow profile,

$$\frac{V_{0\theta}}{v_A} = M_\theta(\rho) \tag{6.21}$$

where the poloidal Mach number,

$$M_\theta(\rho) = \rho \frac{a\Omega(\rho)}{v_A}$$

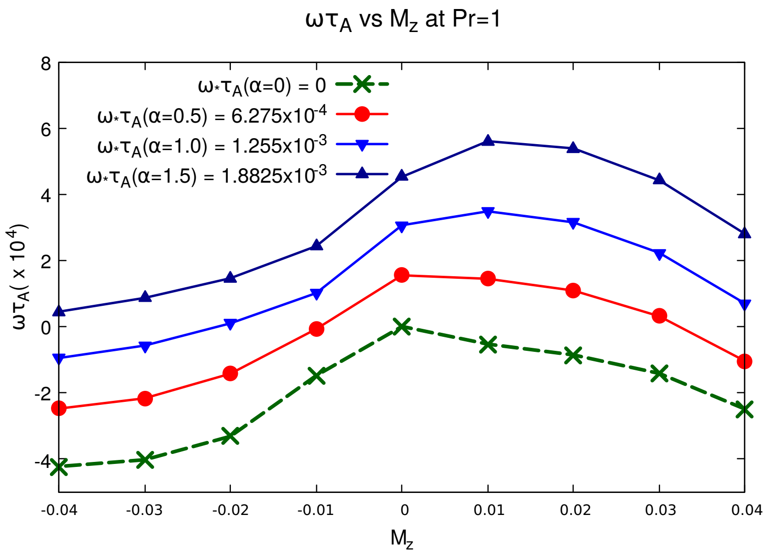

Figure 6.7: Frequency vs Axial Flow(Axial Mach Number) for different density gradients at a fixed Pr=1

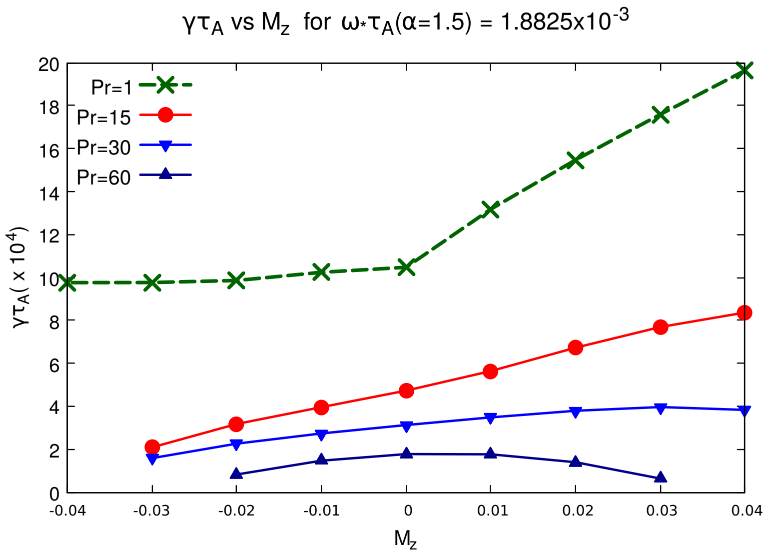

Figure 6.8: Reduced growth rate vs Axial Flow(Axial Mach Number) for different Pr at a fixed density gradient

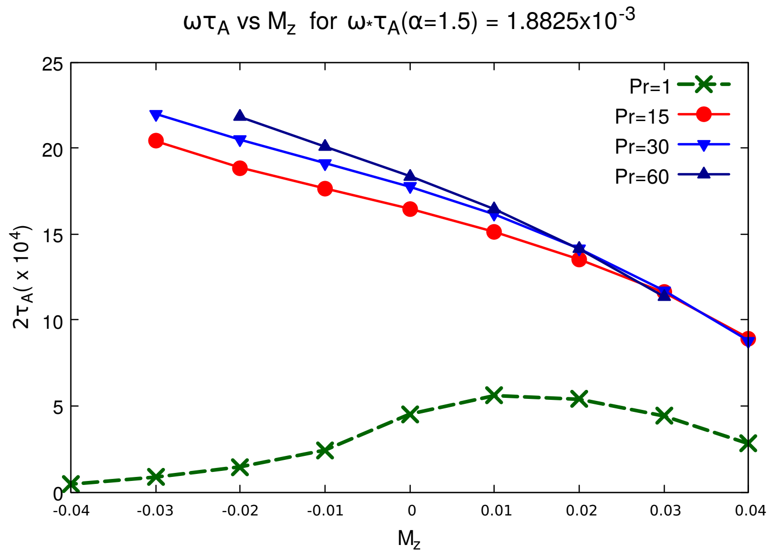

Figure 6.9: Frequency vs Axial Flow(Axial Mach Number) for different Pr at a fixed density gradient

and

$$\Omega(\rho) = \left(1-\rho^2\right)^2$$

Here, $V_{0\theta}$ is the equilibrium poloidal flow, and $\Omega(\rho)$ is the poloidal angular frequency at $\rho = r/a$. The following Fig. 6.10 is a typical flow profile:

In Fig. 6.11, we have plotted mode reduced growth rate vs poloidal flow for different density gradients at a fixed Pr. In the Fig. 6.11, we see that poloidal flow is stabilising the mode with increasing $M_\theta\left(\rho_{q=1}\right)$ and decreases it in the negative direction. This is consistent with our finding that there is a positive $\omega_*\tau_A$ present in the system, thus it adds when the flow is positive, stabilising the mode, and cancels when the flow is negative, so the mode gets destabilised. We see further evidence of this in the $\alpha = 0$ curve which is symmetric when the sign of $M_\theta\left(\rho_{q=1}\right)$ is changed.

Our hypothesis is further strengthened by observing Fig. 6.12 where we see that the frequencies vary linearly with $M_\theta\left(\rho_{q=1}\right)$, and the curves for different $\omega_*\tau_A$, i.e., α values are parallel to each other.

In Fig. 6.13, where we have plotted reduced growth rates vs $M_\theta\left(\rho_{q=1}\right)$ for different Pr at a fixed α. We notice that the trend for $Pr = 1$ in Fig. 6.13 is qualitatively dif-

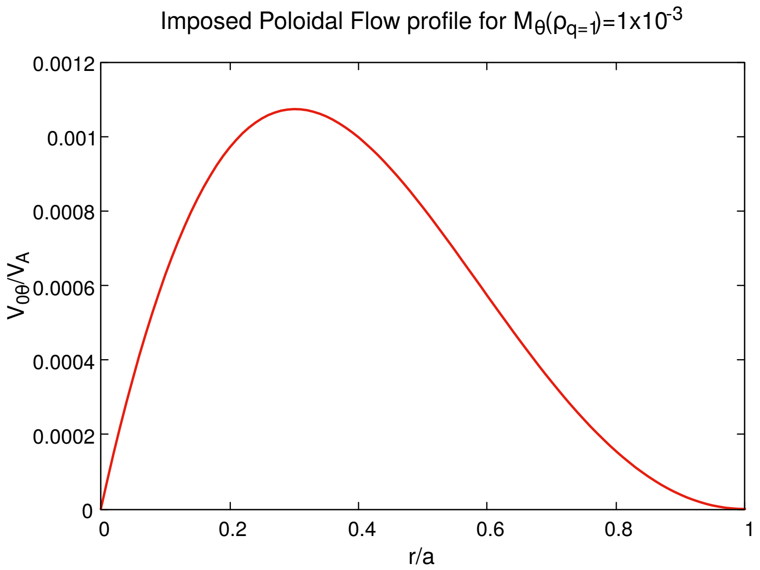

Figure 6.10: Imposed poloidal flow profile

ferent from the other curves, but not substantially so. In the case of the corresponding frequency curve in Fig. 6.14, we notice similarly that the $Pr = 1$ curve is parallel from the other curves, which are almost overlapping. This is also consistent with our Fig. 6.4, where the frequency actually rises with Pr.

In conclusion, we notice that the reduced growth rates are symmetric in the case of $\alpha = 0$ as function of the sign of M_θ, which is consistent from what we see in the RMHD case. After we introduce a finite α, we see curves which are broadly parallel, indicating a fixed ω_* in the system. Importantly, therefore, unlike in the axial flow case, the system is symmetric as a function of poloidal flow. The frequencies confirm this, being linear functions of $M_\theta\left(\rho_{q=1}\right)$ and are parallel for different values of α. When we vary Pr for a fixed α, the curves display broadly the same shape, indicating that Pr does not affect poloidal flow in an asymmetric fashion as it did in the case of axial flow. The frequencies in this case show an expected increase in frequency with Pr as we observed in the benchmarking section.

Helical Flow

In this section we discuss helical flow results. Helical flows are a combined effect of axial and poloidal flows. We have used a fixed poloidal flow of $M_\theta\left(\rho_{q=1}\right)$, without loss of generality as our results are similar when we change the sign of the poloidal flow.

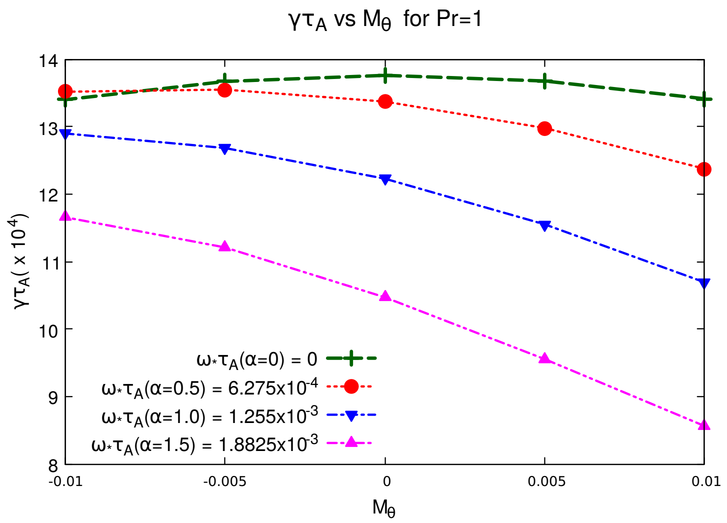

Figure 6.11: Reduced growth rate vs Poloidal Flow(M_θ $(\rho_{q=1})$) for different density gradients at a fixed Pr=1

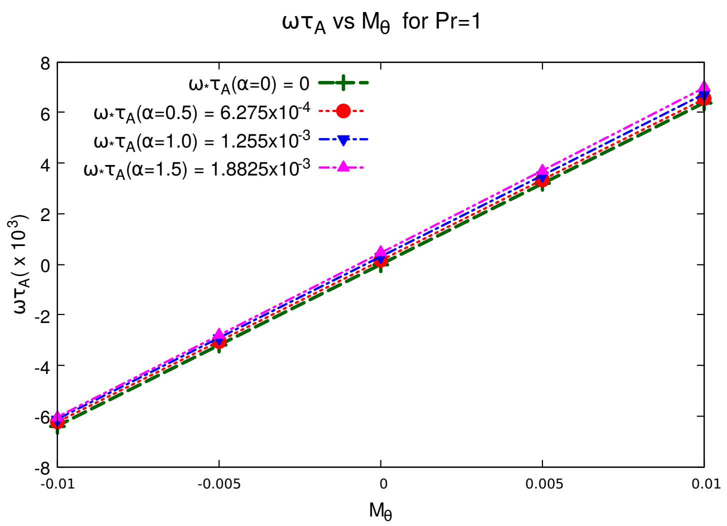

Figure 6.12: Frequency vs Poloidal Flow(M_θ $(\rho_{q=1})$) for different density gradients at a fixed Pr=1

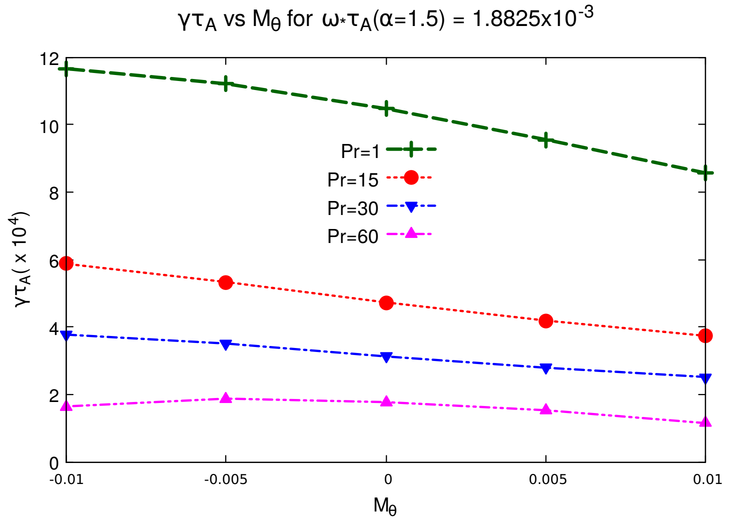

Figure 6.13: Reduced growth rate vs Poloidal Flow($M_\theta\,(\rho_{q=1})$) for different Pr at a fixed density gradient

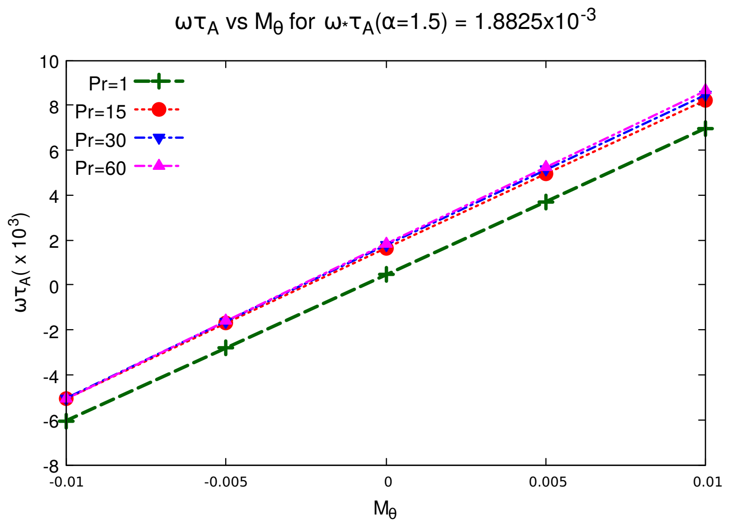

Figure 6.14: Frequency vs Poloidal Flow($M_\theta\,(\rho_{q=1})$) for different Pr at a fixed density gradient

The two fluid has an intrinsic poloidal flow present, and its behaviour is at variance from helical flow V-RMHD results. In the V-RMHD case [41], we have an asymmetry in the effect of the helical flows. The present case is considerably more complicated as it there are both imposed axial and poloidal flows, in addition to the intrinsic poloidal flows. In Fig. 6.15, we observe the variation of mode reduced growth rate with increasing axial flow while keeping poloidal flow constant, for different density gradients at a fixed Pr, the difference between the reduced growth rates trends is significant. The trends show a similarity to the axial flow case, but the big difference is that for $\alpha = 0$, the curve nearly coincides with $\alpha = 0.5$, for M_z negative, showing the strong influence of poloidal flow in modifying the behaviour of the mode here. The other curves are parallel to each other, instead of coinciding as in the case of pure axial flow. The frequency curves in Fig. 6.16 show a similar trend to the corresponding pure axial flow case, 6.7, however, the frequency curves have a greater distance between them, showing that the poloidal flow has increased mode frequencies, and contributed to symmetry breaking.

In Fig. 6.17 we present the variation of reduced growth rate with Pr. We observe a similarity with the corresponding axial flow case Fig. 6.8, with the addition of poloidal flow only changing the relative distance between the curves. This indicates that the axial flow dominates the dynamics in the case of using combined imposed flows. However, the effect of poloidal flows is also noticeable, despite being minor.

A similar situation is noticed in the case of Fig. 6.18, which is very similar to 6.9, showing that the axial flow dominates the dynamics of the system. The frequency curves are very similar, and the addition of imposed poloidal flow has only seemed to slightly widen the distance between the curves.

In conclusion, we have discussed the effects of imposing an axial and poloidal flow simultaneously on the (1,1) kink mode. We see that overall, axial flow dominates the dynamics, but poloidal flow has a smaller but noticeable effect. The figures are very similar to those obtained with a pure axial flow in the system.

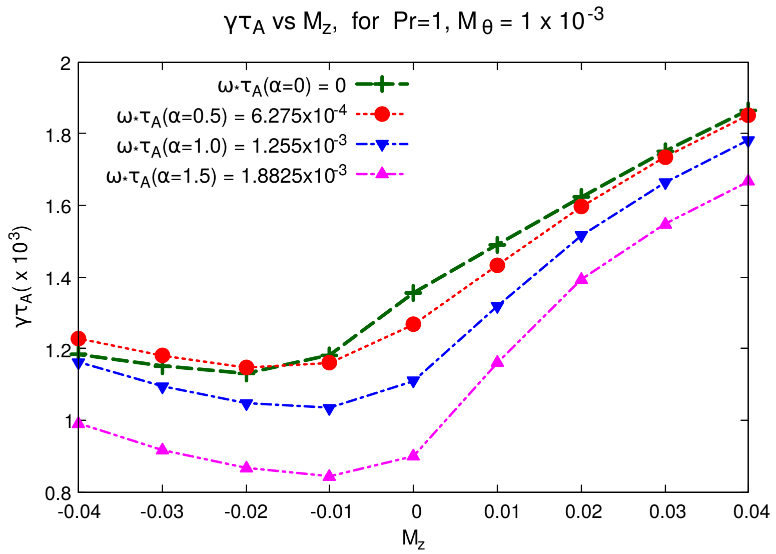

Figure 6.15: Reduced growth rate vs Helical Flow(M_z,fixed M_θ $(\rho_{q=1}) = 1 \times 10^{-3}$) for different density gradients at a fixed Pr=1

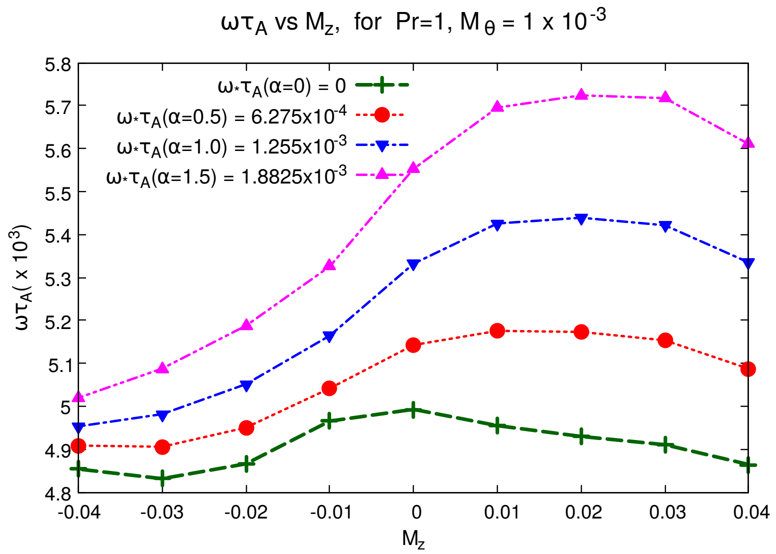

Figure 6.16: Frequency vs Helical Flow(M_z,fixed M_θ $(\rho_{q=1}) = 1 \times 10^{-3}$) for different density gradients at a fixed Pr=1

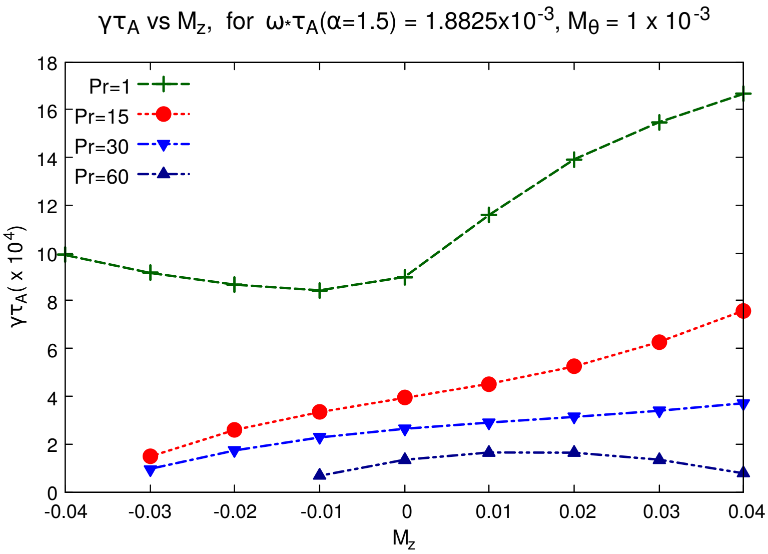

Figure 6.17: Reduced growth rate vs Helical Flow(M_z,fixed M_θ $(\rho_{q=1}) = 1\times10^{-3}$) for different Pr at a fixed density gradient

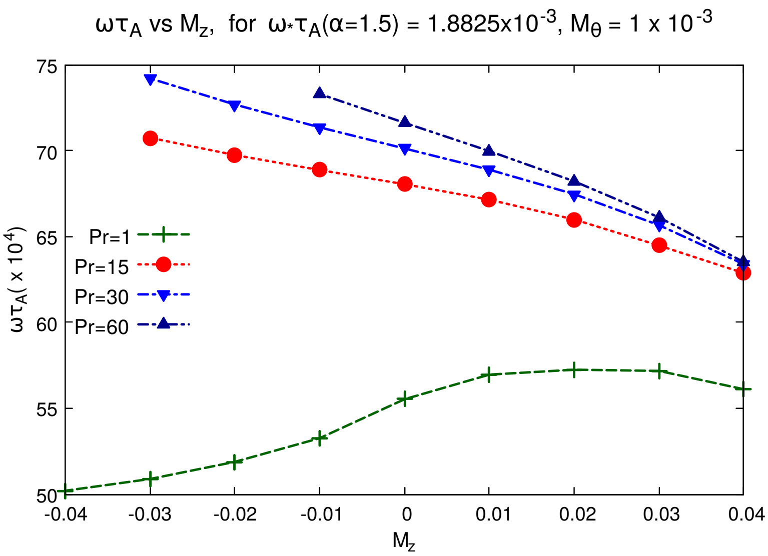

Figure 6.18: Frequency vs Helical Flow(M_z,fixed M_θ $(\rho_{q=1}) = 1\times10^{-3}$) for different Pr at a fixed density gradient

Nonlinear Studies

We present results of our nonlinear simulations in this Section. The nonlinear results here differ from the nonlinear results we obtained in our V-RMHD case[41]. It is worth mentioning here that the nonlinear results differ from the linear in a non trivial sense, which is to say, due to the coupling of the equations, it is not possible to isolate the effect of the individual nonlinear terms. There is an interaction of the nonlinear terms, which cannot be captured by an asymptotic analysis, and a full solution yields results qualitatively different from what an asymptotic analysis would yield. Therefore a numerical solution of the equations is the only way we can understand the true dynamics of this system. There is a discussion about these issues in Thyagaraja et al[35]. Profile-fluctuation interactions as described are the strength of the CUTIE code, and enables us to understand the long term evolution of the visco-resistive modes better. Further, in our system nonlinear mode coupling is allowed but we have held the profiles of the equilibrium flows constant during the evolution. We describe below the variation of the energy levels at saturation as a function of Pr. We observe that at low Pr, the general trend is that the saturated energy level increases with α, and also as a function of Pr. At a high Pr, here $Pr > 15$, we see that the saturated energy levels fall with increasing α.

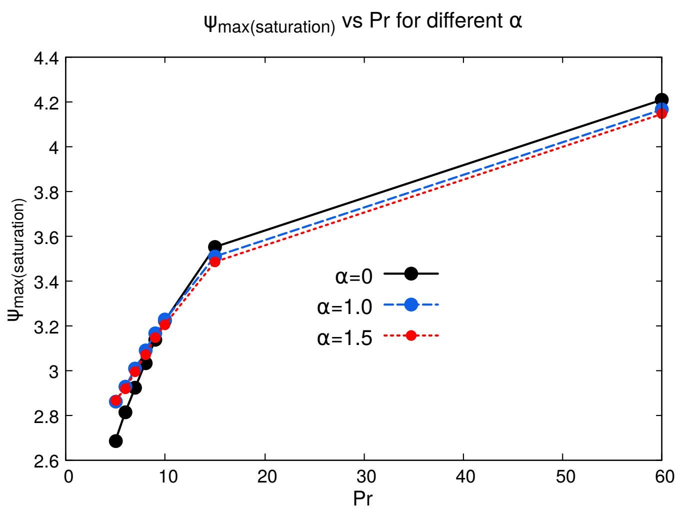

Figure 6.19: $|\psi_{max}|$ $(|\frac{dBr}{(B_0)^2}|)$ at saturation vs Pr for different α, and thus corresponding $\omega_* \tau_A(\alpha) = 1.255 \times \alpha \times 1 \times 10^{-3}$

The nonlinear runs presented in this section were all carried out with a $\alpha = 1.5$, thus the $\omega_* \tau_A(\alpha) = 1.8825 \times 1 \times 10^{-3}$. In Fig. 6.20, we observe the nonlinear evolution of $|\psi|$, for the case with imposed axial flow with a fixed Mach number but opposite directions in comparison with the no flow case for $Pr = 15$. We notice that positive axial flow leads to a higher initial rise of magnetic fluctuation amplitude as compared to the no flow case, followed by certain oscillations leading to a higher saturation amplitude. The situation is reversed with a negative axial flow, leading to a lower saturation level than the no flow case.

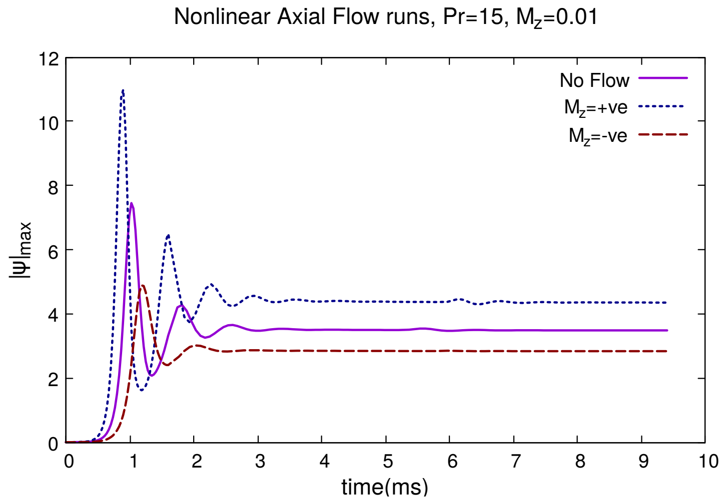

Figure 6.20: Nonlinear Axial Flow results for Pr=15

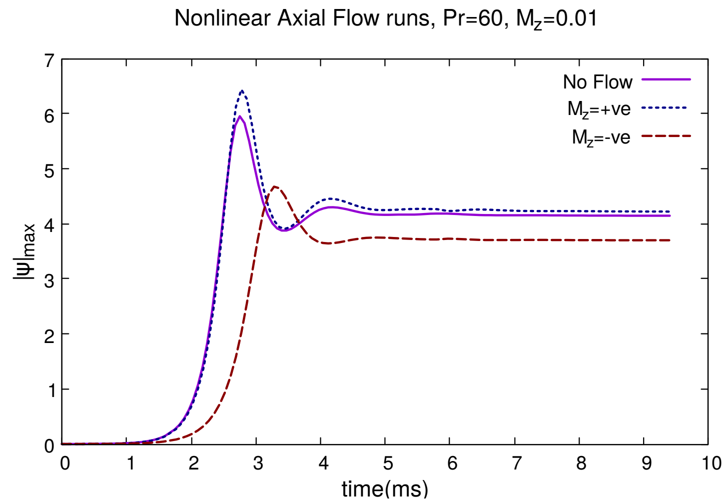

Figure 6.21: Nonlinear Axial Flow results for Pr=60

In the Fig. 6.21, we examine the case when we change the Pr to 60. As opposed to

$Pr = 15$, at the higher viscosity, positive flow hardly differs form the no imposed axial flow case, whereas the saturated amplitude is significantly lower than the no flow case. However, the saturated amplitudes in Fig. 6.21 are higher than the corresponding in Fig. 6.20, consistent with Fig. 6.19. If we compare these results with our previous results with V-RMHD, we see that in the V-RMHD case, at low viscosity, axial flow cases had higher linear growth rates and saturated amplitudes than the no flow case. However, the high viscosity case, there at $Pr = 100$, look similar to the high viscosity case here at $Pr = 60$.

In the next figure, Fig. 6.22 we observe the nonlinear evolution of $|\psi|$, for the case with imposed poloidal flow with a fixed Mach number, $M_\theta\left(\rho_{q=1}\right) = 1\times10^{-3}$ but opposite directions in comparison with the no flow case for $Pr = 15$, we examine the cases with an imposed poloidal flow. Here, the negative imposed poloidal flow case shows destabilisation, that is the saturated amplitude and linear growth rate is higher than the no flow case. It is the opposite for case with imposed positive poloidal flow, the saturated amplitudes and linear growth rates are lower than the no flow case but to a lesser extent.

For the $Pr = 60$ case, in Fig 6.23 we observe that the positive flow exhibits similar behaviour as in Fig. 6.22 but the negative flow has also shown stabilisation, that is a smaller saturated amplitude than the no flow case, but very slightly, as compared to the larger stabilisation shown in the positive flow case.

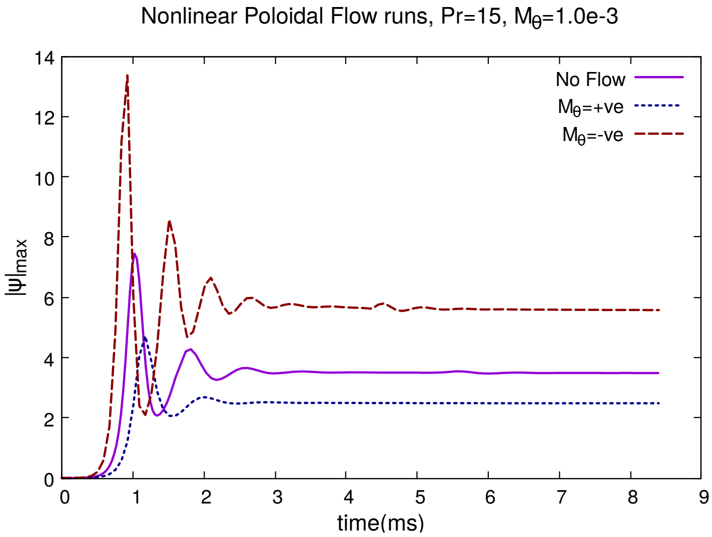

Figure 6.22: Nonlinear Poloidal Flow results for Pr=15

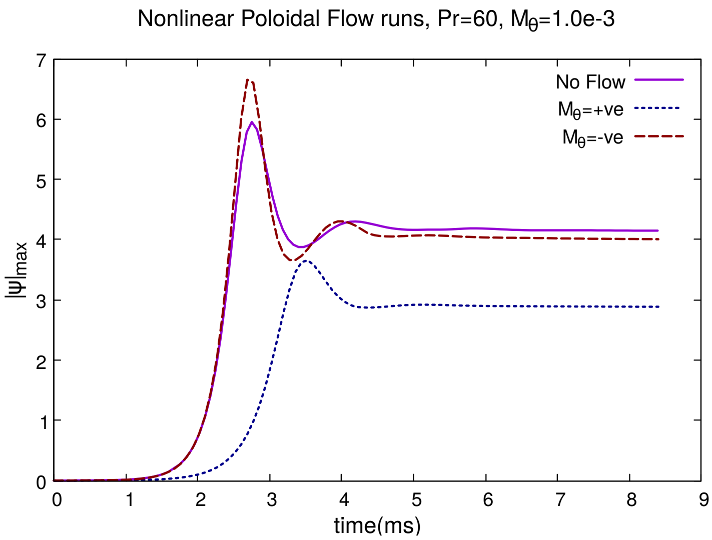

Figure 6.23: Nonlinear Poloidal Flow results for Pr=60

Finally, we turn to the cases with combined imposed flows. In Fig. 6.24, where we observe the nonlinear evolution of $|\psi|$, with helical flows, that is, we use the positive and negative combinations of a fixed axial Mach number $M_z = 0.01$ and poloidal Mach number $M_\theta\left(\rho_{q=1}\right) = 1\times10^{-3}$. This results in four case, as there are two cases each of axial and poloidal flow. An examination of the Fig. 6.24 shows us that it exhibits features of both the nonlinear axial flow Fig. 6.20 and Fig. 6.22 for the same Pr. We notice an asymmetry having runs with two helicities destabilised, that is, with higher saturated amplitudes, and two cases more stable than the no flow case. As in Fig. 6.22, the cases with $M_\theta\left(\rho_{q=1}\right)$ positive are stabilised and vice versa. Negative axial flow is stabilising and positive axial flow destabilises if we fix the poloidal flow. This is similar qualitatively to what we had seen in Fig. 6.20. This also indicates that the intrinsic poloidal flow and imposed poloidal flow have the same effects on the mode and it is the overall poloidal flow, the sum of both which affects the linear and nonlinear characteristics of the mode. In the V-RMHD, we had obtained a destabilisation in all cases of imposed helical flow, unlike the present case which is more complicated.

The behaviour of the mode in the presence of helical flow in Fig. 6.25 similarly exhibits the features of Fig. 6.21 and Fig. 6.23. Here, for positive poloidal flow, positive axial flow is destabilising but for negative poloidal flow, negative axial flow is destabilising. Conversely, for a fixed negative axial flow, positive poloidal flow is stabilising while for a fixed positive axial flow, positive poloidal flow is destabilising. In comparison to the $Pr = 15$ case, we see that case with positive axial and negative poloidal flow which had the highest saturated amplitude, now comes at third place, while the others remain at the same relative position. In comparison to V-RMHD, we see a similarity in that the most stable case is the one with axial and poloidal flows negative, but the important difference is that in V-RMHD, all the cases had a lower saturated amplitude than the no flow case.

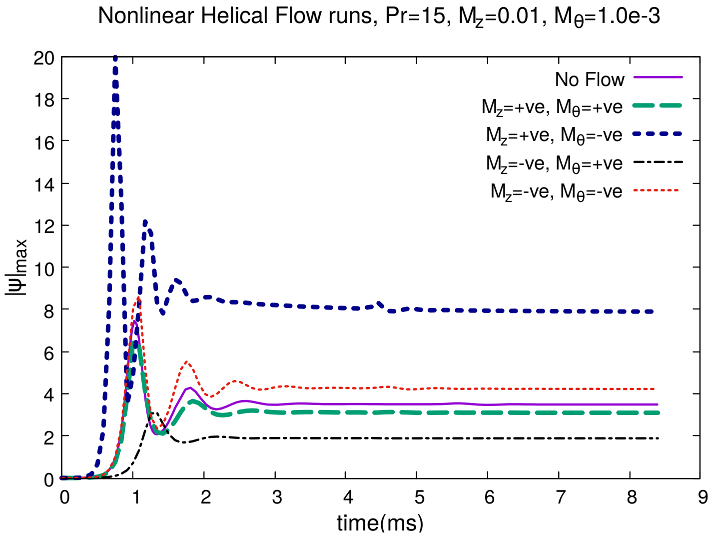

Figure 6.24: Nonlinear Helical Flow results for Pr=15

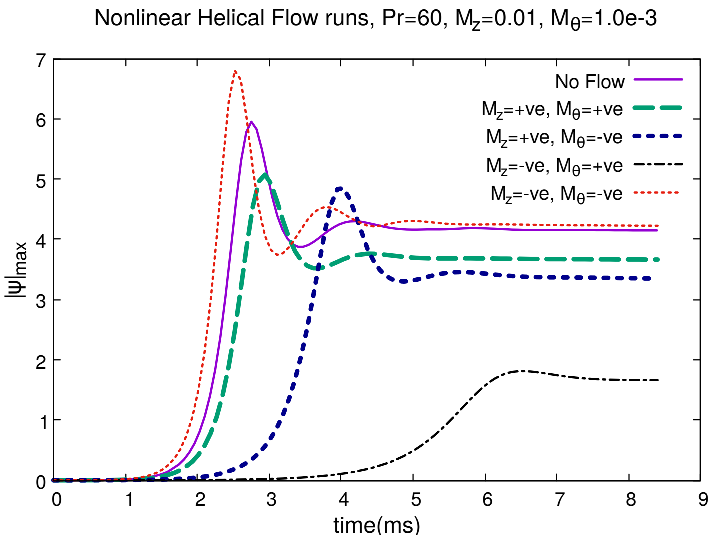

Figure 6.25: Nonlinear Helical Flow results for Pr=60

Summary and Discussion

In summary, we have done linear and nonlinear studies of the $m = 1, n = 1$ mode in a two fluid regime using the CUTIE code. In the absence of any imposed flow, we have observed significant diamagnetic stabilisation in the growth rate of the $m = 1, n = 1$ mode but the effect diminishes as we increase the viscosity. In low viscosity, the mode rotation frequencies are smaller compared to the respective diamagnetic flow frequencies but they approach the diamagnetic flow frequency asymptotically as we increase the viscosity. In the work of Porcelli et. al.[80], they have observed an increase of frequency with viscosity for a low viscosity case. The nonlinear saturation levels of the modes also increase with higher viscosity values, however its behaviour with change in diamagnetic flow is different for the low viscosity and high viscosity regime. At low viscosity it increases slightly with diamagnetic flow but decreases for high viscosity. In case of imposed axial flow, there is asymmetry with respect to the direction of the axial flow, for all cases, including zero diamagnetic flow. This is because parallel dynamics also introduce an asymmetry in the linear growth rate other than diamagnetic flow. Unlike axial flow, in the case of poloidal flow, there's a symmetry in the growth rate for the zero diamagnetic flow case. However, after the introduction of diamagnetic flow, the growth rates are not symmetric with respect to changing the direction of the imposed poloidal flow. In one direction it is destabilising and in the other direction it is stabilising the mode. This is very different from the single fluid result that the poloidal flow is always stabilising and agrees with recent experimental observations in JET[72] which shows that the poloidal flow destablises the internal kink mode.

7

Conclusion and future scope

We have summarised our findings and enumerate the likely areas of investigation to be carried out arising out of our studies in this chapter. We discuss the importance of these results in expanding our knowledge of the physics of MHD modes in the tokamak such as kink and tearing modes. We also attempt to identify lines of investigation for future work, and the improvement in techniques that encompasses.

Summary and conclusions

In this thesis we have studied MHD instabilities, particularly the tearing and kink instabilities in the presence of flow. We have also devoted our attention to the effect of viscosity in modifying the effect of flow. The thesis has thus investigated these matters in detail, extending our understanding of the role played by equilibrium flows in the growth of these instabilities in a tokamak plasma. We have also provided examples of experimental results from tokamaks like JET, MAST, NSTX which observe the type of phenomena we have dealt with in our simulations. In particular, the relative direction of flows applied to a tokamak plasma which we observe in our simulations is not well understood, for example, change of the neoclassical tearing mode stability as well as change of sawtooth period with the change in direction of NBI as observed in several experiments was not well understood based on simple RMHD model equations [58, 59, 81]. Also, most of the analytical and simulation studies in this area are in low viscosity regimes, however viscosity can be very high in tokamaks due to the presence of turbulence etc. as seen in several studies [16, 79]. So, in this thesis we have tried to address these issues by performing simulations of resistive MHD modes using

V-RMHD, two fluid equations for a wide range of viscosity regimes. After providing a background to the subject in the first three chapters, our results have been presented in chapters 4,5,6. In the following, we summarise the contents of the chapters.

In **chapter 4**, we have presented our results on the effect of flows on the $m = 2$, $n = 1$ tearing mode. We have examined the (2,1) tearing mode in various situations, single fluid, two fluid and finally in a toroidal geometry. Throughout, we have studied the effect of flow on the mode, particularly how shear and flow direction affect the evolution of the mode. To begin with, we used a cylindrical visco-resistive magnetohydrodynamic V-RMHD model to study the (2,1) mode in the linear regime. We found that while sheared axial flows destabilise the mode, sheared poloidal flows are stabilising in nature. We also observed that the effects of both flows are independent of the direction of flow. We then proceeded to study the effect of helical flows on the (2,1) mode. We found that the sign of the shear in the flow is significant here, unlike the previous cases. We further notice that this type of symmetry breaking is also noticed in the nonlinear regime where we see that the island saturation level depends on the sign of the flow. After this, we proceeded to a two fluid study. We found that the linear mode is more stable in this regime as compared to the V-RMHD regime. However, it is found that when we introduce sheared axial flows, a negative sheared flow destabilises the mode and a positive flow stabilises it, as compared to the corresponding result in the V-RMHD regime. The next study was done in a toroidal geometry using the NEAR code. Here it is found that unlike the cylindrical model, the equivalent of axial flows, that is, toroidal flows are always stabilising. This is attributed to a 'Shafranov' like shift induced by the flow in the profiles of the equilibrium current that brings about a stabilising change in Δ' and the saturated island size.

In **chapter 5**, we have studied the effect of sheared equilibrium flows on the $m = 1$, $n = 1$ resistive internal kink mode. We have used a V-RMHD model in a cylindrical geometry throughout in the CUTIE code for our investigations. We find that scaling dependence of the mode growth rate in the Lundquist number changes significantly in the presence of axial flows as compared to the no flow case. On the other hand, when we repeat this study in the presence of poloidal flows, we observe no corresponding change. We further observe that viscosity strongly modifies the effect of flows on the (1,1) mode. This is true both in the linear and nonlinear regime. Axial flows are found to increase the linear growth rate for low viscosity values, but on increasing viscosity they decrease linear growth rate of the mode. The poloidal flow on the contrary, tends to reduce the growth rate in all viscosity regimes. We also observe that in the presence of high viscosity, there is a strong symmetry breaking in the behaviour of linear growth rates, as well as in the nonlinear saturation levels of the modes as function of the helicities of the flows. We find a flow induced stabilisation for the axial, poloidal and majority of the helical flow cases, of the nonlinear saturation level in the high viscosity regime and a destabilisation in the presence of low viscosity.

We have extended these V-RMHD studies to the two fluid regime in **chapter 6**. We began with studies in the absence of imposed flow. We obtain significant diamagnetic destablisation in the growth rate of the $m = 1$, $n = 1$ mode, but the effect decreases as increase the viscosity in the system. In the low viscosity regime, we find that the mode rotation frequencies are smaller in comparison to the respective diamagnetic flow frequencies but they approach the diamagnetic flow frequencies as viscosity is increased. We observe similar behaviour qualitatively by performing a dimension analysis of the two fluid equations which agrees well with our numerical results. The paper of Porcelli *et al*[80] have presented a result in which they observe an increase in frequency with viscosity for low values of viscosity. We also observe that nonlinear saturation levels of the modes also increase when we increase viscosity values. The behaviour of the nonlinear saturation levels with a change in diamagnetic flow is different in the low viscosity regime as compared to the high viscosity regime. In the low viscosity regime, the saturation levels increase slightly with diamagnetic flow in the system, whereas a decrease in the saturation level is observed in the high viscosity regime. When we apply an imposed axial flow, we find an asymmetry with respect to the direction of the flow, including in the case of no diamagnetic flow. This is due to the role of the parallel momentum which introduces an asymmetry in the linear growth rate, in addition to the effects of the diamagnetic flow. In contrast, in the poloidal flow case, we find a symmetry in the growth rate when the diamagnetic flow is zero. This symmetry does not persist in the case with a finite diamagnetic flow. In the low viscosity regime, the positive shear poloidal flow is stabilising while the negative flow is destablising, while in the high viscosity regime, positive shear flow is still stabilising but the negative sheared poloidal flow is linearly destabilising and nonlinearly slightly more stable than the no flow case, but less stable than the positive flow case.

Outlook for future work

In this thesis, we have examined several interesting results which pertain to the effect of flows on the tearing and kink instabilities. We have also noted the effect of viscosity in modifying the effects of flows. Our results indicate that flows have a significant influence on the linear growth and the nonlinear saturation levels of the kink and tearing instabilities. These results are of relevance to experiments, and we have cited instances where behaviour which qualitatively indicates results of a similar nature as ours in tokamaks like JET. In particular, flow helicity, shear and the viscosity regime in which these flows are applied have a significant influence on the dynamics of MHD instabilities and thus on the tokamak plasma itself. In addition, flows are important in other situations in tokamak operations, for example to control resistive wall modes. We therefore believe that these studies can be extended to explain tokamak experiments in a more detailed and accurate fashion. In the following, future lines of investigation are outlined, along with possible refinements of our studies.

1. We begin by describing the limitations of our present model and possible extensions to study the physics of MHD instabilities more deeply. In our model we used a cylindrical geometry, and as such it is a crude approximation to a toroidal geometry used in tokamaks. Also, we did not allow the evolution of density and temperature. This would introduce a lot of interesting physics and make our model more realistic. Also, if we allow the evolution of density and temperature in the simulation, this would introduce a lot of interesting physics and we can investigate its effect on our present results.

2. Following from the above, one line of investigation we wish to pursue is to extend these results to allow coupling of different modes that are naturally present in a toroidal geometry. In a toroidal geometry, classical tearing modes excite NTMs and CUTIE needs to be extended to be able to carry out these studies. The presence of neoclassical effects and bootstrap current not only makes the physics considerably richer, but closer to the experimental situation. Toroidal geometry enables coupling and stabilisation of MHD modes, and we anticipate our results will be modified in this scenario. It also enables us to study phenomena like the Shafranov shift, which is absent in our present model

3. Another possible extension is to introduce heating into the code. By doing so, we can have sawteeth in our system. Sawteeth are a common occurrence in most tokamaks, and are not well understood despite decades of intense research. As we use a visco-resistive model, we believe we can get valuable insights into sawteeth behaviour by extending our studies to incorporate it, and examine its effects on the plasma, other modes it triggers, overall transport etc. Sawteeth are also thought to trigger NTMs. Therefore an extension of the code to incorporate these effects can shed light on the physics underlying these phenomena.

The above are some possible lines of investigations and avenues for refining our present work, which we believe can produce interesting results. The area of MHD instabilities and more broadly of disruption physics, particularly in the presence of flows in tokamaks is an area of active research, and we wish to continue contributing to expanding our understanding of it.

Bibliography

[1] J. Wesson and D. Campbell, *Tokamaks*. International Series of Monographs, OUP Oxford, 2011.

[2] R. J. Bickerton, J. W. Connor, and J. B. Taylor, "Diffusion Driven Plasma Currents and Bootstrap Tokamak," *Nature Physical Science*, vol. 229, pp. 110–112, Jan. 1971.

[3] M. Kikuchi, "Steady state tokamak reactor based on the bootstrap current," *Nuclear Fusion*, vol. 30, pp. 265–276, feb 1990.

[4] J. P. Freidberg, *Ideal MHD*. Cambridge University Press, 2014.

[5] H. Zehrfeld and B. Green, "Stationary toroidal equilibria at finite beta," *Nuclear Fusion*, vol. 12, no. 5, p. 569, 1972.

[6] E. K. Maschke and H. Perrin, "Exact solutions of the stationary mhd equations for a rotating toroidal plasma," *Plasma Physics*, vol. 22, no. 6, p. 579, 1980.

[7] R. Betti and J. P. Freidberg, "Radial discontinuities in tokamak magnetohydrodynamic equilibria with poloidal flow," *Physics of Plasmas*, vol. 7, no. 6, pp. 2439–2448, 2000.

[8] L. Guazzotto, R. Betti, J. Manickam, and S. Kaye, "Numerical study of tokamak equilibria with arbitrary flow," *Physics of Plasmas*, vol. 11, no. 2, pp. 604–614, 2004.

[9] E. Hameiri, "The equilibrium and stability of rotating plasmas," *The Physics of Fluids*, vol. 26, no. 1, pp. 230–237, 1983.

[10] G. N. Throumoulopoulos and G. Pantis, "Analytic axisymmetric magnetohydrodynamic equilibria of a plasma torus with toroidal mass flow," *Physics of Fluids B: Plasma Physics*, vol. 1, no. 9, pp. 1827–1833, 1989.

[11] I. Hofman, "Resistive tearing modes in a sheet pinch with shear flow," *Plasma Physics*, vol. 17, no. 2, p. 143, 1975.

[12] X. L. Chen and P. J. Morrison, "Resistive tearing instability with equilibrium shear flow," *Physics of Fluids B*, vol. 2, pp. 495–507, Mar. 1990.

[13] R. G. Kleva and P. N. Guzdar, "Stabilization of sawteeth in tokamaks with toroidal flows," *Physics of Plasmas*, vol. 9, no. 7, pp. 3013–3018, 2002.

[14] C. Wahlberg and A. Bondeson, "Stabilization of the internal kink mode in a tokamak by toroidal plasma rotation," *Physics of Plasmas*, vol. 7, no. 3, pp. 923–930, 2000.

[15] I. Chapman, T. C. Hender, S. Saarelma, S. Sharapov, R. Akers, N. Conway, and MAST, "The effect of toroidal plasma rotation on sawteeth in MAST," *Nuclear Fusion*, vol. 46, pp. 1009–1016, 2006.

[16] T. Tala, "Parametric dependences of momentum pinch and Prandtl number in JET," *Nuclear Fusion*, vol. 51, p. 123002, 2011.

[17] P. Maget, "Non linear MHD Modelling of NTMs in JET Advanced Scenarios," *IAEA CONFERENCE*, pp. 3–10, 2010.

[18] S. Wang and Z. W. Ma, "Influence of toroidal rotation on resistive tearing modes in tokamaks," *Physics of Plasmas*, vol. 22, no. 12, p. 122504, 2015.

[19] K. Takeda, O. Agullo, S. Benkadda, A. Sen, N. Bian, and X. Garbet, "Nonlinear viscoresistive dynamics of the m=1 tearing instability," *Physics of Plasmas*, vol. 15, p. 022502, 2008.

[20] H. P. Furth, J. Killeen, and M. N. Rosenbluth, "Finite-Resistivity Instabilities of a Sheet Pinch," *Physics of Fluids*, vol. 6, pp. 459–484, Apr. 1963.

[21] S. Von Goeler, W. Stodiek, and N. Sauthoff, "Studies of internal disruptions and m=1 oscillations in tokamak discharges with soft-X-ray tecniques," *Physical Review Letters*, vol. 33, no. 20, pp. 1201–1203, 1974.

[22] B. B. Kadomtsev, "Disruptive instability in Tokamaks," *Fizika Plazmy*, vol. 1, pp. 710–715, Sept. 1975.

[23] M. N. Rosenbluth, R. Y. Dagazian, and P. H. Rutherford, "Nonlinear properties of the internal mâĂĽ=âĂĽ1 kink instability in the cylindrical tokamak," *The Physics of Fluids*, vol. 16, no. 11, pp. 1894–1902, 1973.

[24] F. Porcelli, D. Boucher, and M. N. Rosenbluth, "Model for the sawtooth period and amplitude," *Plasma Physics and Controlled Fusion*, vol. 38, pp. 2163–2186, Dec. 1996.

[25] D. A. Monticello, W. Park, R. Izzo, and K. McGuire, "A review of calculations of the resistive internal m = 1 mode in Tokamaks," *Computer Physics Communications*, vol. 43, no. 1, pp. 57–67, 1986.

[26] A. Y. Aydemir, "Nonlinear $m = 1$ mode and fast reconnection in collisional plasmas," *Phys. Rev. Lett.*, vol. 78, pp. 4406–4409, Jun 1997.

[27] D. Biskamp, "Algebraic nonlinear growth of the resistive kink instability," *Physics of Fluids B: Plasma Physics*, vol. 3, no. 12, pp. 3353–3356, 1991.

[28] D. Biskamp and J. F. Drake, "Dynamics of the sawtooth collapse in tokamak plasmas," *Phys. Rev. Lett.*, vol. 73, pp. 971–974, Aug 1994.

[29] A. Y. Aydemir, J. C. Wiley, and D. W. Ross, "Toroidal studies of sawtooth oscillations in tokamaks," *Physics of Fluids B: Plasma Physics*, vol. 1, no. 4, pp. 774–787, 1989.

[30] A. Y. Aydemir, "Magnetohydrodynamic modes driven by anomalous electron viscosity and their role in fast sawtooth crashes," *Physics of Fluids B: Plasma Physics*, vol. 2, no. 9, pp. 2135–2142, 1990.

[31] R. Hastie, "Sawtooth instability in tokamak plasmas," *Astrophysics and space science*, vol. 256, no. 1-2, pp. 177–204, 1997.

[32] S. Migliuolo, "Theory of ideal and resistive m=1 modes in tokamaks," *Nuclear Fusion*, vol. 33, no. 11, p. 1721, 1993.

[33] R. Fitzpatrick, *Plasma Physics: An Introduction.* CRC Press, 2014.

[34] F. Militello, G. Huysmans, M. Ottaviani, and F. Porcelli, "Effects of local features of the equilibrium current density profile on linear tearing modes," *Physics of Plasmas*, vol. 11, pp. 125–128, 2004.

[35] A. Thyagaraja, "Numerical simulations of tokamak plasma turbulence and internal transport barriers," *Plasma Phys. Control. Control. Fusion*, vol. 42, p. B255, 2000.

[36] A. Thyagaraja, M. Valovič, and P. J. Knight, "Global two-fluid turbulence simulations of l-h transitions and edge localized mode dynamics in the compass-d tokamak," *Physics of Plasmas*, vol. 17, no. 4, p. 042507, 2010.

[37] A. Thyagaraja, "Is the Hartmann number relevant to tokamak physics?," *Plasma Physics and Controlled Fusion*, vol. 36, pp. 1037–1050, June 1994.

[38] A. Thyagaraja, P. Knight, and N. Loureiro, "Mesoscale plasma dynamics, transport barriers and zonal flows: simulations and paradigms," *European Journal of Mechanics - B/Fluids*, vol. 23, no. 3, pp. 475 – 490, 2004. Invited papers from the 9th EUROMECH European Turbulence Conference.

[39] D. Chandra, A. Thyagaraja, A. Sen, C. Ham, T. Hender, R. Hastie, J. Connor, P. Kaw, and J. Mendonca, "Modelling and analytic studies of sheared flow effects on tearing modes," *Nuclear Fusion*, vol. 55, no. 5, p. 053016, 2015.

[40] D. Chandra, A. Thyagaraja, A. Sen, and P. Kaw, "Nonlinear simulation of elm dynamics in the presence of resonant magnetic perturbations," *Nuclear Fusion*, vol. 57, no. 7, p. 076001, 2017.

[41] J. Mendonca, D. Chandra, A. Sen, and A. Thyagaraja, "Visco-resistive mhd study of internal kink (m = 1) modes," *Physics of Plasmas*, vol. 25, no. 2, p. 022504, 2018.

[42] R. J. La Haye, D. P. Brennan, R. J. Buttery, and S. P. Gerhardt, "Islands in the stream: The effect of plasma flow on tearing stability," *Physics of Plasmas*, vol. 17, no. 5, p. 056110, 2010.

[43] S. Fietz, M. Maraschek, H. Zohm, M. Reich, L. Barrera, R. M. McDermott, and the ASDEX Upgrade Team, "Influence of rotation on the (m , n) = (3, 2) neoclassical tearing mode threshold in the asdex upgrade," *Plasma Physics and Controlled Fusion*, vol. 55, no. 8, p. 085010, 2013.

[44] X. L. Chen and P. J. Morrison, "The effect of viscosity on the resistive tearing mode with the presence of shear flow," *Physics of Fluids B: Plasma Physics*, vol. 2, no. 11, pp. 2575–2580, 1990.

[45] A. Thyagaraja, “Is the hartmann number relevant to tokamak physics?,” *Plasma Physics and Controlled Fusion*, vol. 36, no. 6, p. 1037, 1994.

[46] S. E. Kruger, C. C. Hegna, and J. D. Callen, “Generalized reduced magnetohydrodynamic equations,” *Physics of Plasmas*, vol. 5, no. 12, pp. 4169–4182, 1998.

[47] D. Chandra, A. Sen, P. Kaw, M. Bora, and S. Kruger, “Effect of sheared flows on classical and neoclassical tearing modes,” *Nuclear Fusion*, vol. 45, no. 6, p. 524, 2005.

[48] “TOQ, a toroidal equilibrium code,” *https://fusion.gat.com/THEORY/toq/*.

[49] A. Thyagaraja, N. Loureiro, and P. J. Knight, “Spectral and evolutionary analysis of advection-diffusion equations and the shear flow paradigm,” *Journal of Plasma Physics*, vol. 68, no. 5, pp. 363 - 388, 2002.

[50] J. G. I. Douglas, *Linear stability analysis of non ideal tokamak plasma fluid models*. PhD thesis, University of Sheffield, 2012.

[51] C. G. Gimblett, R. J. Hastie, R. A. M. V. der Linden, and J. A. Wesson, “Non - uniform rotation and the resistive wall mode,” *Physics of Plasmas*, vol. 3, no. 10, pp. 3619–3627, 1996.

[52] B. Carreras, B. Waddell, and H. Hicks, “Poloidal magnetic field fluctuations,” *Nuclear Fusion*, vol. 19, no. 11, p. 1423, 1979.

[53] A. Thyagaraja, “Perturbation analysis of a simple model of magnetic island structures,” *The Physics of Fluids*, vol. 24, no. 9, pp. 1716–1724, 1981.

[54] D. Chandra, A. Sen, and P. Kaw, “Dynamical origin of shear flow induced modifications of magnetic islands,” *Nuclear Fusion*, vol. 47, no. 9, p. 1238, 2007.

[55] J. Rice, A. Ince-Cushman, J. deGrassie, L.-G. Eriksson, Y. Sakamoto, A. Scarabosio, A. Bortolon, K. Burrell, B. Duval, C. Fenzi-Bonizec, M. Greenwald, R. Groebner, G. Hoang, Y. Koide, E. Marmar, A. Pochelon, and Y. Podpaly, “Inter-machine comparison of intrinsic toroidal rotation in tokamaks,” *Nuclear Fusion*, vol. 47, no. 11, p. 1618, 2007.

[56] J. Menard, M. Bell, R. Bell, E. Fredrickson, D. Gates, S. Kaye, B. LeBlanc, R. Maingi, D. Mueller, S. Sabbagh, D. Stutman, C. Bush, D. Johnson, R. Kaita, H. Kugel, R. Maqueda, F. Paoletti, S. Paul, M. Ono, Y.-K. Peng, C. Skinner, E. Synakowski, and the NSTX Research Team, "Beta-limiting mhd instabilities in improved-performance nstx spherical torus plasmas," *Nuclear Fusion*, vol. 43, no. 5, p. 330, 2003.

[57] J. E. Menard, R. E. Bell, E. D. Fredrickson, D. A. Gates, S. M. Kaye, B. P. LeBlanc, R. Maingi, S. S. Medley, W. Park, S. A. Sabbagh, A. Sontag, D. Stutman, K. Tritz, W. Zhu, and NSTX Research Team, "Internal kink mode dynamics in high-β NSTX plasmas," *Nuclear Fusion*, vol. 45, pp. 539–556, July 2005.

[58] I. Chapman, S. D. Pinches, J. P. Graves, R. J. Akers, L. C. Appel, R. V. Budny, S. Coda, N. J. Conway, M. de Bock, L.-G. Eriksson, R. J. Hastie, T. C. Hender, G. T. a. Huysmans, T. Johnson, H. R. Koslowski, A. Krämer-Flecken, M. Lennholm, Y. Liang, S. Saarelma, S. E. Sharapov, and I. Voitsekhovitch, "The physics of sawtooth stabilization," *Plasma Physics and Controlled Fusion*, vol. 49, pp. B385–B394, 2007.

[59] M. F. F. Nave, H. R. Koslowski, S. Coda, J. Graves, M. Brix, R. Buttery, C. Challis, C. Giroud, M. Stamp, and P. De Vries, "Exploring a small sawtooth regime in Joint European Torus plasmas with counterinjected neutral beams," *Physics of Plasmas*, vol. 13, no. 1, pp. 1–4, 2006.

[60] I. Chapman, J. P. Graves, and C. Wahlberg, "The effect of Plasma Profile Variation on the Stability of the n=1 Internal Kink Mode in Rotating Tokamak Plasmas," *Nuclear Fusion*, vol. 50, p. 025018, 2008.

[61] U. Shumlak and C. Hartman, "Sheared Flow Stabilization of the m=1 Kink Mode in Z Pinches," *Physical Review Letters*, vol. 75, no. 18, pp. 3285–3288, 1995.

[62] R. Gatto, P. Terry, and C. Hegna, "Tearing mode stability with equilibrium flows in the reversed-field pinch," *Nuclear Fusion*, vol. 42, no. 5, p. 496, 2002.

[63] H. Naitou, T. Kobayashi, and S. Tokuda, "Stabilization of the kinetic internal kink mode by a sheared poloidal flow," *Journal of Plasma Physics*, vol. 61, no. 4, pp. 543 – 552, 1999.

[64] A. B. Mikhailovskii, J. G. Lominadze, R. M. O. Galvão, A. P. Churikov, N. N. Erokhin, V. D. Pustovitov, S. V. Konovalov, A. I. Smolyakov, and V. S. Tsypin, "Ideal internal kink modes in a differentially rotating cylindrical plasma," *Plasma Physics Reports*, vol. 34, no. 7, pp. 538–546, 2008.

[65] F. L. Waelbroeck, "Gyroscopic stabilization of the internal kink mode," *Physics of Plasmas*, vol. 3, no. 3, pp. 1047–1053, 1996.

[66] D. Brunetti, E. Lazzaro, and S. Nowak, "Ideal and resistive magnetohydrodynamic instabilities in cylindrical geometry with a sheared flow along the axis," *Plasma Physics and Controlled Fusion*, vol. 59, p. 055012, May 2017.

[67] L. Ofman, X. L. Chen, P. J. Morrison, and R. S. Steinolfson, "Resistive tearing mode instability with shear flow and viscosity," *Physics of Fluids B: Plasma Physics*, vol. 3, no. 6, pp. 1364–1373, 1991.

[68] C. Ren, M. S. Chu, and J. D. Callen, "Magnetic island deformation due to sheared flow and viscosity," *Physics of Plasmas*, vol. 6, no. 4, pp. 1203–1207, 1999.

[69] R. J. L. Haye and R. J. Buttery, "The stabilizing effect of flow shear on m/n=3/2 magnetic island width in DIII-D," *Physics of Plasmas*, vol. 16, no. 2, p. 022107, 2009.

[70] F. Porcelli, "Viscous resistive magnetic reconnection," *Physics of Fluids*, vol. 30, no. 6, p. 1734, 1987.

[71] I. Chapman, R. Scannell, W. A. Cooper, J. P. Graves, R. J. Hastie, G. Naylor, and A. Zocco, "Magnetic reconnection triggering magnetohydrodynamic instabilities during a sawtooth crash in a Tokamak plasma," *Physical Review Letters*, vol. 105, no. 25, pp. 1–4, 2010.

[72] K. Crombé, Y. Andrew, M. Brix, C. Giroud, S. Hacquin, N. C. Hawkes, A. Murari, M. F. F. Nave, J. Ongena, V. Parail, G. Van Oost, I. Voitsekhovitch, and K.-D. Zastrow, "Poloidal rotation dynamics, radial electric field, and neoclassical theory in the jet internal-transport-barrier region," *Phys. Rev. Lett.*, vol. 95, p. 155003, Oct 2005.

[73] M. V. Barkov and S. S. Komissarov, "Relativistic tearing and drift-kink instabilities in two-fluid simulations," *MNRAS*, vol. 458, pp. 1939–1947, May 2016.

[74] L. Zakharov and B. Rogers, "Two fluid magnetohydrodynamic description of the internal kink mode in tokamaks," *Physics of Fluids B: Plasma Physics*, vol. 4, no. 10, pp. 3285–3301, 1992.

[75] P. H. Yoon, A. T. Y. Lui, and H. K. Wong, "Two - fluid theory of drift-kink instability in a one-dimensional neutral sheet," *Journal of Geophysical Research: Space Physics*, vol. 103, no. A6, pp. 11875–11886, 1998.

[76] W. Daughton, "Two - fluid theory of the drift kink instability," *Journal of Geophysical Research: Space Physics*, vol. 104, no. A12, pp. 28701–28707, 1999.

[77] C. Akcay, C. C. Kim, B. S. Victor, and T. R. Jarboe, "Validation of single-fluid and two-fluid magnetohydrodynamic models of the helicity injected torus spheromak experiment with the nimrod code," *Physics of Plasmas*, vol. 20, no. 8, p. 082512, 2013.

[78] a. Thyagaraja and F. a. Haas, "Asymptotic theory of the nonlinearly saturated m=1 mode in tokamaks with q0<1," *Physics of Fluids B: Plasma Physics*, vol. 3, no. 3, p. 580, 1991.

[79] K. Itoh, S.-I. Itoh, A. Fukuyama, M. Yagi, and M. Yazumi, "Prandtl number of toroidal plasmas," *Journal of the Physical Society of Japan*, vol. 62, no. 12, pp. 4269–4276, 1993.

[80] F. Porcelli and S. Migliuolo, "Ion viscosity stabilization of resistive internal kink modes," *The Physics of Fluids*, vol. 29, no. 5, pp. 1741–1743, 1986.

[81] I. Chapman, T. C. Hender, S. E. Sharapov, G. T. A. Huysmans, and A. B. Mikhailovskii, "Modelling the effect of toroidal plasma rotation on magnetohydrodynamic instabilities in MAST," *Physics of Plasmas (1994-present)*, vol. 13, pp. 39–50, 2006.

[82] G. Ara, B. Basu, B. Coppi, G. Laval, M. N. Rosenbluth, and B. V. Waddell, "Magnetic reconnection and m = 1 oscillations in current carrying plasmas," *Annals of Physics*, vol. 112, no. 2, pp. 443–476, 1978.

[83] A. Bierwage, S. Benkadda, S. Hamaguchi, and M. Wakatani, "Nonlinear evolution of the m=1 internal kink mode in the presence of magnetohydrodynamic turbulence," *Physics of Plasmas*, vol. 13, no. 3, pp. 1–14, 2006.

[84] A. Bierwage, Y. Todo, N. Aiba, and K. Shinohara, "Dynamics of low - n shear alfven modes driven by energetic n - nb ions in jt - 60u," *Nuclear Fusion*, vol. 54, no. 10, p. 104001, 2014.

[85] A. Bondeson, G. Vlad, and H. Lütjens, "Resistive toroidal stability of internal kink modes in circular and shaped tokamaks," *Physics of Fluids B: Plasma Physics*, vol. 4, no. 7, p. 1889, 1992.

[86] J. A. Breslau, "Fluid Modeling of Macroscopic Tokamak Instabilities with the M3D Code Acknowledgments," 2009.

[87] D. J. Campbell, D. F. Start, J. A. Wesson, D. V. Bartlett, V. P. Bhatnagar, M. Bures, J. G. Cordey, G. A. Cottrell, P. A. Dupperex, A. W. Edwards, C. D. Challis, C. Gormezano, C. W. Gowers, R. S. Granetz, J. H. Hamnen, T. Hellsten, J. Jacquinot, E. Lazzaro, P. J. Lomas, N. Lopes Cardozo, P. Mantica, J. A. Snipes, D. Stork, P. E. Stott, P. R. Thomas, E. Thompson, K. Thomsen, and G. Tonetti, "Stabilization of sawteeth with additional heating in the JET tokamak," *Physical Review Letters*, vol. 60, pp. 2148–2151, May 1988.

[88] I. Chapman, S. Pinches, H. Koslowski, Y. Liang, A. Krämer-Flecken, and M. de Bock, "Sawtooth stability in neutral beam heated plasmas in TEXTOR," *Nuclear Fusion*, vol. 48, no. 3, p. 035004, 2008.

[89] I. Chapman, S. D. Pinches, L. C. Appel, R. J. Hastie, T. C. Hender, S. Saarelma, S. E. Sharapov, I. Voitsekhovitch, and J. P. Graves, "Modeling sawtooth stabilization by energetic ions from neutral beam injection," *Physics of Plasmas*, vol. 14, no. 7, pp. 1–4, 2007.

[90] I. T. Chapman, "Controlling sawtooth oscillations in tokamak plasmas," *Plasma Physics and Controlled Fusion*, vol. 53, no. 1, p. 013001, 2011.

[91] J. W. Connor, R. J. Hastie, and A. Zocco, "Unified theory of the semi-collisional tearing mode and internal kink mode in a hot tokamak: implications for sawtooth

modelling," *Plasma Physics and Controlled Fusion*, vol. 54, no. 3, p. 035003, 2012.

[92] B. Coppi, R. Galvao, R. Pellat, M. Rosenbluth, and P. Rutherford, "Resistive internal kink modes," *Soviet Journal of Plasma Physics*, vol. 2, pp. 961–966, Nov. 1976.

[93] D. F. Escande and M. Ottaviani, "Simple and rigorous solution for the nonlinear tearing mode," *Physics Letters A*, vol. 323, pp. 278–284, 2004.

[94] G. Fogaccia and F. Romanelli, "On the stability of the internal kink mode in the banana regime," *Physics of Plasmas (1994-present)*, vol. 2, no. 1, p. 227, 1995.

[95] I. Furno, T. P. Intrator, D. D. Ryutov, S. Abbate, T. Madziwa-Nussinov, A. Light, L. Dorf, and G. Lapenta, "Current-Driven Rotating-Kink Mode in a Plasma Column with a Non-Line-Tied Free End," *Physical Review Letters*, vol. 97, p. 015002, July 2006.

[96] C. G. Gimblett, R. J. Hastie, and T. C. Hender, "An analytic study of the magnetohydrodynamic stability of inverse shear profiles," *Physics of Plasmas*, vol. 3, no. 9, p. 3369, 1996.

[97] F. A. Haas and A. Thyagaraja, "The relationship between q profiles, transport, and sawteeth in tokamaks," *Physics of Fluids B: Plasma Physics*, vol. 3, no. 12, p. 3388, 1991.

[98] Q. Hu, Q. Yu, and X. Hu, "Linear and nonlinear effect of sheared plasma flow on resistive tearing modes," *Physics of Plasmas*, vol. 21, no. 12, p. 122507, 2014.

[99] P. Marshall .N. Rosenbluth, R.Y. Dagazian, "Nonlinear properties of the internal m=1 kink instability in the cylindrical tokamak," *The Physics of Fluids*, vol. 16, no. 1973, pp. 1689–1699, 1973.

[100] K. G. McClements and M. J. Hole, "On steady poloidal and toroidal flows in tokamak plasmas," *Physics of Plasmas*, vol. 17, no. 8, pp. 1–9, 2010.

[101] F. Militello, D. Borgogno, D. Grasso, C. Marchetto, and M. Ottaviani, "Asymmetric tearing mode in the presence of viscosity," *Physics of Plasmas*, vol. 18, p. 112108, 2011.

[102] F. Militello, D. Grasso, and D. Borgogno, “The deceiving delta prime: on the equilibrium dependent dynamics of nonlinear magnetic islands,” *Physics of Plasmas*, vol. 21, no. 10, pp. 1–5, 2014.

[103] W. Park, D. a. Monticello, R. B. White, and S. C. Jardin, “Non-linear saturation of the internal kink mode,” *Nuclear Fusion*, vol. 20, no. 9, pp. 1181–1185, 1980.

[104] E. N. Parker, “Sweet’s Mechanism for Merging Magnetic Fields in Conducting Fluids,” *Journal of Geophysical Research*, vol. 62, pp. 509–520, Dec. 1957.

[105] F. Porcelli, “Fast particle stabilisation,” *Plasma Physics and Controlled Fusion*, vol. 33, no. 13, p. 1601, 1991.

[106] P. H. Rutherford, “Nonlinear growth of the tearing mode,” *Physics of Fluids*, vol. 16, pp. 1903–1908, Nov. 1973.

[107] M. J. Schaffer, “ITER test blanket module error field simulation experiments at DIII-D,” *Nuclear Fusion*, vol. 51, p. 103028, 2011.

[108] T. Tala, “Toroidal and poloidal momentum transport studies in tokamaks,” *Plasma Physics and Controlled Fusion*, vol. 49, p. B291, 2007.

[109] B. Lehnert, ed., *The Neutral Point Theory of Solar Flares*, vol. 6 of *IAU Symposium*, 1958.